FOR OFFICIAL USE ONLY

JPRS L/8451

10 May 1979

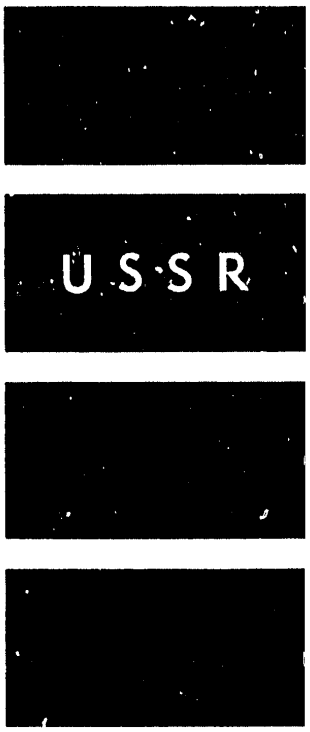

TRANSLATIONS ON USSR SCIENCE AND TECHNOLOGY
PHYSICAL SCIENCES AND TECHNOLOGY
(FOUO 26/79)

U. S. JOINT PUBLICATIONS RESEARCH SERVICE

FOR OFFICIAL USE ONLY

APPROVED FOR RELEASE: 2007/02/09: CIA-RDP82-00850R000100050022-1

NOTE

JPRS publications contain information primarily from foreign newspapers, periodicals and books, but also from news agency transmissions and broadcasts. Materials from foreign-language sources are translated; those from English-language sources are transcribed or reprinted, with the original phrasing and other characteristics retained.

Headlines, editorial reports, and material enclosed in brackets [] are supplied by JPRS. Processing indicators such as [Text] or [Excerpt] in the first line of each item, or following the last line of a brief, indicate how the original information was processed. Where no processing indicator is given, the information was summarized or extracted.

Unfamiliar names rendered phonetically or transliterated are enclosed in parentheses. Words or names preceded by a question mark and enclosed in parentheses were not clear in the original but have been supplied as appropriate in context. Other unattributed parenthetical notes within the body of an item originate with the source. Times within items are as given by source.

The contents of this publication in no way represent the policies, views or attitudes of the U.S. Government.

APPROVED FOR RELEASE: 2007/02/09: CIA-RDP82-00850R000100050022-1

JPRS L/8451

10 May 1979

TRANSLATIONS ON USSR SCIENCE AND TECHNOLOGY
PHYSICAL SCIENCES AND TECHNOLOGY

(FOUO 26/79)

CONTENTS PAGE

CONTENTS (Continued) Page

CONTENTS (Continued) Page

ELECTRONICS AND ELECTRICAL ENGINEERING

UDC 621.37/39.029.64.004:634

MICROWAVE RADIATION SPECTRA OF FOREST FIRE FOCI

Moscow RADIOTEKHNIKA I ELEKTRONIKA in Russian No 1, Jan 79 pp 177-180

[Article by Yu. P. Stakankin, submitted 13 Jan 77]

[Text] 1. The possibility of using microwave radiometry in studying forest fires was discussed in work [1]. It was shown that the flame spectrum is determined by the dimensions and concentration of particles in the flame and by its height. It was also established that, for detecting and mapping forest fire foci when the area is screened by smoke and under the canopy of the forest, the optimal working wave band is 0.8-1.5 cm. Data of experiments in determining the radiation capacity of fire foci on 0.8 and 3.4 cm waves were given.

For the purposes of further studies on forest fire foci by the methods of microwave radiometry, it became necessary to examine models of various types of forest fire foci from the viewpoint of the special characteristics of their spectra of radio-brightness temperatures, as well as to conduct experimental studies on microwave radiation of the foci in a wide wave range.

2. The main components of a foci which form the spectrum of radio-brightness temperature are the flame, smoke trail, crown, and underlying surface.

As a rule, the focus has a complex geometrical shape, and for calculating spectra of various foci, it is practical to examine a simplified model in the form of homogeneous isothermal layers of flame, smoke and the crown situated on an underlying surface.

It is possible to show that the radio-brightness temperature of the stratified model described above is determined by the following relation:

$$T_{\text{я}}(\lambda) = \{[\varkappa(\lambda) T_1 e^{-\tau_2(\lambda)} + T_2(1-e^{-\tau_2(\lambda)})] e^{-\tau_3(\lambda)} + T_3(1-e^{-\tau_3(\lambda)})\} e^{-\tau_4(\lambda)} + T_4(1-e^{-\tau_4(\lambda)}), \quad (1)$$

where $\varkappa(\lambda)$ is the radiation capacity of the underlying surface; T_1, T_2, T_3 T_4 are thermodynamic temperatures of the underlying surface, flame, smoke, and the crown, respectively; τ_2, τ_3, τ_4 are the optical thicknesses of the flame, smoke, and crown, respectively.

The optical thickness in the direction of probing is determined by the relation

$$\tau(\lambda) = \gamma(\lambda) L, \tag{2}$$

where $\gamma(\lambda)$ is the absorption coefficient at a unit of path; L is the layer thickness.

If the volume concentration of the particles of radius a in the layer is equal to N(a), and σ_n (a) is the value of the effective absorption cross section, then the absorption coefficient

$$\gamma(\lambda) = \int_0^{a_{\text{макс}}} \sigma_n(a) N(a)\, da. \tag{3}$$

Methods for calculating absorption coefficients for flame, smoke and the crown are given in [1].

3. Various foci of forest fires are characterized by different degrees of heating of the underlying surface, different power of the smoke trail, and different flame parameters.

Calculations for the spectra of radio-brightness temperature for various foci were done by the above formulas (1)-(3) with the following general assumptions.

The radiation capacity of the underlying surfaces was taken to be equal to one for all waves. The height of the flame was 2 m, and the weight concentration of particles was $3 \cdot 10^{-5}$ g/cm^3. The thickness of the smoke layer was 10 m, and the weight concentration of smoke particles was $3 \cdot 10^{-6}$ g/cm^3. Particles of flame and smoke have the Rayleigh distribution with respect to size with maximums of 150 and 100 micrometers respectively. The thickness of the crown was taken to be equal to 2 m. The thermodynamic temperature of the crown and smoke was equal to 300 degrees K, and that of flame was 900 degrees K. The coefficient of absorption in the crown at various waves was selected according to the data given in work [1]. Cases of changes in these parameters will be mentioned specially.

The results of the calculations of the spectra of the radio-brightness temperature of various foci are shown in Figure 1.

Curves 1 and 2 characterize the spectra of foci covered by the smoke trail and located under the crowns of trees. The temperature of the underlying surface T_1 for case 1 is taken to be equal to 400 degrees K, and for case 2 it is equal to 300 degrees K.

It can be seen from the curves that temperature changes in the underlying surface lead to substantial changes only in the long-wave part of the spectrum.

Curve 3 characterizes radiation of the burning section situated in an open area in the absence of the smoke trail.

In this case, in formula (1) $\tau_3 = 0$ and $\tau_4 = 0$. The temperature of the underlying surface was taken to be 400 degrees K.

It can be seen from the above curves that in the absence of the screening effect of smoke and the crown, a higher radio-brightness temperature of the foci is observed in the shortwave part of the spectrum than in the case of foci 1 and 2.

It is of interest to calculate the spectrum of a focus in which there is no flame ($\tau_2 = 0$). By comparing it with other spectra, it is possible to evaluate the contribution of flame to the microwave radiation of the foci. In the absence of flame, the radio-brightness temperature of the fire focus will be determined in the region of shortwaves by the radiation of the crown and the smoke trail, and in the area of long waves it will be determined by the radiation of the underlying surface (curve 4). Calculation showed that flame makes the main contribution to the radiation of foci in the microwave range.

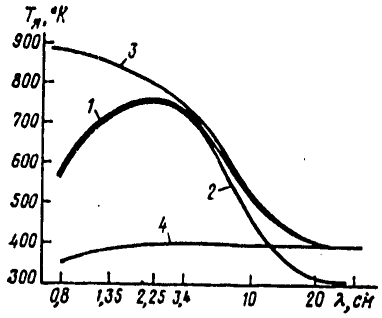

Figure 1. Calculated Spectra of the Radio-Brightness Temperatures of Forest Fire Foci: 1 -- a focus under the canopy of the forest covered by a smoke trail, temperature of the underlying surface 400 degrees K; 2 -- a focus of type 1, temperature of the underlying surface 300 degrees K; 3 -- a focus in an open area without the smoke trails; 4 -- burnt part of a focus without flame.

Analysis of curves 1-4 showed that various components of a focus (flame, smoke, crown, underlying surface) affect substantially various sections of the spectrum of radio-brightness temperatures, which makes it possible to evaluate their parameters.

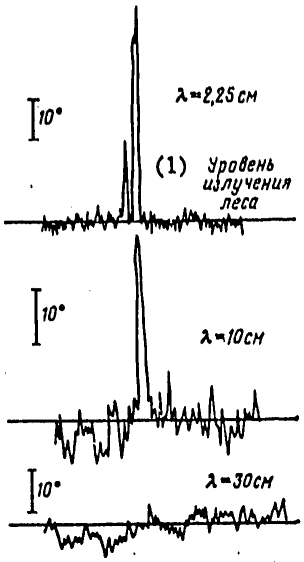

Figure 2. Profile of the Radio-Brightness Temperature of a Forest Fire Focus on 2.25, 10, and 30 cm Waves.
Key: 1. Level of forest radiation

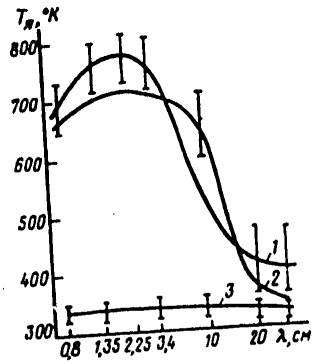

Figure 3. Experimental Spectra of Radio-Brightness Temperatures of Forest Fires:
1 and 2 -- spectra of burning sections of the focus; 3 -- spectrum of a burnt part of the focus.

4. Experimental studies on the microwave radiation of forest fires were conducted from aboard an airborne laboratory "IL-18" on 0.8, 1.35, 2.25, 3.4, 10, 20, and 30 cm waves.

The main characteristics of the radiometers used for measuring self-radiation of forest fires are given in the table

Flight No	Waveband, cm	Fluctuation Sensitivity at τ = 1 sec	Antenna Pattern Width, degrees
1	0.8	0.4	3
2	1.35	0.3	4
3	2.25	0.2	5
4	3.4	0.6	7
5	10	0.5	7
6	20	0.4	15
7	30	0.4	26

The flights were conducted at heights of 100-400 m. Radiometric instruments were calibrated by the radio-brightness temperature gradient of homogeneous sections of the forest and water surface with known radiation capacity. The experimental results were processed with consideration for the antenna patterns. Natural fires in Krasnoyarskiy Kray were studied. As a result of the analysis of large volume of experimental material, it was established that maximums of the radio-brightness temperatures of fire foci, depending on their special characteristics, can occur in a rather wide waveband, 0.8-10 cm. In the long-wave part of the spectrum of 10-30 cm, the radio-brightness temperature of fire foci is very low.

The characteristic radio-brightness temperature distribution in a forest fire focus on waves of 2.25, 10, and 30 cm is shown in Figure 2. As can be seen from the figure, the maximum radio-brightness temperature in the focus zone is observed on a wave of 2.25 cm. The increment of the radio-brightness temperature in the focus zone on a 30 cm wave is small.

Figure 3 shows typical spectra of burning edges of forest fire foci (curves 1 and 2), as well as the spectrum of the burnt part of the focus (curve 3). It can be seen from the curves that the radio-brightness temperature of the burning edge reduced to its dimensions is considerably higher than the radio-brightness temperature of the burnt part. This indicates a predominant contribution of flame to the microwave radiation of the foci.

The special characteristics of the spectra (1-3) can be explained by the influence of various components of the focus described above.

Analysis of the obtained theoretical and experimental results makes it possible to make the following conclusions.

1. The spectra of radio-brightness temperatures of forest fire foci depend on the parameters of the flame, on the power of the smoke trail and the crown, and the degree of heating of the underlying surface.

2. The maximum of the radio-brightness temperature of a forest fire focus is determined by the special characteristics of the focus. For forest fires, it lies within the 0.8-10 cm wave range, which it is most practical to use for detection and mapping of foci.

3. In the 0.8-10 cm wave range, the radio-brightness temperature of the burning edge is considerably higher than the radio-brightness temperature of the burnt part of the focus, which confirms the predominant contribution of flame to the radiation of foci in this range. In the 10-30 cm region of the spectrum, the radio-brightness temperature of the focus is determined both by the radiation of the flame, and by the radiation of the underlying surface.

Bibliography

1. Borodin, L. F.; Kirdyashev, K. P.; Stakankin, Yu. P.; and Chukhlantsev, A. A. RADIOTEKHNIKA I ELEKTRONIKA, 1976, 21, 9, 1945.

10,233
CSO: 1870

ELECTRONICS AND ELECTRICAL ENGINEERING

UDC 621.396.96

DETERMINATION OF THE EFFECTIVENESS OF AN EVALUATION-CORRELATION DETECTOR OF SIGNALS WITH UNKNOWN DELAY BY THE METHOD OF STATISTICAL SIMULATION

Moscow RADIOTEKHNIKA I ELEKTRONIKA in Russian No 1, Jan 79 pp 184-185

[Article by M. A. Gostyukhina, submitted 6 May 1977]

[Text] The work [1] gives the results of a theoretical analysis and experimental studies of an evaluation-correlation detector of signals with an unknown delay which uses a follow-up system as a signal delay evaluation unit with constant parameters and astaticism of the first order and compares it with an ordinary gated detector. This article gives the results of the determination of the effectiveness of the above-mentioned detectors with post-detection processing of a group of radio pulses fluctuating simultaneously by the method of statistical digital simulation.

In simulating the detectors, the following assumptions were made. The observation time was fixed and was equal to the length of the group of radio pulses n_0. The input signal was a group of radio pulses of the Gaussian shape. The amplitude distribution law of each pulse was the Rayleigh Law, and the distribution law of the initial phase was uniform in the interval (0.2π). The correlation function of amplitude fluctuations was exponential with the time of correlation exceeding the duration of the group. The frequency characteristic of the UPCh [intermediate frequency amplifier] was coordinated with the spectrum of the input radio pulse. In order to ensure a wide dynamic range, the detectors were provided with an ARU [automatic gain control] system. The detector was a linear inertia-free envelope detector. The post-detector integrator was a synchronous equilibrium adder.

In preparing a digital simulation algorithm of the formation of the input process and its conversion in the UPCh and the detector, the method described in work [2] is used. For the formation of discrete components of the signal and noise, recurring algorithms of the simulation of the realization of random processes are used. The envelope method is used in simulating the conversion of narrow-band processes by the selective circuits of the UPCh. The UPCh is replaced by an optimal filter with a transmission factor on the resonance frequency equal to one and an inertia-free amplifier with the gain factor controlled by means of the ARU which are connected in series. A sequence with a random pulse shape at the input of the ARU system is replaced

with a sequence of δ -functions with a random amplitude proportional to the mean value of the envelope of the signal and noise mixture at the UPCh output within the limits of the gating pulse.

The voltage at the output of the integrator of the evaluation-correlation detector (at the unit transmission coefficients of the coincidence circuit and the integrator) in the n-th period of repetition is expressed in the form of

$$z[n]=\sum_{m=N_0+t_\varepsilon[n]}^{N_0+m_0+t_\varepsilon[n]} V[n,m],$$

where N_0 is the initial position of the reference pulse; m_0 is the number of discrete values of the envelope within the limits of the duration of the reference pulse; $t_\varepsilon[n]$ is the time mismatching of the signal pulse and the gating pulse; $m = t/\Delta t$ is the integral argument (t is the time from the moment of the arrival of the signal pulse; Δt is the quantification spacing); $V[n,m]$ is the envelope of the mixture of the signal with the noise at the UPCh output [2].

The time mismatching is equal to [3]

$$t_\varepsilon[n]=t_\varepsilon[n-1]-\Delta t_M[n],$$

where $\Delta t_M[n]$ is the change in the time position of the gating pulse during the repetition cycle.

The change in the time mismatching is equal to

$$\Delta t_M[n]=k_M z_\Pi[n],$$

where k_M is the transmission coefficient of the time modulator; $z_\Pi[n]$ is change in control voltage during the repetition cycle.

The change in the control voltage at unit transmission coefficients of the coincidence circuits of the time discriminator is proportional to the value of

$$z_\Delta[n]=\frac{1}{N_1}\sum_{m=N_1+t_\varepsilon[n]}^{N_1+m_1+t_\varepsilon[n]} V[n,m]-\frac{1}{N_2}\sum_{m=N_2+t_\varepsilon[n]}^{N_2+m_2+t_\varepsilon[n]} V[n,m].$$

where N_1, N_2 are the initial time positions of "half-strobes"; m_1, m_2 represent the number of discrete values within the limits of "half-strobes".

The voltage at the output of the integrator of an ordinary detector with a fixed time position of the gating pulse is expressed in the form of

$$z'[n]=\sum_{m=Nc}^{N_c+m_0} V[n,m],$$

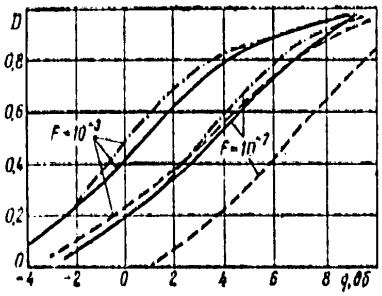

Detection Characteristics: solid curves -- of evaluation-correlation detector at $\varepsilon_0 = 0.5$; dashed curves -- of a detector with gating at $\varepsilon_0 = 0.5$; dash-and-dot curves -- of a detector with gating at $\varepsilon_0 = 0$; $n_0 = 64$.
Key: 1. dB

where N_c is the initial time position of the gating pulse; m_c is the number of discrete values within the limits of the gating pulse.

The characteristics of the detector are determined by means of the method of the Monte-Carlo statistical tests and the extreme statistics method [4]. The simulating algorithms were realized on a digital computer "M-4030". The solving was done with the following values of the parameters: $\Delta t = \tau_и / 6$ ($\tau_и$ -- length of the signal pulse), the ratio of the signal correction time to the repetition cycle is equal to $2n_0$, the transmission coefficient of the ARU feedback circuit is equal to 1000, the ARU time constant is equal to the signal correlation time. The number of realizations was taken to be equal to 100 in determining the detection characteristic by the Monte-Carlo method and equal to 10^6 in determining the dependence of the probability of false alarm F on the detection threshold.

Detection characteristics of the evaluation-correlation detector were determined at the greatest initial time mismatching equal to one-half of the aperture of the discrimination characteristic of the follow-up system. Detection characteristics of the ordinary detector were determined both when the signal and gating pulses completely coincided in time, and when there was the greatest time mismatching ε_0 expressed in the duration of the signal pulse.

The figure shows the dependence of the probability of correct detection D on the signal-noise ratio q for the studied detectors when the duration of the signal pulse is equal to the aperture of the discrimination characteristic in the evaluation-correlation detector and to the duration of the gating pulse in the ordinary detector. As can be seen, the sensitivity of the evaluation-correlation detector in the presence of the initial time mismatching of the signal and gating pulses is higher than the sensitivity of the ordinary detector. For example, at $\varepsilon_0 = 0.5$, $D = 0.5$, $F = 10^{-7}$, the gain in sensitivity is 2.9 dB.

Thus, as a result of statistical digital simulation of post-detector processing of a group of radio pulses fluctuating simultaneously with an unknown delay, it is possible to consider established that the evaluation-correlation processing is more effective than the ordinary processing.

Bibliography

1. Gostyukhina, M. A., and Sosulin, Yu. G. RADIOTEKHNIKA I ELEKTRONIKA, 21, 7, 1434, 1976.

2. Bykov, V. V. "Tsifrovoye modelirovaniye v statisticheskoy radiotekhnike" [Digital Simulation in Statistical Radio Engineering], Izd Sovetskoye radio, 1971.

3. Saybel', A. G. "Osnovy radiolokatsii" [Fundamentals of Radar], Izd Sovetskoye radio, 1961.

4. Likharev, V. A. "Tsifrovyye metody i ustroystva v radiolokatsii" [Digi- Methods and Devices in Radar], Izd Sovetskoye radio, 1973.

10,233
CSO: 1870

ELECTRONICS AND ELECTRICAL ENGINEERING

UDC 621.394.326:621.396.96

OPTIMAL SELECTION OF INTERFERENCE BY DURATION IN A PASSIVE INFRARED SYSTEM

Moscow RADIOTEKHNIKA I ELEKTRONIKA in Russian No 1, Jan 79 pp 186-188

[Article by N. A. Dolinin, submitted 23 June 76]

[Text] Until the present time, receivers with a relatively large time constant have been used in passive radar systems. In this case, when it is necessary to select targets and identify them, it is very advantageous to use a system of selection by duration, because different objects in the infrared range create signals of various lengths at the input of the receiver depending on the angular dimensions of each object due to the scanning of the optical system. The functional diagram of the selector (Figure 1) consists of a photoelectric converter (FEP) whose output is delivered to a linear filter (LF), and then to a threshold device (UPS [device for conversion of signals]) to whose second input a pulse with the duration $T_{\text{п}}$ is sent from a generator of threshold-duration pulses (GIP) which is triggered by the leading edge of the signal from LF. The decision regarding the presence or absence of a useful signal is registered at the output of the UPS circuit. Let us note that FEP is a receiver performing angle scanning in space.

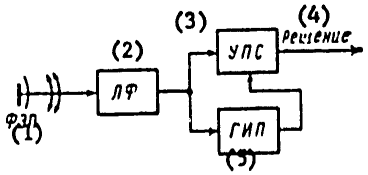

Figure 1

Key: 1. FEP
2. LF
3. UPS
4. Decision
5. GIP

Let us now describe the properties of the useful signal and the complex of interfering effects on the selector. Let us assume that the amplitudes of the useful signal and the interference are much greater than the fluctuations of the internal noise of the FEP, and, consequently, it is possible to select a sufficiently high value of the threshold C ($C \gg 4\sigma_{\text{ш}}$, where $\sigma_{\text{ш}}$ is the root-mean-square value of the internal noise of the FEP) at which false crossing

of the threshold by noise or by fluctuations of the intensity of the useful signal in the gently sloping section of the pulse is practically impossible. Signals at the FEP input from the interference and the targets are considered to be rectangular pulses with a random amplitude x distributed according to the normal law with different average values (A_c, $A_п$) and dispersions (σ_c, $\sigma_п$) for the signal and the interference. We shall have the following signal at the FEP and LF output:

$$s_1(t)=xz(t),$$

where

$$z(t)=\begin{cases}0, & t<0;\\ \dfrac{1-\exp(-\alpha_0 t)}{\alpha_0}, & 0\leqslant t\leqslant T_0;\\ \dfrac{1-\exp(-\alpha_0 T_0)}{\alpha_0}e^{-\alpha_0(t-T_0)}, & t>T_0.\end{cases}$$

Here, α_0 is the FEP inertness index; T_0 is the pulse duration. The duration of the excess of $s_1(t)$ over the threshold C (duration of overshooting) will be defined by the formula

$$\bar{T}_в=t_2-t_1=T_0-\frac{1}{\alpha_0}\ln\left[\frac{C\alpha_0}{(1-\exp(-\alpha_0 T_0))(A_в-C\alpha_0)}\right]. \qquad (1)$$

In the absence of fluctuations of the signal and interference, $x = A_c$ or $A_п$, respectively. Let us find the dispersion of the duration of overshooting with consideration for fluctuations and interference. Let us use Δt_1, Δt_2 to designate the deviations of the moments of crossing from the values of t_1, t_2 corresponding to the mean value of the amplitude and the absence of interference. Then

$$xz(t_1+\Delta t_1)+n(t_1)=C=A_в z(t_1),$$
$$xz(t_2+\Delta t_2)+n(t_2)=C=A_в z(t_2),$$

where $n(t_1)$ and $n(t_2)$ represent the FEP self-noise at the moments of time t_1 and t_2 which, as it is always accepted in [1], we shall consider to be white Gaussian noise in the reception band. Expanding $z(t_1+\Delta t_1)$ and $z(t_2+\Delta t_2)$ in a Taylor series, we shall obtain the following from the last equalities:

$$\Delta T_в=\Delta t_2-\Delta t_1=\frac{x-A_в}{A_в}\left(\frac{z(t_1)}{z'(t_1)}-\frac{z(t_2)}{z'(t_2)}\right)+\frac{n(t_2)}{A_в z'(t_2)}+\frac{n(t_1)}{A_в z'(t_1)},$$

from which the dispersion of the duration of the overshooting will be defined by the formula

$$\sigma_в^2=\frac{\sigma_в^2}{A_в^2}\left(\frac{z(t_1)}{z'(t_1)}-\frac{z(t_2)}{z'(t_2)}\right)^2+\frac{\sigma_ш^2}{A_в^2 z'^2(t_1)}+\frac{\sigma_ш^2}{A_в^2 z'^2(t_1)}= \qquad (2)$$
$$=\frac{\sigma_в^2}{(A_в-C\alpha_0)^2\alpha_0^2}+\sigma_ш^2\left(\frac{1}{(A_в-C\alpha_0)^2}+\frac{1}{(C\alpha_0)^2}\right).$$

where $\sigma_{ш}$ 2 is the dispersion of the FEP self-noise; $\sigma_{п}$ 2 is the dispersion of the fluctuations of the interference pulse. Due to the fact that the ratio of the signal to the noise in the selection system is great, the duration of the overshooting can be considered to be random values distributed according to the normal law [2] with a mean value of $\overline{T}_{в}$ and the dispersion of $\sigma_{в}$2. It is easy to calculate the probabilities of errors of the first and second kinds. By writing the expression for average risk in the form of

$$R=\gamma C_0\alpha+(1-\gamma)C_1\beta,$$

where α, β are the probabilities of errors of the first and second kinds, respectively; γ, $(1-\gamma)$ are the a priori probabilities of the appearance of errors of the first and second kinds, respectively; C_0, C_1 are the cost functions for the errors of the first and second kinds, respectively, it is possible to select the parameters of the selector in such a way that the average risk would be minimal. Finding a derivative of R by the threshold $\partial R/\partial C$ and threshold duration $T_{п}$ - $\partial R/\partial T_{п}$ and equating them to zero, we shall find the optimal values of C_{opt}, T_{opt}.

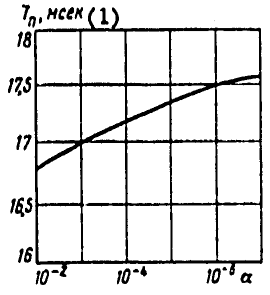

Figure 2 ($T_{в}$=16,1; $\sigma_{в}$=0,3)
Key: 1. msec

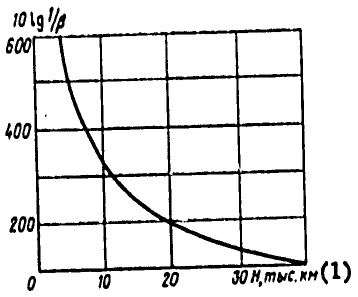

Figure 3 ($\alpha=10^{-4}$.
Key: 1. thousand kilometers

Let us illustrate these results with an example. Let us examine the infrared self-radiation of the earth in the band of 9-12 micrometers as the target which we have to select from the interference. In this case, the interference will be the radiation of the sun, moon, and other space objects within the same band. The slow-responding detector will be a standard bolometer with the inertia index α_0 = 1000/3 [1/sec], the band F_0 = 160 Hz, $\sigma_{ш}$ = $\sqrt{NF}$ = 0.3 microvolt; the scanning system covers a 120 degree angle and is based on standard scanning motors; it scans this angle in 150 msec. Then, for the sun, T_0 = 5 msec, because its angle of rotation is 4 degrees. Works [3, 4] give experimental data for the infrared self-radiation of the earch within a band of 9-12 micrometers. Let us assume that $\sigma_{п}$ /$A_{п}$ = $\sigma_{с}/A_{с}$ = 16/300. The fact that we took identical energy characteristics for the signal and the interference does not worsen the quality of the operation of the selection system. We have $A_{п}/\alpha_0\cdot(1-\exp(-\alpha_0 T_0))$ = 60 microvolts, and C_{opt} = 4 microvolts; in this case, we obtain $T_{в}$ = 16.1 msec, $\sigma_{в}$ = 0.3 msec. Having been given the values of the probabilities of the first kind α, we find $T_{п}$.

The curve of function $T_п = f(\alpha)$ is given in Figure 2. Substituting the appropriate constants in expressions (1) and (2), we find that $\sigma_{ВС} = 0,28$ msec, $\overline{T}_{ВС} = (T_о + 8,32)$ msec. In this case, $T_о = f(H)$, where H is the flight altitude of the ISZ [artificial earth satellite]. If the scanning is done along the diameter of the earth, then

$$T_0 = 2,5 \arcsin \frac{R}{R+H} \text{ [мсек]},$$

where R is the radius of the earth; H is the flight altitude of the ISZ. Using the formula for the probability of a second-kind error

$$\beta = \Phi\left(\frac{T_п - \overline{T}_{вс}}{\sigma_{вс}}\right),$$

where $\Phi(x) = (1/\sqrt{2\pi}) \int_{-\infty}^{x} \exp(-t^2/2)\,dt$ is the probability integral, we compute the probability of a second-kind error for $\alpha = 10^{-4}$ and various H. This curve is shown in Figure 3. We can see that the probability of confusing the interference with the useful signal is negligibly small.

Bibliography

1. Rays, S. O. "Theory of Fluctuation Noise" in collection "Teoriya peredachi elektricheskikh signalov pri nalichii pomekh" [Theory of the Transmission of Electric Signals in the Presence of Interference], edited by N. A. Zheleznov, IL [Foreign Literature Publishing House], 1953.

2. Tikhonov, V. I. "Vybrosy sluchaynykh protsessov" [Overshooting of Random Processes], Izd Sovetskoye radio, 1969.

3. Dolinin, N. A. IZV VUZOV MVSSO SSSR [Vuz Proceedings of the USSR Ministry of Higher and Secondary Specialized Education] (Radio Electronics), 20, 11, 82, 1977.

4. Boldarev, V. G. METROLOGIYA I GIDROLOGIYA [Metrology and Hydrology], 10, 23, 1970.

10,233
CSO: 1870

ELECTRONICS AND ELECTRICAL ENGINEERING

UDC 621.396.962.25

TOWARD THE EVALUATION OF THE ACCURACY OF ECHOLOCATION RANGE MEASUREMENTS BY MEANS OF FREQUENCY-MODULATED SIGNALS

Moscow RADIOTEKHNIKA I ELEKTRONIKA in Russian No 1, Jan 79 pp 188-190

[Article by V. I. Aleshchenko, A. A. Belousov, Yu. I. Zdorovyy, and V. V. Ustimenko, submitted 20 Dec 1976]

[Text] The works [1,2] mention a property of LChM [linearly frequency modulated]-signals which makes it possible to "predict" the range of a uniformly moving object and to minimize its measurement error (i.e., to reduce it to an error obtained for motionless objects or objects moving at a known rate of speed). It is also mentioned (see, for example, [1]) that, in order to realize this property, it is necessary to use radars "designed on other principles differing from the principles of a system... with a classical circuit for obtaining evaluations of parameters" ([1], page 344).

The purpose of this article is to show that, firstly, this property follows directly from the classical theory of radio engineering measurements of the parameters of a moving target and, secondly, that it is characteristic not only of LChM, but also other frequency modulation laws having a high value of the frequency-time coupling coefficient.

Let us write the equation of motion of the target in the form

$$r(t)=r_0-v(t-t_0), \tag{1}$$

where r(t) is the distance to the target changing with time; r_0 is the distance to the target at the moment of the reflection of the leading edge of the signal t_0; v is the speed of the uniform motion of the target.

The values given in [1, 3] are taken as evaluations of the distance $\hat{r}_0$ and speed $\hat{v}$:

$$\hat{r}_0=\frac{c\hat{\tau}}{2},\quad \hat{v}=\frac{\hat{\varphi}c}{2f_0}, \tag{2}$$

where $\hat{\tau}$ and $\hat{\varphi}$ are the evaluations of the time and frequency shifts of the signal, repectively.

Then, at a certain moment of time T_x (counted from the moment of the reflection of the leading edge of the signal) the evaluation of the distance can be obtained as

$$\hat{r}(T_x) = r_0 - \hat{v}T_x. \tag{3}$$

Let us find the dispersion of this evaluation:

$$D(r(T_x)) = \frac{c^2}{4}\left(\sigma_\tau^2 + \sigma_\varphi^2 \frac{T_x^2}{f_0^2} - 2\sigma_\tau\sigma_\varphi\rho\frac{T_x}{f_0}\right), \tag{4}$$

where σ_τ^2 and σ_φ^2 are the dispersions; ρ is the coefficient of cross-correlation of the evaluations of the time τ and frequency φ shifts of the signal being received; f_0 is the carrier frequency of the radio signal.

Let us designate in expression (4) $T_x/f_0 = x$ and study $D(\hat{r}(T_x))$ for the extremum. We shall obtain the following equation

$$\frac{\partial D(\hat{r}(T_x))}{\partial x} = \frac{c^2}{4}(2x\sigma_\varphi^2 - 2\sigma_\tau\sigma_\varphi\rho) = 0,$$

whence

$$x = \frac{\sigma_\tau}{\sigma_\varphi}\rho, \quad T_x = \frac{\sigma_\tau}{\sigma_\varphi}\rho f_0; \tag{5}$$

in which case

$$D(\hat{r}(T_x)) = \frac{c^2}{4}\sigma_\tau^2(1-\rho^2) = \frac{c^2}{4}\sigma^2_{\tau\,\min}, \tag{6}$$

where $\sigma^2_{\tau\,\min}$ is the minimum obtainable value of dispersion in the evaluation of the time delay.

Thus, relating the value of distance which is being measured to the moment of time T_x defined by relation (5), it is possible to obtain a minimal value of the measurement error, the same as for a motionless object or an object moving at a known rate of speed.

For signals for which the measurement errors of the frequency and time shifts are not correlated ($\rho = 0$), the most accurate evaluation of distance corresponds to $T_x = 0$, i.e., to the true moment of reflection. The evaluation of the distance for the moments of time T different from T = 0 by means of such signals will have a greater dispersion equal to

$$D(\hat{r}(T)) = \frac{c^2}{4}\left(\sigma_\tau^2 + \sigma_\varphi^2\frac{T^2}{f_0^2}\right). \tag{7}$$

Kind of Signals	ρ	T_x/f_0	K_r	Remarks
LChM (for all kinds of envelopes)	1	$T/\Delta f$	5500	For $T\Delta f = 100$ (Δf -- signal band width; T -- duration)
Nonlinear FM				
1) cosine power spectrum, envelope rect (t/T)	0.994	$1.32\ T/\Delta f$	100	
2) cosine-square power spectrum, envelope rect (t/T)	0.987	$1.58\ T/\Delta f$	40	
3) power spectrum described by the Hemming function, envelope rect (t/T)	0.974	$1.46\ T/\Delta f$	17.7	
4) parabolic one-sided FM, envelope rect (t/T)	0.968	$0.94\ T/\Delta f$	16	

For signals for which $\rho < 0$ (particularly, with a decreasing FM law) $T_x < 0$, i.e., $r(T_x)$ refers to the moment of time preceding the moment of reflection, and for signals for which $\rho > 0$ (particularly with an increasing FM law), $T_x > 0$, i.e., the property of distance "prediction" mentioned in [1] shows itself.

The table gives the values of T_x/f_0 calculated for various kinds of signals and the corresponding coefficients of the decrease of the dispersion of distance evaluation

$$K_r = \frac{D(r_0)}{D(\hat{r}(T_x))}.$$

Thus, for any laws of frequency modulation it is possible to obtain minimal values of the dispersion in the evaluations of the distance to an object moving at a steady radial speed.

In conclusion, let us note that in formula (3) it is possible to use an evaluation of distance r_0 corresponding to any velocity channel (if the echo signal does not go beyond the limits of the area of strong correlation), including the channel of $\hat{v} = 0$. In the latter case, the evaluation algorithm of $r(T_x)$ amounts simply to finding $\hat{r}_0$.

Bibliography

1. Kuk, Ch., and Bernfel'd, M. "Radiolokatsionnyye signaly" [Radar Signals], Izd Sovetskoye radio, 1971.

2. Rikhachek, TIIER, 53, 475, 1965.

3. Varakin, L. Ye. "Teoriya slozhnykh signalov" [Theory of Compound Signals], Izd Sovetskoye radio, 1970.

10,233
CSO: 1870

ELECTRONICS AND ELECTRICAL ENGINEERING

UDC 621.376

LINEAR REGENERATOR FABRICATED WITH HYBRID INTEGRATED TECHNOLOGY

Moscow ELEKTROSVYAZ' in Russian No 1, Jan 79 pp 33-36

[Article by A. M. Mekkel', Yu. V. Minikov, E. V. Novikov, E. N. Rubinshteyn and E. P. Savost'yanov: "A Linear Regenerator of Hybrid Integrated Design for the Speed 8448 Mbit/sec"]

[Text] The secondary digital transmission system (TsSP) IKM-120 (1) is implemented on a modern component base: standard integrated microcircuits (IMS), transistors and mounted electronic components (ERE) with printed single-layer wiring and bunched connections between terminals. Further improvement of the TsSP equipment can only be done with difficulty without the extensive incorporation of hybrid integrated (GI) components.

The most important and highest-volume single-type unit for cable TsSP's is the linear regenerator (LR). The degree of its development depends greatly on the advantages and outlook for the whole developed system. Because of this, implementing an LR in hybrid integrated design is of particular interest. Experimental development is being done on a linear regenerator for the TsSP for the speed 8448 Mbit/sec in microdesign. Several linear microregenerators (LMR) have been fabricated and tested whose size and weight are 70 to 75 times smaller than LR's constructed of mounted discrete components and whose reliability is higher by a factor of one to two.

Considerations in Fabricating a Linear Regenerator

The LMR prototype is still in the developmental stage and it is LR's of discrete components that are considered factors determining the potential for its fabrication in hybrid integrated design: the difficulty of implementing inductance and several other circuit quantities with hybrid integrated technology, the availability of mass-produced "caseless" transistors and other active components and the development and production of new radio components such as varicaps and transformers.

It should be noted that the listed new components have been developed with the potential for their application in LMR's taken into account. Thus, caseless "ultrasharp" type KV118A varicaps have been structurally implemented

which are similar to caseless transistors. Serially developed TIIl-255 and TIIl-256 miniature transistors are fabricated in a beryllium ceramic package with ball leads and symmetrical windings on a flat permalloy substrate.

Regardless of the overall theoretical and functional identity of the LMR and its prototype of discrete components, they have significant differences. The nature of these differences is manifested by a simple comparison of the number and designation of the complete parts set used for the LR and the component base of the LMR.

Table

Circuit Components	Number of Components in LR	LMR
Active Components	50	85
Capacitors	85	87
Resistors	100	170
Inductors	3	—
Microcircuits	4	—
Total	250	365

An increase in the number of components, especially the active ones, is associated with the specific nature of hybrid integrated technology for fabricating LMR's while the individual regenerator terminals are more easily fabricated of circuits with active components and not by means of circuits containing inductance, large value capacitors and so on. However, an increase in the number of components does not result in a reduction of the reliability indicators but, due to the use of hybrid integrated technology, the size and weight of the parts are reduced considerably.

Construction Characteristics of Some LMR Terminals

An LMR is a device consisting of two large-scale, linear-pulse hybrid integrated circuits with a small degree of integration. The schematic diagram of an LMR (fig. 1) differs little in principle from familiar circuits of conventional linear regenerators (2,3). An LMR consists of four main blocks: a tuned discriminating amplifier RKU, a regeneration unit UR, time delay circuits VVI and a regulated power supply SIP. The LMR may be arbitrarily divided into an analog and a digital part.

The RKU is part of the analog section consisting of an amplifier US with sloping automatic gain control accomplished by detectors D, a coincidence circuit SS with floating threshold (relative to the reference voltage U_{on}), a d-c amplifier UPT and control components UE. The distinguishing characteristic of the digital part — the VVI and the UR — is the extensive use of matched pairs of p-n-p and n-p-n transistors in the circuits of these units.

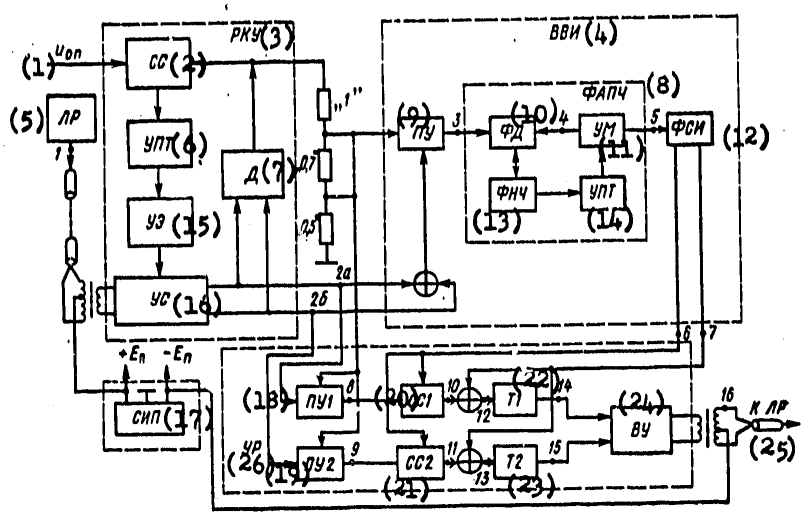

Figure 1

Key:

1. U_{on} -- reference voltage
2. SS -- coincidence circuit
3. RKU -- tuned discriminating amplifier
4. VVI -- time delay circuit
5. LR -- linear regenerator
6. UPT -- d-c amplifier
7. D -- detector
8. FAPCh -- phased automatic frequency control unit
9. PU -- threshold device
10. FD -- phase detector
11. UM -- controlled multivibrator
12. FSI -- strobe pulse shaper
13. FNCh -- low-frequency filter
14. UPT -- d-c amplifier
15. UE -- control component
16. US -- amplifier
17. SIP -- regulated power supply
18. PU1 -- threshold device 1
19. PU2 -- threshold device 2
20. SS1 -- coincidence circuit 1
21. SS2 -- coincidence circuit 2
22. T1 -- Schmitt trigger 1
23. T2 -- Schmitt trigger 2
24. VU -- output unit
25. K LR -- linear regenerator terminal
26. UR -- regeneration unit

The RKU circuit is divided into variable and fixed discriminators and is constructed of standard RC components. The variable discriminator matches the cable attenuation in a defined frequency band and the amplifier is automatically retuned to compensate for the electrical parameters of the regeneration section resulting from the cable attenuation distribution in these sections, the effect of temperature fluctuation and so on. A type KV118A varicap with ultrasharp variation of the capacitance by the bias voltage, that is with reverse bias of the doping density, is chosen for the tuned control components of the variable discriminator. Because of this, the required variation in the capacitance is achieved with small variations in the bias voltage.

The fixed discriminator makes it possible to obtain optimum low-frequency and high-frequency "skirts" for the RKU's amplitude and frequency characteristic. The main RKU circuit is identical to the prototype implemented of discrete components (4).

The VVI consists of a threshold device PU, a phased automatic frequency control unit FAPCh and a strobe pulse shaper FSI. The FAPCh includes a controlled multivibrator UM, a phase detector FD, a low-frequency filter FNCh and a d-c amplifier UPT. A characteristic of the VVI circuit is the presence of the FAPCh where a controlled multivibrator is used as an autooscillation generator with phased automatic frequency control. As a result, resonance circuits not technologically adviseable for GI fabrication were excluded.

The VVI threshold unit is an unsaturated Schmitt trigger. A pulse discriminated in the RKU and applied to the PU input has a bell-shaped form; its duration at the 0.5 amplitude level is about 60 nanoseconds. The trigger has a floating response threshold on each of two inputs which ensures invariability of the response level of the PU with amplitude oscillations of the input pulses. When the algebraic sum of the constant negative voltage of the detector FD and the instantaneous voltage of the signal at the trigger input reaches the level of the response threshold, the trigger flip-flops. In this case, one of the input transistors of the Pu is off and the second one is on, that is the Schmitt trigger circuit operates as a conventional trigger but with switching of the input triggers.

The phase detector of the FAPCh is implemented on a balanced circuit. An FNCh is included in each leg of the FD for quenching an in-phase composite output signal. The UPT coordinates the FNCh output with the multivibrator and obtains the required gain.

Matched pairs of transistors of different conductances are used in the controlled multivibrator circuit. Frequency control of the multivibrator is accomplished by the UPT by varying the bias voltage on the transistor bases.

The regeneration unit is composed of a threshold device for each of the two channels PU1 and PU2, the coincidence circuits SS1 and SS2, the triggers T1 and T2 and the output unit VU. The design of the VU should be noted. It consists of two legs, each of which is a dual-cascade emitter follower with

in-phase output depending on the switching of the primary winding of the output transformer. Paired p-n-p and n-p-n transistors with increased capacitance are used in the output cascades.

Diagrams illustrating the operating principle of the individual LMR circuit terminals are shown in figure 2. The line numbers correspond to the points in figure 1.

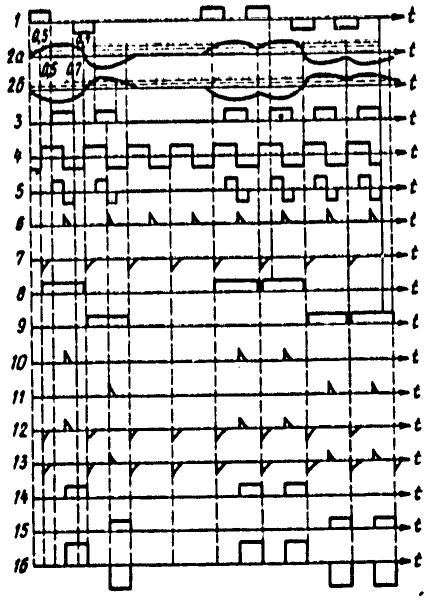

Figure 2

LMR Design and Fabrication Process

The technological cycle of LMR fabrication involves more than 30 basic operations including monitoring the electrical parameters. The fabrication sequence is standard for hybrid integrated technology described, for example, in (5,6). Listed below are the main design specifications incorporated in LMR development. The dimensions of the regenerator package should be minimal and comply with GOST 17467-72. The package design should provide for normal operating conditions (particularly provision for heat dissipation) and also storage and handling. The LMR design should provide for interchangeability of the generator itself and as far as possible for the repairability of its individual terminals at the fabrication stage.

These specifications govern the regenerator design in the form of two identical packages with the dimensions 60 X 60 X 7.5 mm (fig. 3a,b) in each of which are housed the analog or digital part of the LMR. The package includes

a certain number of functionally complete blocks, "chips" 6 (see fig. 3b) positioned on two sides of a ceramic substrate with multilayered separation. The heat sinks 3 make contact in three places with the brass end shield of the package. On the perimeter of the package is enclosed a plastic frame 4 fabricated by pressure-molding the terminal 2 of the package and the heat sink with a special molding powder. The terminals 2 on the package are flat, tinplated and produced from 3 mm thick brass.

The chips are fabricated in a plastic package on an inert glass substrate in contact with the heat sinks. The active components in the chips are fastened to the glass substrate with a special glue.

The net cost of an LMR even at the research and development stage seems to be on the same order as the prototype of discrete components.

Brief Electrical Specifications of the LMR

Expansion of "eye-curve" at RKU output with maximum length of regeneration section corresponding to 70 dB attenuation at half-power frequency according to laboratory measurement data, %	80
Limits of tuning of automatic RKU discrimination at half-power frequency, dB	±15
Output pulse parameters:	
Amplitude, volts	±3
Duration, nanoseconds	59
Edge width, watts	not worse than 8
Reliability of regeneration according to laboratory measurement data	not worse than 10^{-9}
Power supply, volts	±6
Input, watts	2

Conclusion

LMR development is the first stage in developing a complete, functionally complex, linear-pulse LR, more highly developed by a factor of one or two than an LR of discrete components. The weight and size of the regenerator are reduced considerably. It can be anticipated that with mass production of LMR's using hybrid integrated technology, the density of component integration will be increased, the individual blocks (chips) of regenerators for various frequencies of hierarchical systems will be unified and the net cost of their production will be lowered.

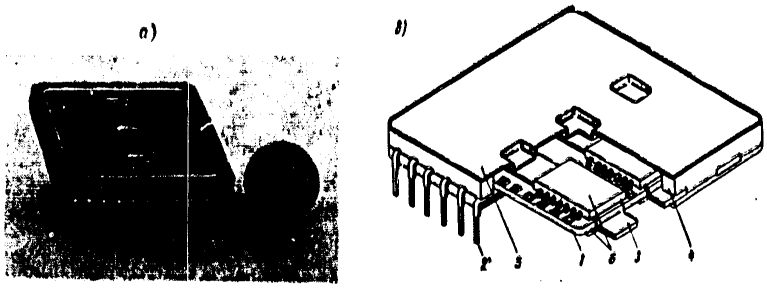

Figure 3a and b

Future improvement of the LMR fabrication process is expected as a result of reducing the number of fabrication operations by using, for instance, MDP structures, complementary (mutually completing) transistors and so on. This will make it possible to increase significantly the degree of LMR integration, to lower the input power and to reduce their size and the units in the hybrid integrated design for TsSP's at the speed 8448 Mbit/sec. Laboratory research and experiments on existing TsSP series has shown that the electrical specifications of LMR's coincide with the specifications of the prototype and the estimated and tested LMR reliability with the mass. A more distant prospect is the development of monolithic, multipurpose for various hierarchical systems, functional linear regenerator units and after that multipurpose LMR's with plug-in frequency blocks (components) for each actual transmission system.

BIBLIOGRAPHY

1. Lopushnyan, Yu. G. and others. "A Device for the Secondary Digital Transmission System IKM-120," ELEKTROSVYAZ', No 12, 1977.

2. Abolitsa, I. A. (ed). "Mnogokanal'naya svyaz'" [Multichannel Communication], Moscow, Svyaz', 1971.

3. Ketermoul, K. V. "Printsipy impul'sno-kodovoy Modulyatsii" [Principles of Pulse-Code Modulation], Moscow, Svyaz', 1974.

4. Strongin, R. G. and others. "On optimization of the Specifications of a Linear Regenerator Discriminator for a Cable TsSP," in "Trudy TsNIIS" [TsNIIS Works], Issue 1, 1978.

5. Shtern, L. "Osnovy proyektirovaniya integral'nykh skhem" [Foundations of Integrated Circuit Design], Moscow, Energiya, 1973.

6. Medlend, G. R. and others. "Integral'nyye skhemy. Osnovy proyektirovaniya i tekhnologii." [Integrated Circuits. Foundations of Design and Engineering], Moscow, Sovetskoye Radio, 1970.

8945
CSO: 1870

ELECTRONICS AND ELECTRICAL ENGINEERING

UDC 621.391

INTERFERENCE IMMUNITY IN COMMUNICATION SYSTEMS

Moscow ELEKTROSVYAZ' in Russian No 1, Jan 79 pp 42-47

[Article by L. E. Varakin in the column "Systems and Communication Networks": "Interference Immunity in Communication Systems with Noise-type Signals"]

[Text] Introduction. During information transmission from a great distance, in some cases the power of preformed interference at the receiver input and in its bandwidth may increase the signal power considerably (by 20 to 50 dB). Preventing such high-power interference always has been and remains a serious engineering problem in communication systems. Solving this problem has a great importance even now since the number of different electronic devices is growing and the frequency bands remain the same.

Noise-type or complex signals and matched filters or correlators (1) may be used to prevent high-power preformed interference. This method is used successfully in various radio equipment systems including communication systems. Those signals whose base is the product of the spectrum width F at duration T are also called noise-type signals:

$$B = FT \gg 1. \qquad (1)$$

The interference immunity of a discrete information receiver with a matched filter (or correlator) is determined completely by the signal-to-noise ratio at the filter output:

$$q_n^2 = 2E/N_n, \qquad (2)$$

where E is the signal energy and N_Π is the spectral density of the noise power at the receiver input. If the average noise power P_Π is limited and there is interference in the frequency band of the signal, then $N_\Pi = P_\Pi/F$. Since the signal energy $E = P_C T$, replacing E and N_Π in (2) we obtain

$$q_n^2 = \frac{P_c}{P_n} 2B. \qquad (3)$$

For example, assume that (P_C/P_Π) dB = - 40 dB and it is necessary to have q^2_{db} = 13 dB at the output. In this case, noise-type signals with the base

$B_{(dB)} = 50$ dB or $B = 10^5$ must be used. As power calculations show, in contemporary communication systems with noise-type signals, $B = 10^4$ to 10^6.

On the other hand, the interference immunity of an optimum receiver exposed to noise with a limited spectral power density does not depend on the form of the signal and its base but is determined only by its energy according to (2). For this reason, interference whose average power is limited will be considered in what follows.

First, formula (3) was obtained for noise interference with limited average power but it also holds true for other interference including narrow-band, pulsed and structured interference (interference having the same structure as the useful signal). With structured interference is classified intrasystem, retransmitted and simulated interference.

For some time past, preventing preformed interference in communication systems has been done on broader terms. The working ability of a communication system must be ensured during concurrent exposure to a group of interferences, such as that of the receiver's internal noise, high-power noise, pulsed and intrasystem structured interference and so on.

In a large portion of the known studies, the combined effect of noise and narrow-band interference is investigated. Here, band-elimination filters which suppress inherent narrow-band interference should be part of the optimum receiver. If the spectral densities of narrow-band and noise interference are added together, then the optimum reception is reduced to reception of a signal in a background of correlated interference (noise with an erratic spectral power density). This problem was solved by V. A. Kotel'nikov in 1947 (4). He showed that the optimum receiver should contain a "whitewash" filter whose transmission factor is smaller the larger the spectral density of the interference. The main point is that the "whitewash" filter is depended on for all optimum methods of signal reception in a background of noise and narrow-band interference with known parameters for the interference and of all self-adjusting reception methods when the parameters of the narrow-band interference are unknown.

The prevention of pulsed noise is also the subject of many studies but in most cases the ShOU (wide band-clipper-narrow-band) circuit proposed by A. N. Shchukin in 1946 is used. The ShOU circuit directly or in modified form is a part of receivers which receive signals in a background of noise and pulsed interference. The clipper eliminates pulsed noise but reduces the signal-to-noise ratio of the interference. The combined use of band-elimination (band) filters and ShOU circuits constitutes the basis of a number of empirical methods for preventing narrow-band, pulsed, noise and structured interference (6,7 and others).

In addition to empirical methods of reception, there are general methods of synthesizing self-adjusting receivers (8,9 and others). The characteristics of a self-adjusting receiver should depend to some extent on the parameters of the noise distribution functions. However, existing methods of synthesizing

self-adjusting receivers still have not given a conclusive answer to the problem of how to construct a receiver for communication systems with noise-type signals and what characteristics it will display, although the general structure of such receivers is known (10), namely that it is a multichannel receiver in which the analyzer measures the interference level in the channels and varies their transmission factor. In study (11) a quasioptimum self-adjusting receiver for a noise-type signal in the form of a phase-modulated signal which either switches the channel over to the output or switches it off is examined. In communication systems, optimum and quasioptimum self-adjusting receivers have already been in use for a long time in space-diversity reception (12 and others). However, space-diversity reception is accomplished with a small number of channels and contemporary noise-type signal receivers are characterized by a large number of channels which is responsible for a number of their characteristics.

For this reason, research on interference immunity of communication systems with noise-type signals is an urgent problem which is confirmed by the conclusion of a book published in our country (13) and by a special magazine issue published abroad (14).

Thus, to prevent high-power interference it is necessary to use noise-type signals with large bases and to accomplish reception by means of receivers which are linear with matched filters, nonlinear and self-adjusting. The purpose of this study is to determine the potential interference immunity of a self-adjusting receiver for noise-type signals and to compare it with linear and nonlinear receivers.

Basic Calculations. To investigate the effect of a set of interferences on a useful signal, let us consider the energy distribution of the signal and interference on the frequency and time plane (fig. 1) where a reference base rectangle is selected whose square equals the base of the useful signal. The carrier frequency of the signal is labeled f_0. The base rectangle is subdivided into frequency and time elements (ChVE) using M for the frequency (horizontal) and M for the time (vertical) bands. The duration and width of the ChVE spectrum equal $T_e = T/M$ and $F_e = F/M$ respectively. The cross-hatches signify those ChVE's in which the energy of random structured interference is distributed in the form of a discrete frequency signal (15). The energy distribution of narrow-band interference with the spectrum width f_b is represented by the wide horizontal line and the wide vertical line represents the energy distribution of pulsed interference with the duration T_p. The energy distribution of the useful signal in the base rectangle depends on the type of signal.

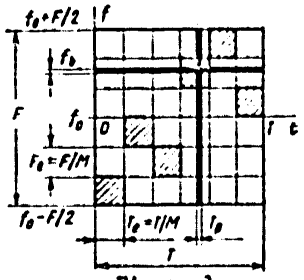

Figure 1

In figure 2 is shown the energy distribution of four of the most common types of noise-type signals (15, 16): a -- for a phase-modulated signal consisting of N pulses of duration $T_0 = T/N$ (the energy of each pulse is distributed in a vertical band of width F and duration T_0; b -- for a discrete frequency (DCh) signal consisting of L pulses each of which is distributed in the rectangle with sides T_0 and F_0; c -- for a discrete composite frequency signal with frequency modulation (DSCh-ChM) consisting of L pulses which are grouped in K ChVE's with duration T'_e and spectrum width F'_e (16); d -- for a discrete composite frequency signal with phase modulation (DSCh-FM) which consists of K ChVE's with duration T'_e and spectrum width F'_e and each ChVE contains S radio pulses. The energy of an individual radio pulse is located in the vertical band with sides T_0 and F'_e. Comparative data on the signals under consideration is given in table 1.

Table 1

Type of signal	Number of elementary pulses	Number of ChVE's (length of external code)	Number of pulses in ChVE (length of internal code)	Signal base
FM	N	--	--	N
DCh	L	L	--	L^2
DCh-ChM	L	K	L/K	$L^2=K^2\left(\frac{L}{K}\right)^2$
DCh-FM	KS	K	S	K^2S

A self-adjusting receiver uses information on the signal energy distribution in a frequency and time plane. Assume that there is coherent reception r of orthogonal signals. The receiver will contain r filters $\phi_1,\ldots,\phi_r$ (fig. 3) whose voltages across the outputs act as a resolver RU. The latter adopts a solution at the moment of signal termination. With noise interference, the filter should be matched; with random interference it should be self-adjusting.

A standard circuit for a self-adjusting filter (one of r) is shown is figure 4. It consists of Q channels in each of which there are a component matched filter, delay lines and an amplifier with variable gain factor. The matched filters $S\phi_1,\ldots,S\phi_2$ are determined for the ChVE of the signal and the delay lines compensate for time lag of the ChVE's, that is at the moment of signal termination ($t = T$) the peaks of the autocorrelation functions ($AK\phi$) of the elements coincide and there is coherent accumulation. The channel analyzer AK produces an analysis of the voltage records across the outputs of the $S\phi$'s at the moment of signal termination and establishes the gain factors, that is the weights with which the voltages across the filter outputs enter into the overall total, according to the adopted algorithm.

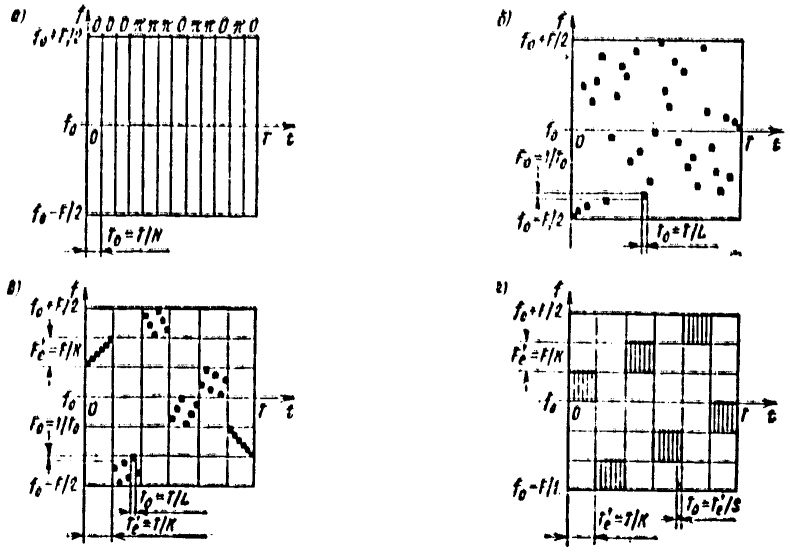

Figure 2

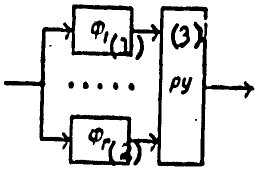

Figure 3

Key:
1. Φ_1 — filter 1
2. Φ_r^1 — filter 2
3. RU — resolver

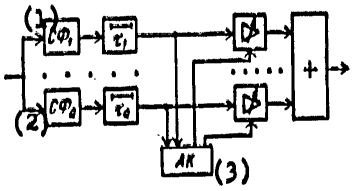

Figure 4

Key:
1. $S\phi_1$ -- matched filter 1
2. $S\phi_2$ -- matched filter 2
3. АК -- channel analyzer

The interference immunity of a self-adjusting receiver exposed to interference whose energy is concentrated in some way in the individual ChVE's of the base rectangle (see fig. 1) depends on the number of coincidences of the ChVE's of the signal and noise and on the signal-to-noise ratio at the outputs of the $S\phi$'s (the component signal-to-noise ratio). To determine the number of coincidences, it is necessary to analyze those ChVE's in which the signal energy is concentrated. The number A of the analyzed ChVE's for the signal types being considered is given in table 2 along with the base of the component matched filters.

Table 2

Type of signal	Number of ChVE's analyzed	Base of component matched filter
FM	M^2	N/M^2
DCh	$M \leq A \leq M^2$	$\geq L^2/M^2$
DSCh-ChM	M	L^2/M
DSCh-FM	M	S

For DSCh-ChM's and DSCh-FM's of signals, it is assumed that K = M. The number of ChVE's analyzed is determined by superimposing figure 1 on figure 2a-d. It is apparent from table 2 that the lowest number of analyzed ChVE's is required for signals of DSCh-ChM's and DSCh-FM's.

In table 3 are shown the values of the number of coincidences of narrow-band (or pulsed) and structured interference with all the considered signals. In determining the number of coincidences, it is assumed that only one interference is active while structured interference belongs to the class of signals under consideration. Correlation characteristics of signal FM's are determined by intercorrelation functions ($VK\phi$) and not by the number of coincidences. It is known that the root-mean-square value of the $VK\phi$ of the signal FM is equal to $1/\sqrt{N} = 1/M$, which coincides with the mean value of the relative number of coincidences for the DCh, DSCh-ChM and DSCh-FM of the signals (17).

Table 3

Type of signal	Narrow-band pulsed interference		Structured interference	
	Number of coincidences	Relative no. of coincidences	Average no. of coincidences	Average value of relative no. of coincidences
FM	M	1/M	--	--
DCh	M	1/M	1	1/M
DSCh-ChM	1	1/M	1	1/M
DSCh-FM	1	1/M	1	1/M

It follows from table 3 that the noise-type signals under consideration have identical characteristics from the point of view of the number of ChVE coincidences of signal and interference, i.e. they do not have basic advantages relative to one another. However, the DSCh-ChM's and DSCh-FM's of signals make it possible to have a smaller number of channels in the self-adjusting receiver. For this reason, hereinafter the formulas are developed for DSCh-ChM's and DSCh-FM's of signals. But the results obtained will be true for any noise-type signals since definitive formulas depend on the relative number of "affected" ChVE's.

Note that the method based on determining the number of "affected" ChVE's and the component signal-to-noise ratio is true for interference not correlated with noise-type signals.

We determine the component signal-to-noise ratio at the output of a random component matched filter in the following manner. Assume that signal reception is always accomplished in a background of the receiver's own noise which is a standard random process with uniform spectral density of power N_0.

Assuming that the number of ChVE's equals M, the energy of the ChVE's is $E_0 = P_c T/M$. The component signal-to-noise ratio at the output of the component matched filter exposed to noise alone is

$$q_0^2 = 2E_0/N_0. \qquad (4)$$

Let us suppose that the preformed interference coincides with m of the ChVE's and, independently of the number of affected components, the power is P_Π = const. In this case, the interference power entering one component equals P_Π/M and the cumulative interference and noise power is $(P_\Pi/M) + P_m$. With this kind of hypothesis, the component signal-to-noise ratio exposed to interference and noise is

$$q_m^2 = \frac{2P_c}{P_a} mB_0 \left(1 + \frac{2P_c}{P_a} \frac{mMB_0}{q_{max}^2}\right)^{-1}, \qquad (5)$$

where $B_0 = F_e T_e$ is the ChVE base and $q^2_{max} = Mq^2_0 = 2E/N_0$ is the maximum signal-to-noise ratio equal to the signal-to-noise ratio at the output of the coherent accumulator, the accumulator (fig. 4) exposed to inherent noise.

Formula (5) like (3) is true for noise, narrow-band and pulsed interference (2,3): for noise interference with uniform spectral density of interference in the limits of the band of the frequency component; for narrow-band interference with a constant in the limits of the frequency band F_0 ratio of the transmission factor for the component matched filter and for pulsed interference with $T_p \approx 1/F$.

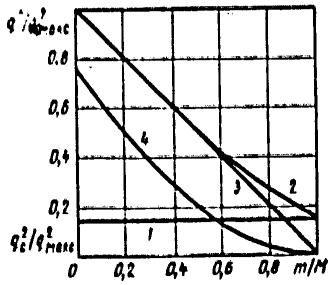

Figure 5

A Matched Filter and Linear Accumulator. First, let us consider the case when the transmission factors of the amplifier in figure 4 are constant, i.e. the filter in figure 4 is matched, the m's of the ChVE's are affected by interference, i.e. in m channels, the signal-to-noise ratio equals q^2_m (5) and in (M - m) channels it equals q^2_0 (4). In this case, the signal-to-noise ratio is

$$q_C = q_{max}\left(1 - \frac{m}{M} + \frac{mq_0^2}{Mq_m^2}\right)^{-1}. \qquad (6)$$

Substituting q^2_0 and q^2_m in (6) according to (4) and (5), we obtain

$$q_C^2 = \frac{q_n^2 q_{max}^2}{q_n^2 + q_{max}^2}, \qquad (7)$$

where q^2_π (2) is the signal-to-noise ratio under the condition that there is no noise and the interference affects all M components. In figure 5 the straight line 1 is the dependence q^2_C / q^2_{max} of m/M constructed according to (7). Since q^2_0 is independent of m, the straight line 1 is parallel to the axis of the abscissa. From (7) two basic conclusions follow. 1. The signal-to-noise ratio at the output of the matched filter in figure 5 does not depend on the number of affected components. This is a result of restricting the overall power of the interference P_π and its uniform distribution on m affected components. 2. The ratio q^2_C is always less than the least of the ratios q^2_{max} or q^2_π. If $q^2_{max} \gg q^2_\pi$, then $q^2_C \approx q^2_\pi$. In this case, it follows from (2) that the signal-to-noise ratio is determined only by the signal base.

Self-adjusting Filter and Optimum Accumulators. In a self-adjusting filter (see fig. 4) the voltages from the outputs of the component matched filters are added in the coherent accumulator with a certain weight. The weights are established in amplifiers with a variable gain factor. A similar problem is solved in the theory of space-diversity reception (12). For this reason, we will take advantage of the known results. With a coherent accumulation weight at the output of the accumulator, the maximum signal-to-noise ratio exists with the following weight factor sample:

$$\varphi_n = V_n/P_{nn}, \qquad (8)$$

where V_n is the signal component and P_{nn} is the interference power at the output of the n channel. From (8) it follows that the greater the interference power, the less the weight factor. Let us recall that such characteristics are possessed by "whitewash" filters. With the sample ϕ_n corresponding to (8) the signal-to-noise ratio at the output of the self-adjusting filter is maximum and equals

$$q_\Lambda^2 = \sum_{n=1}^{M} q_n^2, \qquad (9)$$

where q_n^2 is the signal-to-noise ratio at the output of the n channel. Let us assume that in m channels, the signal-to-noise ratio equals q_m^2 (5) and in (M -m) components it equals q_0^2 (4). Then

$$q_\Lambda^2 = (M-m)q_0^2 + mq_m^2. \qquad (10)$$

Replacing q_0^2 and q_m^2 in agreement with (4) and (5) we obtain from (10)

$$q_\Lambda^2 = q_{max}^2\left[1 - \frac{m}{M} + \frac{mq_n^2}{M^2} \times \right.$$
$$\left. \times \left(q_{max}^2 + \frac{m}{M}q_n^2\right)^{-1}\right]. \qquad (11)$$

With $m \ll Mq_\Lambda^2 \approx q_{max}^2$, (1 - m/M) also differs little from q_{max}^2. It is in this that the self-adjusting filter consists: the portion of ChVE's affected by high-power interference in general has a lower signal-to-noise ratio and when $m \ll M$ with them it can be ignored. With m = M, when all components are affected, the signal-to-noise ratio q_Λ^2 (11) reaches its minimum value $q_\Lambda^2 = q_c^2$ (7), i.e. the self-adjusting filter always provides improved interference immunity compared to a matched filter. The curve 2 in figure 5 represents the dependence q_Λ^2/q_{max}^2 constructed according to (11). When $m/M \ll 1$, the curve 2 coincides with the straight line 3 described as 1 - m/M. With a reduction in q_m^2, the curve 2 approaches straight line 3.

In those cases when the individual values of the signal and noise powers cannot be found, it is possible to use a quasioptimum self-adjusting receiver in which the weight is defined as

$$\varphi_n = a/(V_n^2 + P_{nn}).$$

where a is a defined constant. The calculations show that with high-power interference, quasioptimum and optimum self-adjusting receivers are practically the same in interference immunity.

The Nonlinear Filter. In study (7) a receiver is described with a nonlinear filter which differs from the one described in figure 4 in that, in each channel, there is first a band-pass filter, then a limiter followed by a component matched filter and delay line. In (7) the interference immunity of a receiver with the kind of nonlinear filter associated with coherent and noncoherent reception is analyzed. In the assumed designations, the signal-to-noise ratio at the output of the nonlinear filter is

$$q_{\text{н}}^2 = q_{\text{макс}}^2 \frac{\pi}{4}\left(1 - \frac{m}{M}\right)^2. \qquad (12)$$

In figure 5, the curve 4 characterizes the dependence $q_{\text{н}}^2 / q_{\max}^2$ of m/M. The ratio $\pi/4$ results in 1 dB of loss. The ratio $q_{\text{н}}^2/q_{\max}^2$ is sharply reduced with an increase in m/M since $q_{\text{н}}^2$ depends on m/M with $(1 - m/M)^2$. At the same time, in the optimum self-adjusting filter, the signal-to-noise ratio is reduced by approximately 1 - m/M. This is explained by the fact that in a self-adjusting filter, the signal-to-noise ratio is determined by formula (9) -- the less the component signal-to-noise ratio, the less it affects the overall signal-to-noise ratio, i.e. in essence, affected components are eliminated in a self-adjusting filter. In a nonlinear filter, the affected components always remain and add interference equal to the power of the ChVE's of the useful signal to the voltage across the output. Since the affected components with high-power interference are interferences, their presence as a whole results in a worsening of the interference immunity of the nonlinear filter as compared to a self-adjusting filter. It can be seen from figure 5 that when m/M>0.6, the nonlinear filter will be significantly inferior to a matched filter.

An Analyzer for Self-adjusting Filter Channels. To operate a self-adjusting filter, it is necessary that the channel analyzer establish weight factors corresponding to (8). Into the channel analyzer enters the sample $z_1, z_2 \ldots, z_m$ in which must be found the values of the signal amplitudes $\hat{U}$, the noise power and the interference plus noise power. Detecting such values is a self-instruction problem of the filter (8,9,13). Without considering this problem in this article, let us note that the accuracy of the values is higher, the greater the number of ChVE's in the signal, since the sample number is increased with an increase in M and this increases the accuracy of the values. In turn, an increase in the accuracy of the values results in an approximation of the exact interference immunity of the self-adjusting filter to the potential defined in formula (11).

Conclusions. 1. Exposed to high-power preformed interference, a self-adjusting filter provides maximum interference immunity. 2. A nonlinear filter is inferior in interference immunity to a self-adjusting filter, particularly in the increase in the number of affected components. 3. The least interference immunity of a communication system with a self-adjusting filter will

occur in that case when the interference affects all of the components. In this case, the interference immunity of a self-adjusting filter coincides with the interference immunity of a matched filter.

BIBLIOGRAPHY

1. Turin. "Matched Filters," ZARUBEZHNAYA RADIOELEKTRONIKA, No 3, 1961.

2. Teplov, N. L. "Pomekhoustouchivost' sistem peredachi diskretnoy informatsii" [Interference Immunity of Discrete Information Transmission Systems], Moscow, Svyaz', 1964.

3. Varakin, L. E. "Teoriya slozhnykh signalov" [Theories of Complex Signals], Moscow, Sovetskoye radio, 1970.

4. Kotel'nikov, V. A. "Teoriya potentsial'noy pomekhoustoychivosti" [Theories of Potential Interference Immunity], Moscow-Leningrad, Gosenergozdat, 1956.

5. Shchukin, A. N. "On One Method of Preventing Pulsed Interference," in "Izvestiya AN SSSR" [Journal of the USSR Academy of Sciences], series "fizicheskaya", No 10, 1946.

6. Bendzhamin. "Recent Achievements in Methods of Generating and Processing Radar Signals," ZARUBEZHNAYA RADIOELEKTRONIKA, No 7, 1965.

7. Vlasov, V. N. "Interference Immunity of a Nonlinear Receiver for Multifrequency Signals," in "Izvestiya AN SSSR," series "Radioelektronika", No 4, 1975.

8. Levin, B. R. "Teoreticheskiye osnovy statisticheskoy radiotekhniki" [Theoretical Foundations of Statistical Radio Methods], Moscow, Sovetskoye radio, Book 2, 1968, Book 3, 1976.

9. Repin, V. G. and Tartakovskiy, G. P. "Statisticheskiy sintez_pri apriornoy neopredelennosti i adaptatsiya informatsionnykh sistem" [Statistical Synthesis by A Priori Indeterminancy and Adaptation of Information Systems], Moscow, Sovetskoye radio, 1977.

10. Okunev, Yu. B. "Sistemy svyazi s invariantnymi kharacteristikami pomekhoustoychivosti" [Communication Systems with Invariant Interference Immunity Characteristics], Moscow, Svyaz', 1973.

11. Campbell, M. R.; Hoff, L. E.; and Ziemer, R. E. "A Large Time-Bandwidth Product Signaling Technique for Nonwhite Noise Channels," IEEE TRANS, Vol COM-24, No 10, 1976.

12. Fink, L. M. "Teoriya peredachi diskretnykh soobshcheniy" [Theories of Discrete Communications Transmission], Moscow, Sovetskoye radio, 1970.

13. Sikarev, A. A.; and Fal'ko, A. I. "Optimal'nyy priyem diskretnykh soobshcheniy" [Optimum Reception of Discrete Communications], Moscow, Svyaz', 1978.

14. "IEEE Trans. on Communications," Vol COM-25, No 8, 1977.

15. Varakin, L. E. "Statistical Characteristics of Discrete Composite Frequency Signals with Frequency Modulation," RADIOTEKHNIKA, Vol 32, No 9, 1977.

16. Varakin, L. E.; and Vlasov, V. N. "Systems of Discrete Multifrequency Signals," ELEKTROSVYAZ', No 7, 1974.

17. Varakin, L. E. "Coincidences of Structured Interference in Radio Equipment Systems with Discrete Frequency Signals," RADIOTEKHNIKA I ELEKTRONIKA, Vol 22, No 11, 1976.

8945
CSO: 1870

ELECTRONICS AND ELECTRICAL ENGINEERING

UDC 621.391.28

UNIFIED AUTOMATED COMMUNICATIONS NETWORK TERMS EXPLAINED

Moscow ELEKTROSVYAZ' in Russian No 1, Jan 79 pp 48-53

/Article by T. A. Vladimirova, K. A. Sil'vanskaya and A.Ya. Netes in the column "Questions of Terminology": "Terms for the Unified Automated Communications Network (EASS)"/

/Text/ GOST 22348-77 "A Unified Automated Communications Network. Terms and Definitions" was put into effect on 1 Jan 1978 by decree No 295 of the State Standards Committee of the USSR Council of Ministers of 4 Feb 1977. The GOST /All-Union State Standard/ was developed in accordance with the procedure of the All-Union Scientific Research Institute for Technical Information, Classification and Coding with allowance made for the recommendations of the USSR Academy of Sciences Committee for Scientific and Technical Terminology and other interested organizations based on principles and technical solutions incorporated into EASS's. A wide group of enterprises and organizations of the USSR and union republic ministries of communications, the NTORES /Scientific and Technical Society of Radio Engineering and Telecommunications/ imeni A. S. Popov terminology commission and the USSR Academy of Sciences, scientific research, educational and planning and production organizations took part in discussion of the plan for the standard.

In the standard are terms and definitions which incorporate the basic concepts of the Unified Automated Communications Network. The GOST contains 66 terms classified into two sections: "Primary EASS Network" and "Secondary EASS Network". In a reference appendix to the standard a number of terms are presented from the field of electrical communications which have a direct relationship with EASS's and also structural diagrams of primary and secondary EASS networks, systems and transmission lines. These diagrams facilitate understanding of the terms and their interrelationship.

The GOST does not exhaust all of the various terms used in EASS's but characterizes only the basic and most frequently used terms. The majority of terms of the standard apply to a primary EASS network. The development of a number of terminological state standards for individual secondary EASS networks is considered in what follows.

The GOST was composed taking into account the current state of science of both the equipment and principles incorporated into EASS's and for this reason some of the terms introduced differ in principle from the traditional ones used before.

In this connection, explanations are given in the article for the new EASS terminology and definitions. For convenience, after the terms in the article text are given their series numbers in the standard and a number with the index ТТ designates the series number of a term in the reference appendix.

The first term in the standard is "Unified Automated Communications Network (EASS)" to which the rest of the standardized terms are related. It reveals the concept of EASS's as systems for electrical communications which are systems of technical communications equipment interacting on the basis of certain principles, the main ones of which are the organizational and technical unity and function of EASS's. Its basis is a primary network of standard transmission channels and standard group channels. All secondary EASS networks are constructed on the basis of a primary network and are intended for satisfaction of the needs of enterprises, organizations, institutes and the country's population for transmitting any information converted into electrical communications signals. Attention should be given to the fact that, because of accumulated circumstances, the abbreviation EASS is expanded as Unified Automated Communications Network although the term corresponds to the concept Communications System.

The second term is the term "primary network" which begins the main section of the standard. By primary network is meant a collection of network terminals, network stations and transmission lines which constitute the standard transmission channels and standard group channels in an EASS.

With the standard transmission channels of an EASS primary network are grouped:

a voice frequency channel (TCh) with an effective transmitted frequency band of 300-3400 Hz;

an audio broadcast channel with effective transmitted frequency band of 30-15,000 Hz (higher class), 50-10,000 Hz (first class) or 100-6300 Hz (second class);

a television audio signal transmission channel with effective transmitted frequency band of 30-15,000 Hz (higher class) and 50-10,000 Hz (first class);

a television video signal transmission channel with a frequency band up to 6 MHz;

a wide-band channel based on a group channel (primary, secondary and so on).

With standard group channels of the EASS primary network are classified:

a primary group channel with an operating frequency band of 312.3-551.4 kHz;

a tertiary group channel with an operating frequency band of 812.3-2043.3 kHz;

a group channel of a higher order.

As far as the introduction of digital transmission systems and the development of norms for their parameters in a primary network are concerned, the following standard digital channels are possible:

a subprimary digital channel (STsT) with rated transmission speed of 0.512 Mbit/sec;

a primary digital channel (PTsT) with a rated transmission speed of 2048 Mbit/sec;

a secondary digital channel (VTsT) with a rated transmission speed of 8448 Mbit/sec;

a tertiary digital channel (TTsT) with a rated transmission speed of 34,368 Mbit/sec;

a quarternary digital channel (ChTsT) with a rated transmission speed of 139,264 Mbit/sec.

A transmission channel or group channel is called standard when its parameters are standardized. All of the transmission channels and group channels of an EASS primary network are standard. Because of this, the terms "standard group channel of a primary EASS network" (14) and "standard transmission channel of a primary EASS network" (20) should be used only in individual cases when it is necessary to contrast them with some other kind of nonstandard channels.

Transmission channels and group channels of a primary EASS network may be simple and composite. A simple group channel (16) and simple channel (27) have equipment for producing a group circuit or channel only at their input or output. A composite group channel (17) and composite channel (26) have transits corresponding to group circuits or channels (in the frequency band or with the transmission speed of the group circuit or channel). The transit of group channels of a primary EASS network (29) was previously designated a VCh transit. The transit of transmission channels of a primary EASS network was previously designated an NCh or TCh transit. Terms with the abbreviation "VCh", such as "VCh transmission system" should not be used since the extensive adoption of radio transmission systems has expanded considerably the frequency band used in EASS's and, naturally, wire transmission systems as compared to radio systems cannot be called high frequency systems.

A local primary network (3), an intrazone primary network (4) and a main circuit primary network (6) are component parts of a primary system. The system of intrazone and local primary networks in a territory coinciding with the numeration zone of the Statewide Automatic Keyed Telephone Network (OAKTS) represents a zoned primary network (5). Thus, a primary network of EASS's includes one main circuit primary network and a variety of intrazone and local primary networks.

The term "zoned primary network" is secondary and its use is adviseable in coordinating secondary EASS networks. Not infrequently, the terms (3-6) are used in distorted form. Thus, for instance, instead of "main circuit primary network" is used "primary main circuit network".

A network terminal (7) and a network station are components of a primary network. Network terminals and network stations are systems of technical equipment which accomplish the organization and transit of group channels and transmission channels of a primary network. Network terminals primarily accomplish the organization of transits and the separation of a limited number of channels and circuits to secondary networks and other users. Network stations are the terminal points of the primary network in which a large portion of the channels and circuits are available to secondary networks. Depending on the primary network to which it belongs, a network terminal is assigned the name "main circuit", "intrazone", "local" or terminal of the first, second or third class respectively. Thus, network terminals and network stations of a primary EASS network are called territorial network terminals (first and second class) TSU-1 and TSU-2, network switching terminals (first, second and third class) SUP-1, SUP-2 and SUP-3 , network separation terminals (first and second class) SUV-1 and SUV-2, main circuit network stations MSS, intrazone network stations VSS and local network stations SSM.

A transmission line (9) is a component of a primary network. A related term "communication line" (12П) is given in the appendix. If a transmission line (fig. 1) is a system of linear channels for a single type or diverse types of EASS transmission systems having a common propagation agent, linear construction and maintenance units, then a communication line is a system of transmission systems having a common propagation agent, linear construction and maintenance units, that is it includes in addition to linear channels, group channels and transmission channels. Consequently, in all cases when there is reference to development (planning, construction and so on) not only of linear but also of group channels or transmission channels, it is adviseable to use the term "communication line".

A number of the standard's terms are associated with group channels of a primary EASS network (13-17). Group channels in network terminals and stations are equipped with a special device for correcting amplitude and frequency distortion, the input and protection of control frequencies (KCh) during transmission and their blocking during reception. A standard group channel of a primary EASS network including such a device at its input and output to permit provision of a group channel to all users and also development of group channels with less channelled nature, wide-band channels or TCh channels is

called a "network channel of a primary EASS network" (15) and the device is called a "device for developing network channels". Group channels not equipped with device are used, as a rule, in network terminals and stations only in transit organization.

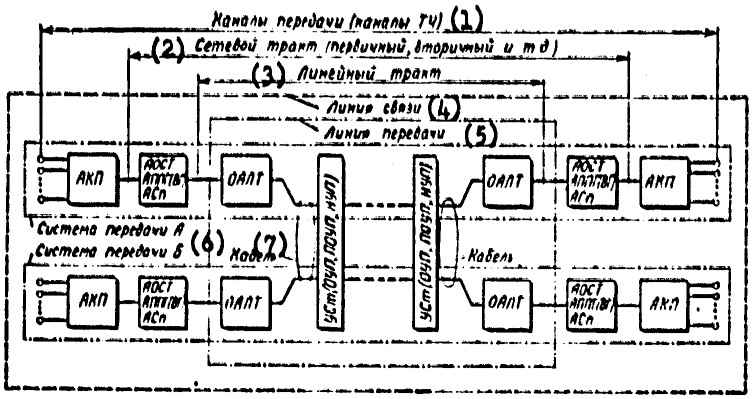

Figure 1. AKP — channel conversion device; AOST -- device for developing network channels (primary, secondary etc.); APPG — device for converting primary groups (APVG — secondary groups etc.); ASp — coupling device; OALT — terminal device of linear channel; USt (OUP, POUP, HUP) — booster stations for served, semi-served and unserved booster points.

Key:
1. Transmission channels (TCh channels)
2. Network channel (primary, secondary etc.)
3. Linear channel
4. Communication line
5. Transmission line
6. Transmission system
7. cable

In addition, the incorrect use of the term "group channel" (13) is frequently encountered in cases when there is reference to network channels.

It is especially necessary to consider the term "EASS transmission system" (32) which is introduced instead of the widely used term "multiplex system" whose use is inadmissible. A transmission system is a system of technical equipment which accomplishes the development of a linear channel, standard group channels and transmission channels of a primary EASS network consisting of the transmission system stations and the propagation agents of electrical communication signals. Consequently, the wire systems K-1920, K-60П, IKM-30 and ones like them are transmission systems since they directly accomplish

the organization of transmission channels and standard group channels.

In contrast to wire systems, many radio systems (radio relay in direct line-of-sight, tropospheric radio relay, satellite relay and so on) produce only trunks and for developing channels and group channels, cable transmission system equipment is also used. Such radio systems by themselves (by GOST definition) are not transmission systems (fig. 2). Depending on the type and consequently on the number of trunks, the radio system may accomplish the organization of a corresponding number of transmission systems. These transmission systems receive the name corresponding to the name of the trunk, such as "analog radio relay transmission system", "digital radio relay transmission system", "satellite system for transmitting audio broadcasts" and so on. In this case, the KURS-4 radio relay system is able to accomplish the organization of up to six transmission systems, the Orbita satellite system up to three transmission systems and so on.

The section of the standard "Secondary EASS network" contains 11 terms. A secondary EASS network (56) is a system of switching stations, switching terminals, terminal subscribers' units and secondary network channels organized on the basis of the transmission channels of the primary EASS network. Depending on the form of electrical communication (1TT), a secondary network takes an appropriate name. In EASS's, the following secondary networks are organized: a telephone network, a general use telegraph network, a subscribers' telegraph network, an audio broadcasting network, a television broadcasting network and a data transmission network.

The majority of secondary networks like the primary EASS network have a three-stage structure, i.e. they consist of main circuit, intrazone and local secondary networks. Since the telephone network has its own historically evolved terminology (GOST 19472-74), the term "intercity telephone network" corresponding to the term "main circuit secondary network" is retained at a certain stage.

The switching station (59), channel switching terminal (60), communication switching terminal (62) and secondary network channel (64) are the component parts of each secondary network. Switching stations and switching terminals should not be confused with network stations and network terminals of a primary EASS network. The function and composition of the technical equipment of the terminals and stations of primary and secondary networks differ.

To ensure normal operation of the primary network and its individual parts as well as secondary networks in EASS's, a control system is included for the primary network (55) and, in each secondary network, a control system for a secondary network (66) is included. Such control systems are systems for special organizational and technical services and facilities by means of which monitoring of the network operation and required switching are carried out to accomplish network operation in various circumstances. The terms "primary network control system" and "secondary network control system" should not be used for representing concepts associated with control in establishing connections, control in networks with communications switching and so on.

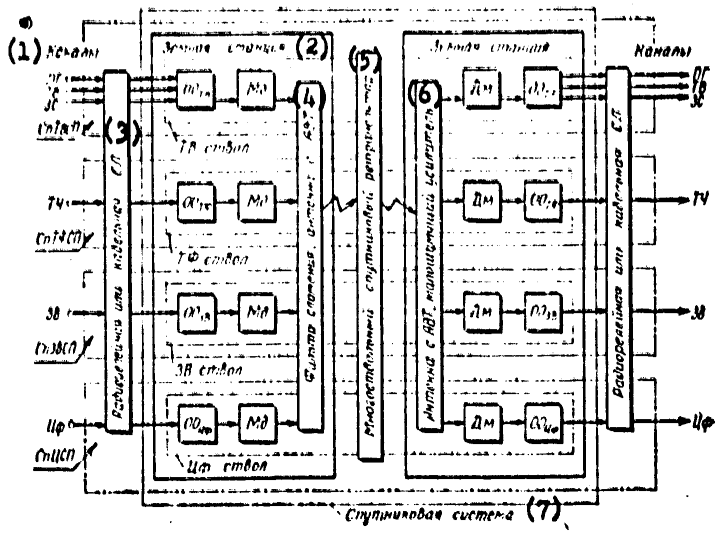

Figure 2. SpTVSP — satellite television transmission system; SpTFSP — satellite telephone transmission system; SpZVSP — satellite audio broadcasting transmission system; SpTsSP — satellite digital transmission system; OO_{TV}, OO_{TF}, OO_{ZV}, OO_{TsF} — terminal equipment of trunks of television, telephone, audio broadcasting and digital respectively; AVT — antenna-waveguide channel; Md — modulator; Dm — demodulator; channels PG, TV, ZS, TCh, TsF — channels for newspaper transmission, television video signal transmission, television audio signal transmission, voice-frequency and digital respectively.

Key:
1. Channels
2. Ground station
3. Radio relay or cable SL communication line
4. Accumulation filter, antenna with AVT
5. Multitrunk satellite retranslator
6. Antenna with AVT, noiseless amplifier
7. Satellite system

Primary network channels have the general term "transmission channel" (19) and individual names (21-25). The general term should be used when all or some transmission channels are referred to. In a secondary network, the terms "EASS electrical communication channel" (65) and "EASS secondary network channel" (64) are different. By EASS electrical communication channel is meant a system of technical equipment and a propagation agent which, during switching of terminal subscribers' units, accomplish the transmission of any form of

communications from their source to a receiver by means of electrical communication signals. The terminal subscribers' units themselves are not part of the electrical communications channel.

An EASS electrical communications channel and the terminal subscribers' units in various secondary networks have their own historically evolved terminology which has been retained without change. Thus, for instance, it is "information transmission channel" in a telephone network and "telegraph network" in a telegraph network. In some secondary networks, there is no term for linking an electrical communications channel with terminal units (for instance, in data transmission networks). This has also been the reason why, in the GOST under consideration, a single term is not given for linking an electrical communications channel with terminal subscribers'units. Depending on the form of communications transmitted, the designation "telephone communications channel", "telegraph communications channel", "data transmission channel" and so on is conferred on the electrical communications channel.

An EASS secondary network channel (64) is any part of an electrical communications channel: between switching points of two adjacent switching terminals or two switching stations or a switching station and a switching terminal or between a terminal subscriber's unit and switching points of a switching station or switching terminal. Depending on the form of secondary network, the secondary network channel assumes a name such as "telephone network channel", "telegraph network channel" and so on.

In conclusion, it should be noted that in connection with the introduction of GOST 22348-77 it is necessary in reviewing previously issued standards on statewide communication systems to refer to them according to the terms and definitions for the Unified Automated Communication Network.

It is also necessary to adhere strictly to the established contemporary standards for a term both in all forms of documentation and in records, plans, technical and reference literature, textbooks and educational manuals.

8945
CSO: 1870

GEOPHYSICS, ASTRONOMY AND SPACE

'AIR & COSMOS' REPORTS ON 'SOYUZ-33' ABORTED MISSION

Paris AIR & COSMOS in French No 762 (21 Apr 79) p 42

/Article by Pierre Langereux: "The Soviet-Bulgarian Crew ('Soyuz-33') Could Not Dock with 'Salyut-6'"/

/Text/ The Soviet-Bulgarian crew on board the Soviet "Soyuz-33" transport ship, which was launched by the USSR from the Tyuratam-Baykonur cosmodrome on 10 April 1979 at 1734 GMT (cf. Air & Cosmos, No 761), could not fulfill the mission as planned because of the failure to rendezvous and dock with the Soviet "Salyut-6" orbital station.

This was the first time that such a failure has occurred during an "international" flight organized by the USSR. Many Soviet cosmonauts, however, had already experienced similar difficulties in earlier missions: in October 1977 the "Soyuz-25" crew could not dock with the "Salyut-6" station also due to a failure of the "Soyuz" docking system, and the crews of "Soyuz-23" (in October 1976) and "Soyuz-15" (in 1974) also failed to dock with orbital stations.

The "Soyuz-33" crew should have docked with the "Salyut-6" orbital station on 11 April 1979 at 2100 hours GMT. A deviation in the approach system prevented the docking, and the crew was forced to return to earth at night. The descent vehicle safely softlanded on 12 April at 1635 GMT in Kazakhstan, 320 kilometers from the town of Dzhezkazgan.

The failure of this mission will probably force the Soviets to modify the flight program for the "Soyuz-32" crew, which has been on board "Salyut-6" since 25 February 1979. Vladimir Lyakhov and Valeriy Ryumin had been waiting for their colleagues in order to proceed with 27 new experiements in space physics, space metallurgy, space biology and medicine and earth observations.

"Soyuz-33" would have delivered, in particular, three new Bulgarian-made instruments: a "DAGA" photometer, a 15-channel "SPECTRA 15" multispectral camera, and a "SREDETZ" instrument for psychophysiological analysis. Some materials would also have been supplied by the Bulgarians for the "PIRINE" experiments in metallurgy in microgravity.

The "Progress-5" Reaupply Mission

The flight of the Soyuz-32" crew, which has been in orbit for 6 weeks (cf. Air et Cosmos, No 760), could be cut short because, if we can judge by previous "Salyut-6" operations (the "Soyuz-29" crew used the "Soyuz-31" transport ship for their return to earth), Lyakhov and Ryumin will not have "Soyuz-33" at their disposal. On the other hand, the crew will be able to prolong its flight thanks to the fuel and supplies delivered by the "Progress-5" freight transport ship on 14 March 1979. "Progress-5" had been launched on 12 March at 0847 hours Moscow time and docked automatically with the station 2 days later at 1020 hours. Once the resupply mission had been completed, "Progress-5" was undocked on 3 April at 1910 hours Moscow time and burned up in the atmosphere. But, most important, the thrusters of the freight transport ship were used twice to correct the "Salyut-6" station's orbit (on 30 March and 2 April), thus saving the fuel on board. Thus the station was placed into an orbit with the following parameters:

--apogee, 357 kilometers;

--perigee, 284 kilometers;

--inclination, 51.6 degrees;

--period, 90.6 minutes.

It is no longer possible to return in "Soyuz-33" the samples from the French ELMA metallurgy experiments conducted in the station's "Kristall" and "Splav" furnaces; normally they would have been returned in "Soyuz-33" one week after it was launched. The samples will probably be returned by the "Soyuz-32" crew.

But even more serious might be that the failure of "Soyuz-33" occurred on Cosmonautics Day in the USSR, which would have celebrated the 18th anniversary of Yuriy Gagarin's flight with a new international flight. The prestige of Soviet astronautics has been tarnished.

A Disappointment for the First Bulgarian Cosmonaut

This is also a disappointment for the first Bulgarian cosmonaut, Georgiy I. Ivanov (age 39), who was sent into space on board "Soyuz-33" as flight engineer along with Soviet cosmonaut Nikolay Rukavishnikov (age 46), flight commander and veteran of "Soyuz-10" (11 April 1971) and "Soyuz-16" (2 December 1974) flights. Georgiy Ivanov, a laborer's son who became a military pilot instructor (1800 hours flight time) had been preparing for space flight since March 1978.

Nevertheless, Bulgaria made its entrance into the ranks of cosmonauts. It is the fourth East European country to have set a cosmonaut into space on board a "Soyuz" transport ship--in order to spend about a week on board the

"Salyut-6" station--within the framework of cooperation between the USSR and socialist countries organized by the USSR Academy of Sciences' "Intercosmos" council. These joint flights began in 1978 with the successive flights of a Czech (Vladimir Remek), a Pole (Miroslaw Hermaszewski) and an East German (Sigmund Jaehn). The next flight will involve a Cuban, a Romanian and a Mongolian. All of them will have flown by 1981, according to the Soviets, before the first West European astronaut--to be chosen from among German, Swiss and Dutch candidates--who will be launched on board "Spacelab" around August 1981.

France also foresees sending a man into space on board a Soviet transport ship some time in the next decade, according to announcement by the president of CNES (cf. Air & Cosmos, No 759). /5/

CSO: 3100

GEOPHYSICS, ASTRONOMY AND SPACE

UDC 551.465.153

STATISTICAL CHARACTERISTICS OF THE HORIZONTAL STRUCTURE OF THE FIELD OF SMALL-SCALE TURBULENCE IN THE OCEAN

Moscow IZVESTIYA AKADEMII NAUK SSSR, FIZIKA ATMOSFERY I OKEANA in Russian Vol 15, No 3, 1979 pp 300-306

[Article by I. D. Lozovatskiy, R. V. Ozmidov and M. L. Pyzhevich, Institute of Oceanology USSR Academy of Sciences, submitted for publication 13 April 1978]

[Text] [Abstract] On the basis of data from measurements of fluctuations of current velocity and conductivity of sea water in the upper homogeneous layer and the thermocline the authors analyze the horizontal structure of the field of small-scale ocean turbulence. The separation of the current mean square values of signals into zones of background turbulence and turbulent spots made it possible to obtain estimates of the coefficient of horizontal intermittence of turbulence in dependence on the level of turbulent energy in the spot. There is an anisotropy in the horizontal distribution of turbulent inhomogeneities in the considered region of the ocean. The distribution of the dimensions of zones of background turbulence is approximated by a log-normal law, whereas the distribution of dimensions of individual turbulent spots is approximated by an exponential distribution law, which is associated with different mechanisms of generation of these turbulent formations.

Measurements of small-scale fluctuations of hydrophysical fields, carried out during recent years, demonstrated [1, 2] that the distribution of turbulent energy in the thickness of the ocean is extremely noniform. As a rule, there was no monotonic change in the energy level of turbulent fluctuations either vertically or horizontally. There was an intermittent structure of the turbulent formations, representing a random alternation of zones of weak and strong turbulence of the fluid.

The dimensions of zones with active turbulence, so-called turbulent spots, in most cases were several meters vertically and several tens of meters horizontally. However, these results, obtained using individual measurements of short duration and with the limited statistics for turbulent spots, are naturally only rough estimates which require further refinement. In particular, a problem which is unclear (see [3]) is the types of intermittence of turbulent formations in different hydrophysical fields in the ocean and the influence of stratification on the statistical characteristics of intermittence. It is also of interest to investigate the anisotropy of spatial structure of turbulent inhomogeneities in the ocean.

For an experimental study of the intermittence of turbulence it is necessary to have extended and long-term measurements of the fluctuations of current velocity and scalar fields (temperature, conductivity, etc.) in the vertical and horizontal planes in regions of the ocean which are different with respect to large-scale hydrological processes. The first data on the statistical characteristics of vertical intermittence of sea turbulence can be found in [3] and the first experiment for investigating the horizontal structure of turbulent formations in the ocean was carried out on the 19th voyage of the scientific research ship "Dmitriy Mendeleyev" (autumn of 1977) [4].

In the western tropical part of the Pacific Ocean specialists carried out long-term measurements of small-scale fluctuations of current velocity and conductivity of sea water in a towing regime on two perpendicular runs of 10 miles each. Hydroresistor sensors for the fluctuations of current velocity u' and conductivity σ' were towed at a depth of 100 m in the upper part of the thermocline (mean temperature gradient $\overline{T}_z = 0.07°C \cdot m^{-1}$, runs Nos 1 and 2) and on one of the runs (No 2a) at a depth of 45 m in the upper temperature-quasiuniform layer. The speed of towing was 2 $m \cdot sec^{-1}$. A detailed description of the measuring instrumentation used was cited in [5]. The registry of u' and σ' signals was with a three-channel N327-3 high-frequency recorder. In addition, a signal s_u -- mean square value of the velocity fluctuations, obtained using a mean-square voltmeter with an averaging time constant $\tau = 1$ sec, was fed to one of the channels of the automatic recorder.

The measurement data were then processed in such a way as to obtain the statistical characteristics of the horizontal dimensions of the turbulent formations in dependence on the level of turbulent energy in them. Due to the high noise level of the hydroresistor sensor of velocity fluctuations ($s_{u_{noise}} = 0.3$ $cm \cdot sec^{-1}$) it was impossible in the processing of the signals to discriminate purely laminar and slightly turbulent zones, since the evaluations of the characteristic s_u values for turbulence in the upper layer of the ocean have the order of magnitude 10^{-1}–10^{0} $cm \cdot sec^{-1}$ [6]. Therefore, the segments of the record on which the u' signal appreciably exceeded the noise level ($s_u > 0.5$ $cm \cdot sec^{-1}$) were henceforth identified as turbulent spots; however, those sectors where $s_u < 0.5$ $cm \cdot sec^{-1}$ were considered zones of background turbulence. The threshold level

of zones of active conductivity fluctuations was assumed equal to $5 \cdot 10^{-6}$ $ohm^{-1} \cdot cm^{-1}$ ($5 \cdot 10^{-3}$ equivalent Celsius degrees). In order to exclude brief interference in the discrimination of turbulent spots it was assumed that the minimum duration of a significant signal on individual parts of the record had to exceed 1 sec (that is, a study was made of turbulent inhomogeneities with horizontal scales not less than 2 m). Figure 1 shows an example of separation of the record into individual parts.

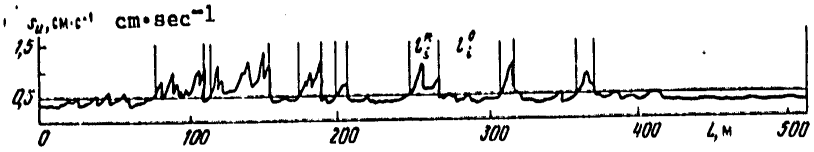

Fig. 1. Example of discrimination of zones of background turbulence l^0 and turbulent spots l^* on record of signal of mean square values of velocity fluctuations s_u.

Table 1

Statistical Characteristics of Distributions of Horizontal Dimensions of Turbulent Spots l^* and Zones of Background Turbulence l^0

1 № гала	2 Горизонт буксировки, м	3 Величина	4 Количество членов ряда	5 Минимальное значение, м	6 Максимальное значение, м	7 Среднее значение, м	8 Среднеквадратичное отклонение, м	9 Коэффициент вариации	10 Коэффициент асимметрии	11 Стандартное отклонение асимметрии	12 Коэффициент эксцесса	13 Стандартное отклонение эксцесса	χ^2
1	100	l^0	107	6	1344	194	278	1,4	2,2	0,2	4,8	0,5	18,0
		l^*	107	4	696	32	78	2,5	6,5	0,2	50,4	0,5	2594,0
2	100	l^0	122	6	896	115	170	1,5	2,9	0,2	9,6	0,4	21,5
		l^*	122	6	614	35	78	2,2	5,7	0,2	37,3	0,4	303,6
2а	45	l^0	122	6	856	106	148	1,4	3,0	0,2	10,6	0,4	20,0
		l^*	122	6	320	36	56	1,5	3,0	0,2	9,6	0,4	83,3

KEY:

1. No of run
2. Towing horizon, m
3. Parameter
4. Number of terms in series
5. Minimum value, m
6. Maximum value, m
7. Mean value, m
8. Standard deviation, m
9. Variation coefficient
10. Asymmetry coefficient
11. Standard deviation of asymmetry
12. Excess coefficient
13. Standard deviation of excess

On the basis of the resulting series of horizontal dimensions of turbulent spots l_i^* and zones of background turbulence l_i^0 we carried out computations of the statistical characteristics l^* and l^0 for each individual

run. As an example, Table 1 gives the limits of change in the first four distribution moments for ℓ^* and ℓ^0, as well as the variation coefficients $V = \sigma/\bar{\ell}$ (where $\bar{\ell}$ is the mean value and σ is the standard deviation of the ℓ_i series), standard deviations in computations of asymmetry D_A and excess D_E from records of the signal s_u on all runs.

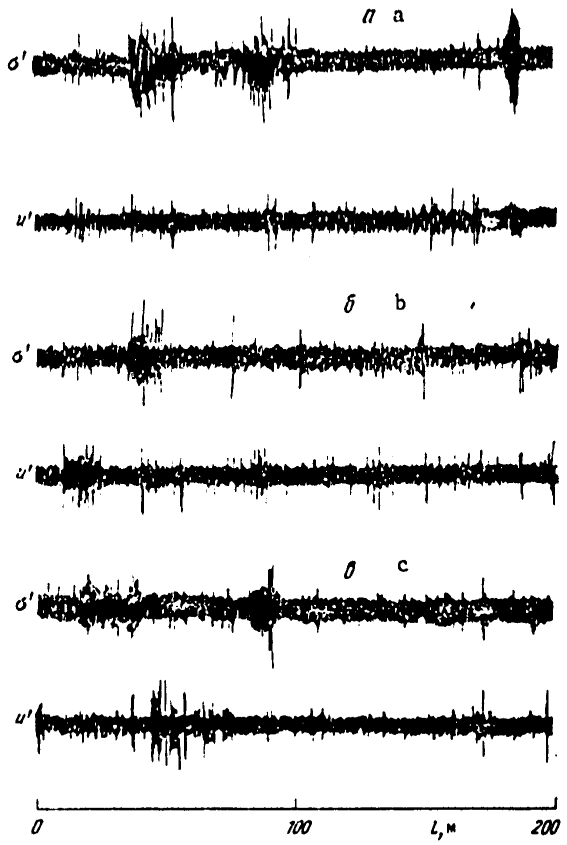

Fig. 2. Examples of zones of "fossil" turbulence (a), microfronts (b) and density-homogeneous layers (c) on records of signals u' and σ'.

We note that the number of turbulent spots on the first run (107) was appreciably less than on the two subsequent runs (122), despite the fact that run No 2 was situated, like run No 1, in the thermocline, and run

No 2a -- in the quasihomogeneous layer. The mean horizontal dimensions of the turbulent spots were approximately constant in space and equal to 32-36 m. However, there was an appreciable difference in the very distribution of the dimensions of spots in the homogeneous layer and in the thermocline. For example, the variability of l^* at a depth of 100 m was considerably greater than at a depth of 45 m (V_{100} = 2.2-2.5, V_{45} = 1.5); the maximum dimensions l^*_{max} in the thermocline (614 and 696 m) exceeded l^*_{max} in the uniform layer by a factor of more than 2 (uniform layer, 320 m), and the excess values E^*_{100} were greater by a factor of 4-5 than E_{45}. All this is evidence of the considerably better developed intermittence of the turbulent spots in the thermocline in comparison with the upper quasihomogeneous layer. [The statistical significance in the difference in the dispersions $\sigma_{l^*}^2$ and mean values $\bar{l}^*$ at the horizons 100 and 45 m was checked using the Fisher and Student tests. The ratio of the dispersion for $l^*\sigma^2_{100}/\sigma_{45}^2$ = 1.94 was greater than the tabulated value $F_{0,95}$ (121.121) = 1.35, which means a significant difference between the dispersions of the horizontal dimensions of the turbulent spots at the horizons 100 and 45 m. Although the difference of the mean dimensions $\overline{l^*_{100}}$ and $\overline{l^*_{45}}$ was not significant with this same confidence level, the variation coefficients V_{100} and V_{45} for l^*, characterizing the variability of l^* in the thermocline and the homogeneous layer, significantly differed from one another.]

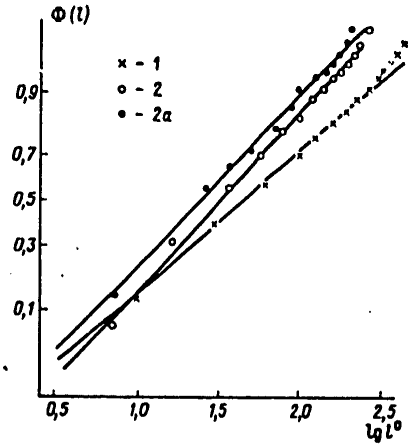

Fig. 3. Empirical distribution functions of dimensions of zones of background turbulence on runs Nos 1, 2 and 2a. The solid curves represent the distribution functions of the log-normal law (1), computed for values of the parameters μ and σ, corresponding to the empirical distributions.

The distribution of the dimensions of the zones of background turbulence l^0 was characterized by an appreciably greater smoothness than l^*. The variation coefficients for all the runs had values $\sim$1.4, and the values

of the excess varied in the range 4.8-10.6. However, the absolute scatter of l^0 values naturally exceeded the scatter of l^*; the maximum dimensions of the zones of background turbulence in the thermocline and the quasihomogeneous layer were equal to 1344 and 856 m respectively.

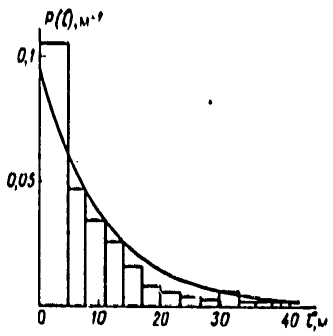

Fig. 4. Histogram of the distribution of dimensions of highly turbulent zones ($s_u^0 > 1.1$ cm·sec^{-1}) on run No 2. The solid curve represents the density distribution of the exponential law (2) for a value of the λ parameter corresponding to an empirical distribution.

Table 2

Values of the Intermittence Coefficient χ for Three Reading Levels of the Mean Square Values of Velocity Fluctuations s_u^0 cm·sec^{-1}

No of run	χ		
	$s_u^0 = 0,5$	$s_u^0 = 0,8$	$s_u^0 = 1,1$
1	0,14	0,07	0,03
2	0,23	0,11	0,06
2a	0,26	0,09	0,05

A reciprocal analysis of the variability of the signals u' and σ' along one of the runs made it possible to draw a series of conclusions concerning the distribution of small-scale turbulence in the thermocline. It was found that on the average the number of sectors with intensive σ' fluctuations exceeds the number of turbulent spots on the u' record and the mean dimensions $\overline{l_{\sigma^*}}$ are greater than $\overline{l_u}^*$. This is evidence of the existence of both individual zones of "fossil" turbulence [2] and microfronts in the thermocline. In the latter case the intensification of conductivity fluctuations must be attributed primarily to an increase in the mean horizontal gradient $\overline{\partial\sigma / \partial l}$. Examples of the possible manifestation of fossil turbulence and microfronts on the records of the σ' and u' signals are shown in Fig. 2,a,b. A rarer phenomenon in the analyzed measurements

was the existence of highly turbulent density-homogeneous layers, within whose limits there was a high level of fluctuations u' and an absence of conductivity fluctuations. One of these examples is shown in Fig. 2,c.

The coefficient of horizontal intermittence of turbulence $\varkappa$ can be determined as the ratio of the sum of the dimensions of all the turbulent spots (with a given reading level s_u^0) on some run to the total length of the entire run. The $\varkappa$ values, computed for the three reading levels $s_u^0 = 0.5$, 0.8, 1.1 cm·sec^{-1}, at the horizons 100 and 45 m are given in Table 2.

The value of the intermittence coefficient on the first run is appreciably less than on the second run, where in turn it remains approximately identical in the thermocline and in the quasihomogeneous layer. This result, together with the appreciable differences in the excess of the distribution of l^0 and l^* on mutually perpendicular runs in the thermocline, can indicate a horizontal anisotropy of the considered turbulent formations. The numerical value $\varkappa$ is essentially dependent on the selected minimum level s_u^0. For example, in the quasihomogeneous layer zones of very intensive turbulence, within which $s_u > 1.1$ cm·sec^{-1}, occupied 5% of the considered space, whereas turbulent spots with mean square values of the velocity fluctuations exceeding 0.5 cm·sec^{-1} occupied 26%.

The dependence of the numerical value $\varkappa$ on the selected minimum level s_u^0 is evidence that the most complete characteristics of the variability of the horizontal structure of turbulence are not the intermittence coefficients, but the distribution functions both for the dimensions of the turbulent zones and the levels of turbulent energy.

The empirical distributions $\tilde{P}(l)$ of the dimensions of turbulent spots and zones of background turbulence were computed from the resulting records for individual runs. Comparison of the empirical dependences $\tilde{P}(l)$ with the analytical expressions for the distribution laws $P(l)$ was carried out using the test χ^2 [7], the computed values for which for a log-normal distribution law are given in Table 1. The comparison of $\tilde{P}(l^0)$ and $\tilde{P}(l^*)$ with 12 different distribution laws indicated that on all runs the distribution of the horizontal dimensions of the zones of background turbulence with a significance level from 0.05 to 0.15 can be approximated by a log-normal law (Fig. 3) with a distribution function in the form

$$\Phi(l^0, \mu, \sigma) = \frac{1}{\sqrt{2\pi}} \int_{-\infty}^{u} e^{-t^2/2}\, dt \qquad \text{when } l^0 > 0, \tag{1}$$

$$u = (\lg l^0 - \mu) / \sigma,$$

where μ and σ are the distribution parameters corresponding to the mathematical expectation of the random value $z = \lg l^0$ and its standard deviation.

It was demonstrated in [8] that the log-normal distribution asymptotically corresponds to the particle-size distribution, obtained as a result of a series of successive independent fragmentations. Such a process of

successive fragmentation, as was noted in [9], can serve as a natural model of the cascade process of formation of ever-smaller turbulent formations. It can therefore be assumed that the formation of zones of background turbulence ($s_u < 0.5$ cm·sec^{-1}) occurred in the ocean as a result of the cascade process of fragmentation of large-scale turbulent inhomogeneities arising due to instability of the averaged motion.

However, the genesis of spots of intensive small-scale turbulence ($s_u > 0.5$ cm·sec^{-1}) of relatively small size had a different nature, related, probably, to the local instability of the vertical gradients of current velocity and destruction of short internal waves at individual moments in time. We note that the appearance of turbulent spots was frequently noted not individually, but in whole groups. One of the examples of such a group of spots is shown in Fig. 1. The random appearance of turbulent spots in turn can cause a "fragmentation" of the field of background turbulence, which is also reflected in the log-normal distribution $\tilde{P}(l^0)$.

A comparison of the empirical distributions of the dimensions of turbulent spots $\tilde{P}(l^*)$ with 12 different theoretical $P(l)$ laws indicated that in most of the considered cases the constructed $\tilde{P}(l^*)$ histograms cannot be approximated by the best-known distribution laws with few parameters (as an example, in Table 1 we give the values for the χ^2 test for a log-normal distribution $P(l^*)$). However, in individual cases, for example, for run No 2, the distribution of the dimensions of spots with an extremely high turbulence level ($s_u > 1.1$ cm.sec^{-1}) can be approximated using the test $\chi^2 = 12.3$ with a significance level 0.35 by an exponential curve (Fig. 4), whose probability density is determined using the formula

$$\varphi(x, \lambda) = \begin{cases} 0, & x \leqslant 0 \\ \lambda e^{-\lambda x}, & x > 0 \end{cases} \qquad (2)$$

where λ is the sole distribution parameter, known as the density of the flow of events and numerically equal to the inverse value of the mathematical expectation and standard deviation of the considered random value. The solid curve in Fig. 4 shows the curve for law (2), computed for a value of the parameter $\lambda = 10.8$ m^{-1}, corresponding to the empirical distribution $\tilde{P}(l_{em}^*)$. We note that with some assumptions concerning the distribution law $P(l^*)$, on the basis of the theory of distribution of the extreme terms in the sample [7] it can be shown that the distribution of the horizontal dimensions of zones with an extremely high turbulence level $\tilde{P}(l_{em}^*)$ asymptotically in the case of a large number of turbulent spots is described by an exponential distribution (2). Since the generation of turbulent spots in the thickness of the ocean, having a broad range of change of both geometrical dimensions and turbulence levels, is related primarily to the mechanisms of local instability, for the $P(l^*)$ density distribution there may not actually exist any universal distribution laws.

BIBLIOGRAPHY

1. ISSLEDOVANIYE IZMENCHIVOSTI GIDROFIZICHESKIKH POLEY V OKEANE (Investigation of the Variability of Hydrophysical Fields in the Ocean), edited by R. V. Ozmidov, "Nauka," 1974.

2. Nasmyth, R. W., "Turbulence and Microstructure in the Upper Ocean," MEM. SOC. ROY. SCI. LIEGE, Ser. 6, 4, 47-56, 1973.

3. Losovatskiy, I. D., Ozmidov, R. V., "Peculiarities of the Vertical Structure of Sea Turbulence," OKEANOLOGIYA (Oceanology), 18, No 1, 1978.

4. Ozmidov, R. V., "Nineteenth Voyage of the Scientific Research Vessel 'Dmitriy Mendeleyev'," OKEANOLOGIYA, 18, No 3, 1978.

5. Paka, V. T., Kushnikov, V. V., "Carrier of Towed Apparatus for Hydrophysical Investigations," OKEANOLOGIYA, 18, No 3, 1978.

6. Monin, A. S., Ozmidov, R. V., Lozovatskiy, I. D., "Small-Scale Ocean Turbulence," GIDROFIZIKA OKEANA (Ocean Hydrophysics), Vol 1, "Nauka," 164-183, 1978.

7. Smirnov, N. V., Dunin-Barkovskiy, I. V., KURS TEORII VEROYATNOSTEY I MATEMATICHESKOY STATISTIKI (Course in the Theory of Probabilities and Mathematical Statistics), "Nauka," 1965.

8. Kolmogorov, A. N., "Log-normal Distribution of the Sizes of Particles During Fragmentation," DOKLADY AN SSSR (Reports of the USSR Academy of Sciences), 31, No 2, 99-101, 1941.

9. Obukhov, A. M., "Some Specific Features of Atmospheric Turbulence," JGR, 67, No 8, 3011-3014, 1962.

5303
CSO: 1870

GEOPHYSICS, ASTRONOMY AND SPACE

UDC 551.465.41:551.466.3

GENERATION OF STATIONARY TEMPERATURE BOUNDARY LAYERS BY SURFACE WAVES

Moscow IZVESTIYA AKADEMII NAUK SSSR, FIZIKA ATMOSFERY I OKEANA in Russian Vol 15, No 3, 1979 pp 314-325

[Article by B. A. Nelep, G. S. Dvoryaninov and A. V. Prusov, Marine Hydrophysical Institute, Ukrainian Academy of Sciences, submitted for publication 24 February 1978]

[Text] [Abstract] Within the framework of a viscous quasi-linear model the authors investigate the stationary temperature boundary layers arising under the influence of surface waves. In contrast to studies [1-4], carried out on the basis of potential theory, it is shown that surface waves cause an averaged vertical convective transport of heat, the maximum of whose spectrum with deepening is shifted into the direction of the low frequencies. These fluxes form stationary temperature boundary layers at the water-air discontinuity which can be interpreted as one of the reasons for existence of a warm surface film. The conclusion is drawn that the greatest contribution to its formation must be from short waves. The joint effect of surface and thermal waves in the averaged transport of mass is also studied.

The physics of boundary layers at the water-air discontinuity of especially complex because this surface itself is mobile and permeable for heat and mass. The most important type of interaction, to a high degree determining the thermodynamic state of the ocean-atmosphere system, is heat exchange. It takes place through the discontinuity and is dependent on the parameters determining the properties of the boundary layers. However, the heat exchange problem has been poorly studied. For example, there are two important phenomena in the thin boundary layer of the sea which have been established experimentally.

1. Under the influence of surface waves an additional vertical heat flow arises; this is a function of the parameters characterizing waves [5].

2. The thin boundary layer in the fluid adjacent to the discontinuity is characterized by a sharp temperature gradient -- a thin warm film [6-10].

These two facts have been poorly investigated experimentally and only preliminary attempts have been made to treat them theoretically and give a physical interpretation. For example, in [4] there is an analysis of the dependence of the amplitude and phase of the temperature fluctuations at the surface of a fluid in the presence of a progressive wave. The analysis was made on the assumption that the wave is potential and that the heat flow through the surface is known. A study of the averaged fields generated by surface waves was studied in [11]; similar effects, caused only by temperature waves, were examined in [12]. In this article we investigate the generation of stationary boundary layers by surface waves; we investigate some of their properties and examine matters related to the phenomena mentioned above. At the same time, both dynamic and thermal factors are taken into account. On the basis of the solutions obtained the conclusion is drawn that surface waves, as a result of the convection excited by them, can make an appreciable contribution to formation of the structure of a warm surface film.

1. Formulation of Problem

Experimental investigations of the upper boundary layer in the ocean show [2, 5] that when there are wind waves or surge exists at its surface the temperature field also oscillates and there is a phase shift between the rise in the ocean surface and temperature variations. Thus, there are temperature waves as well as surface waves. Together they should induce averaged thermohydrodynamic effects within the fluid. We will examine some of them.

Assume that a plane layer of fluid of constant density and the depth d is bounded at the lower surface by a horizontal bottom. We will select a Cartesian coordinate system $\{x, z\}$ with its origin at the bottom; z is directed vertically upward. Motion is excited by a surface wave. On the basis of the above-mentioned observations [2, 5] we will assume that the surface wave leads to the appearance of a surface temperature wave which is displaced in phase relative to it. The existence of a phase shift can be explained by the following physical considerations. The disturbance of the temperature field in the horizontal direction occurs with the phase velocity of propagation of the surface wave. In the vertical direction, however, the velocity of the dynamic disturbance is much greater than the velocity of heat diffusion; therefore, a phase shift already appears in the thin molecular layer between them. And since the diffusion of heat and vorticity in a general case occurs at different rates, a phase shift arises between the fluctuations of velocity and heat. Precisely the phase shift should create a directed vertical heat transfer.

Assume that a is the characteristic amplitude of the surface wave, θ_0 is the amplitude of the temperature disturbance at the fluid surface, ω and k is the characteristic frequency and wave number of the disturbance, g is gravitational acceleration, t is time, ψ is the stream function for our two-dimensional motion. We introduce the following dimensionless variables:

$$x=kx^+,\ z=z^+/d,\ \psi=(a\omega d)^{-1}\psi^+, \tag{1.1}$$

where

$$\{u^+,\ w^+\}=\{\partial\psi^+/\partial z^+,\ -\partial\psi^+/\partial x^+\}, \tag{1.2}$$

u and w are the velocity components along x and z respectively; the cross denotes dimensional parameters.

We will determine the temperature

$$T^+=T_0^+(1+\varepsilon T), \tag{1.3}$$

so that the density, expressed from the equation of state, is

$$\rho^+=\rho_0^+[1+\beta^+(T^+-T_0^+)], \tag{1.4}$$

where T_0^+, ρ_0^+ are equilibrium temperature and density; $\beta=\beta^+T_0^+$ (β^+ is the coefficient of thermal expansion of water).

Then, in dimensionless form the surface wave, stipulated in the form of one Fourier component, has the form

$$\eta=\frac{\varepsilon}{\delta}\cos(x-t), \tag{1.5}$$

where ε = ak is wave steepness; δ = kd. The equations of diffusion of vorticity and heat are

$$\left\{\frac{\partial}{\partial t}+\varepsilon\left(\frac{\partial\psi}{\partial z}\frac{\partial}{\partial x}-\frac{\partial\psi}{\partial x}\frac{\partial}{\partial z}\right)\right\}\nabla^2\psi=\frac{\alpha^2}{2}\nabla^4\psi+\delta\beta_0\frac{\partial T}{\partial x}, \tag{1.6}$$

$$\left\{\frac{\partial}{\partial t}+\varepsilon\left(\frac{\partial\psi}{\partial z}\frac{\partial}{\partial x}-\frac{\partial\psi}{\partial x}\frac{\partial}{\partial z}\right)\right\}T=\frac{\alpha^2}{2P}\nabla^2T, \tag{1.7}$$

where $\alpha=(2\nu/\omega)^{1/2}d$, ν is the kinematic coefficient of exchange of momentum; P is the Prandtl number;

$$\beta_0=g\delta\beta/\omega^2d;\ \nabla^2=\partial^2/\partial z^2+\delta^2\partial^2/\partial x^2.$$

The parameters ε and α entering into equations (1.6), (1.7) characterize the contribution of inertial and viscous forces to the general balance and are assumed to be small, so that $\varepsilon \ll 1$, $\alpha \ll 1$.

The boundary conditions at the sea surface are: condition of absence of shearing stress, which has the form [11]

$$\frac{\partial^2\psi}{\partial z^2}-\frac{\partial^2\psi}{\partial x^2}-4\frac{\partial\eta}{\partial x}\frac{\partial^2\psi}{\partial x\,\partial z}=0 \qquad \text{when } z=1+\eta, \tag{1.8}$$

the kinematic condition is

$$\frac{\partial\eta}{\partial t}+\frac{\partial\psi}{\partial x}+\frac{\partial\eta}{\partial x}\frac{\partial\psi}{\partial z}=0 \qquad \text{when } z=1+\eta, \tag{1.9}$$

and for the temperature wave field -- existence at the discontinuity of a temperature wave displaced in phase relative to η, that is

$$T=\vartheta\cos(x-t+\gamma) \qquad \text{when } z=1+\eta, \tag{1.10}$$

where $\vartheta = \theta_0/\varepsilon T_0^+$; γ is the phase difference between the temperature and surface waves.

On the bottom the boundary conditions are the attachment conditions

$$\psi=\psi_z=0 \qquad \text{when } z=0 \tag{1.11}$$

and the absence of wave disturbances of temperature, so that

$$T=0 \text{ when } z=0. \tag{1.12}$$

2. Nonstationary Fields of Velocity and Temperature

The solution of problem (1.6)-(1.12) will be sought in the form of series for the small parameters ε and α with subsequent use of the method of asymptotically joinable expansions. We will represent ψ and T in the form

$$\{\psi, T\}=\sum_{l,m=0}^{\infty}\varepsilon^l\alpha^m\{\psi_{lm}, T_{lm}\}, \tag{2.1}$$

and the functions ψ_{0m}, T_{0m} as

$$\{\psi_{0m}, T_{0m}\}=\frac{1}{2}[\{\hat{\psi}_{0m}, \hat{T}_{0m}\}e^{i(z-t)}+\{\hat{\psi}_{0m}^*, \hat{T}_{0m}^*\}e^{-i(z-t)}], \tag{2.2}$$

where the asterisk denotes complexly conjugate values.

After the substitution of (2.1), (2.2) into (1.6), (1.7) and equating the coefficients with the corresponding powers of α relative to $\hat{\psi}_{0m}$ and $\hat{T}_{0m}$ we obtain, respectively, first- and second-degree equations which describe the solutions only in the main region, excluding the viscous boundary layers at the free surface and bottom. In order to obtain the equations for the boundary layers, we introduce the corresponding boundary layer variables:

at the free surface

$$z-1=\alpha\xi, \quad \psi(x, z, t)=\varphi(x, \xi, t), \quad T(x, z, t)=\theta(x, \xi, t), \tag{2.3}$$

at the bottom

$$z=\alpha\zeta, \quad \psi(x, z, t)=\Phi(x, \zeta, t), \quad T(x, z, t)=G(x, \zeta, t). \tag{2.4}$$

Then, substituting (2.3), (2.4) into (1.6), (1.7) for the sought-for functions in the upper boundary layer we obtain

$$\left\{\frac{\partial}{\partial t}+\frac{\varepsilon}{\alpha}\left(\frac{\partial\varphi}{\partial\xi}\frac{\partial}{\partial x}-\frac{\partial\varphi}{\partial x}\frac{\partial}{\partial\xi}\right)\right\}\left(\frac{\partial^2\varphi}{\partial\xi^2}+\delta^2\alpha^2\frac{\partial^2\varphi}{\partial x^2}\right)=$$

$$=\frac{1}{2}\left(\frac{\partial^3\varphi}{\partial\xi^3}+2\alpha^2\delta^2\frac{\partial^3\varphi}{\partial x^2\partial\xi^2}+\alpha^4\delta^4\frac{\partial^3\varphi}{\partial x^3}\right)+\alpha^2\delta\beta_0\frac{\partial\theta}{\partial x}, \tag{2.5}$$

$$\left\{\frac{\partial}{\partial t}+\frac{\varepsilon}{\alpha}\left(\frac{\partial\varphi}{\partial\xi}\frac{\partial}{\partial x}-\frac{\partial\varphi}{\partial x}\frac{\partial}{\partial\xi}\right)\right\}\theta=\frac{1}{2P}\left(\frac{\partial^2\theta}{\partial\xi^2}+\alpha^2\delta^2\frac{\partial^2\theta}{\partial x^2}\right). \tag{2.6}$$

The equations for the bottom boundary layer, in which, in place of ξ, φ, θ we have ζ, Φ, G respectively, have the same form.

Before expressing the boundary conditions at the free surface (1.8), (1.9) in terms of the boundary layer variables, they must be expanded into a Taylor series relative to the undisturbed surface z = 1. Performing this procedure and representing the derived expressions in the variables ξ and φ, with an accuracy to $o(\varepsilon^2)$ we have

$$\frac{\partial^3\varphi}{\partial\xi^3}-\delta^2\alpha^2\frac{\partial^3\varphi}{\partial x^2}+\frac{\varepsilon}{\alpha\delta}\left[\frac{\partial^3\varphi}{\partial\xi^3}\cos(x-t)-\alpha^2\delta^4\frac{\partial^3\varphi}{\partial x^2\partial\xi}\cos(x-t)-\right.$$
$$\left.-4\alpha^2\delta^2\frac{\partial^3\varphi}{\partial x\partial\xi}\sin(x-t)\right]=0 \qquad \text{when } \xi=0, \tag{2.7}$$

$$\frac{1}{\delta}\sin(x-t)+\frac{\partial\varphi}{\partial x}+\frac{\varepsilon}{\alpha\delta}\left[\frac{\partial^2\varphi}{\partial x\partial\xi}\cos(x-t)-\frac{\partial\varphi}{\partial\xi}\sin(x-t)\right]=0 \quad \text{when } \xi=0. \tag{2.8}$$

Conditions (1.10)-(1.12) assume the form

$$\frac{\varepsilon}{\delta}\frac{\partial\theta}{\partial\xi}\cos(x-t)+\theta=\theta_0\cos(x-t+\gamma) \qquad \text{when } \xi=0 \tag{2.9}$$

$$\Phi=\Phi_0=0 \qquad \text{when } \zeta=0 \tag{2.10}$$

$$G=0 \qquad \text{when } \zeta=0. \tag{2.11}$$

In addition to the conditions (2.3), (2.4), (2.7)-(2.11) the external and internal solutions must satisfy the joining conditions [13]

$$\lim_{z\to 1}\{\psi, T\}\approx\lim_{t\to-\infty}\{\varphi, \theta\}, \quad \lim_{z\to 0}\{\psi, T\}\approx\lim_{\zeta\to\infty}\{\Phi, G\}. \tag{2.12}$$

For the functions φ, Φ, θ, G we seek a solution in the form (2.1), (2.2). Substituting the expansions of the sought-for functions into a series for the small parameters ε and α into the corresponding equations of motion

and the boundary conditions, taking into account (2.2) and equating the coefficients with identical powers of α, we have the following equations and boundary conditions in the approximations (00) and (01):

$$\left(\frac{\partial^2}{\partial\xi^2}+2i\right)\frac{\partial^2\varphi_{0m}}{\partial\xi^2}=0,\quad \frac{\partial^2\hat{\varphi}_{0m}}{\partial\xi^2}(0)=0,\quad \hat{\varphi}_{0m}(0)=\delta^{-1}(1-m), \tag{2.13}$$

$$\left(\frac{\partial^2}{\partial\xi^2}+2iP\right)\hat{\theta}_{0m}=0,\quad \hat{\theta}_{0m}(0)=(1-m)\theta e^{i\gamma}, \tag{2.14}$$

$$\left(\frac{\partial^2}{\partial z^2}-\delta^2\right)\hat{\psi}_{0m}=-(1-m)\delta\beta_0\hat{T}_{00},\quad \hat{T}_{0m}=0,$$

$$\left(\frac{\partial^2}{\partial\zeta^2}+2i\right)\frac{\partial^2\hat{\Phi}_{0m}}{\partial\zeta^2}=0,\quad \frac{\partial\hat{\Phi}_{0m}}{\partial\zeta}(0)=0,\quad \hat{\Phi}_{0m}(0)=0,$$

$$\left(\frac{\partial^2}{\partial\tau^2}+2iP\right)\hat{G}_{0m}=0,\quad \hat{G}_{0m}(0)=0, \tag{2.15}$$

in which m = 0; 1.

The final form of solution of the problems (2.13)-(2.15), satisfying the joining conditions (2.12), are

$$\begin{aligned}
&\hat{\varphi}_{00}=\delta^{-1}, && \hat{\theta}_{00}=\theta e^{i\gamma}e^{(1-i)\sqrt{P}\zeta},\\
&\hat{\psi}_{00}=(\delta\,\mathrm{sh}\,\delta)^{-1}\,\mathrm{sh}\,\delta z, && \hat{T}_{00}=0,\\
&\hat{\Phi}_{00}=0, && \hat{G}_{00}=0,\\
&\hat{\varphi}_{01}=(\mathrm{cth}\,\delta)\xi, && \hat{\theta}_{01}=0,
\end{aligned} \tag{2.16}$$

$$\hat{\psi}_{01}=\frac{1+i}{2\,\mathrm{sh}^2\delta}\,\mathrm{sh}[\delta(z-1)],\qquad \hat{T}_{01}=0,$$

$$\hat{\Phi}_{01}=\frac{1+i}{2\,\mathrm{sh}\,\delta}[e^{-(1-i)\zeta}\cdot(1-i)\zeta-1],\quad \hat{G}_{01}=0.$$

It can be seen from expressions (2.16) that already in these approximations the vorticity of the observed velocity wave field is different from zero. However, in the future to compute the stationary effects induced by the wave fields it is necessary to find the solutions for the two following approximations for α. The equations and the boundary conditions for them have the form

$$\left(\frac{\partial^2}{\partial\xi^2}+2i\right)\frac{\partial^2}{\partial\xi^2}\hat{\varphi}_{0n}=2i\delta^2\left(\hat{\varphi}_{0n-2}-i\frac{\partial^2}{\partial\xi^2}\hat{\varphi}_{0n-2}-i\frac{\beta_0}{\delta}\hat{\theta}_{0n-1}\right), \tag{2.17}$$

$$\hat{\varphi}_{0n}(0)=0,\quad \frac{\partial^2\hat{\varphi}_{0n}}{\partial\xi^2}(0)=-(3-n)\delta,$$

$$\left(\frac{\partial^2}{\partial\xi^2}+2iP\right)\hat{\vartheta}_{0n}=\delta^2\hat{\vartheta}_{0n-2},\qquad \hat{\vartheta}(0)=0,$$

$$\left(\frac{\partial^2}{\partial z^2}-\delta^2\right)\hat{\psi}_{0n}=\frac{i}{2}\left(\frac{\partial^4}{\partial z^4}-2\delta^2\frac{\partial^2}{\partial z^2}+\delta^4\right)\hat{\psi}_{0n-2}-\delta\beta_0\hat{T}_{0n-2},$$

$$\hat{T}_{0n}=\frac{i}{2P}\left(\frac{\partial^2}{\partial z^2}-\delta^2\right)\hat{T}_{0n-2},$$

$$\left(\frac{\partial^2}{\partial\zeta^2}+2i\right)\frac{\partial^2\hat{\Phi}_{0n}}{\partial\zeta^2}=2i\delta^2\left(\hat{\Phi}_{0n-2}-i\frac{\partial^2\hat{\Phi}_{0n-2}}{\partial\zeta^2}-i\frac{\beta_0}{\delta}\hat{G}_{0n-2}\right),$$

$$\hat{\Phi}_{0n}(0)=0,\qquad \frac{\partial\hat{\Phi}_{0n}}{\partial\zeta}(0)=0,$$

$$\left(\frac{\partial^2}{\partial\zeta^2}+2iP\right)\hat{G}_{0n}=\delta^2\hat{G}_{0n-2},\qquad \hat{G}_{0n}(0)=0,$$

where n = 2, 3.

In addition to the boundary conditions entering into (2.17), the joining conditions for the external and internal solutions are additional. Here we will cite only the final form of the solutions, omitting unwieldy intermediate computations and the joining procedure

$$\hat{\varphi}_{02}=-i\delta e^{(1-i)\xi}-i\frac{\delta\beta_0\vartheta e^{i\tau}}{2(P-1)}\left(e^{(1-i)\xi}-\frac{1}{P}e^{(1-i)\sqrt{P}\xi}\right)+$$
$$+\frac{\delta}{2}\xi^2+\frac{(1+i)\delta}{2\,\mathrm{sh}^2\delta}\xi+\frac{i\delta}{2}\left(2+\frac{\beta_0\vartheta}{P}e^{i\tau}\right),$$

$$\hat{\psi}_{02}=\frac{i\delta}{2\,\mathrm{sh}\,\delta}\left[\left(2+\frac{\beta_0\vartheta}{P}e^{i\tau}\right)\mathrm{sh}\,\delta z+\frac{\mathrm{cth}\,\delta}{\mathrm{sh}\,\delta}\mathrm{sh}[\delta(z-1)]\right] \qquad (2.18)$$

$$\hat{\Phi}_{02}=-\frac{i\delta\,\mathrm{cth}\,\delta}{2\,\mathrm{sh}\,\delta}[1-(1-i)\xi-e^{-(1-i)\xi}],$$

$$\hat{\vartheta}_{02}=\frac{(1+i)\delta^2\vartheta e^{i\tau}}{4\sqrt{P}}\xi e^{(1-i)\sqrt{P}\xi},\qquad \hat{T}_{02}=\hat{G}_{02}=0,$$

$$\hat{\varphi}_{03}=\frac{i\delta^2\,\mathrm{cth}\,\delta}{2}\left(2+\frac{1}{\mathrm{sh}^2\delta}+\frac{\beta_0\vartheta}{P}e^{i\tau}\right)\xi+\frac{\delta^2\,\mathrm{cth}\,\delta}{6}\xi^2,$$

$$\hat{\psi}_{03}=-\frac{(1-i)\delta^2}{4\,\mathrm{sh}^2\delta}\left(\frac{3}{2}+\mathrm{cth}^2\delta+\frac{\beta_0\vartheta}{P}e^{i\tau}\right)\mathrm{sh}[\delta(z-1)],$$

$$\hat{\Phi}_{03}=\left[-\frac{(1-i)\delta^2}{4\operatorname{sh}\delta}\left(\frac{5}{2}+\operatorname{cth}^2\delta+\frac{\beta_0\vartheta}{P}e^{i\tau}\right)-\frac{i\delta^2}{4\operatorname{sh}\delta}(1+i+\zeta)\right]e^{-(1-i)\zeta}+$$
$$+\frac{\delta^2}{6\operatorname{sh}\delta}\zeta^3-\frac{\delta^2(1+i)}{4\operatorname{sh}\delta}\zeta^2+\frac{i\delta^2}{2\operatorname{sh}\delta}\left(2+\operatorname{cth}^2\delta+\frac{\beta_0\vartheta}{P}e^{i\tau}\right)\zeta+$$
$$+\frac{(1-i)\delta^2}{4\operatorname{sh}\delta}\left(\frac{3}{2}+\operatorname{cth}^2\delta+\frac{\beta_0\vartheta}{P}e^{i\tau}\right),$$
$$\theta_{03}=T_{03}=\hat{G}_{03}=0.$$

Thus, we have found four approximations of the nonstationary parts of the stream function and temperature. The internal solutions characterize the distribution of the pulsating velocity and temperature fields in the surface and boundary layers and the external solution -- in the main layer of the fluid. Before proceeding to an examination of the stationary effects we will discuss the solutions obtained.

The solutions, obtained on the basis of all the determined approximations, uniformly suitable in the entire region, have the following form:

$$\tilde{\psi}(z)=\frac{\operatorname{sh}\delta z}{\delta\operatorname{sh}\delta}+\alpha\frac{1+i}{2\operatorname{sh}\delta}\left[\frac{\operatorname{sh}[\delta(z-1)]}{\operatorname{sh}\delta}+e^{-(1-i)z/\alpha}\right]+$$
$$+\alpha^2\frac{i\delta}{2}\left\{\left(2+\frac{\beta_0\vartheta}{P}e^{i\tau}\right)\frac{\operatorname{sh}\delta z}{\operatorname{sh}\delta}+\frac{\operatorname{cth}\delta}{\operatorname{sh}\delta}\frac{\operatorname{sh}[\delta(z-1)]}{\operatorname{sh}\delta}-\right.$$
$$-2e^{(1-i)(z-1)/\alpha}-\frac{\beta_0\vartheta e^{i\tau}}{(P-1)P}\left[Pe^{(1-i)(z-1)/\alpha}-e^{(1-i)\sqrt{P}(z-1)/\alpha}\right]+$$
$$\left.+\frac{\operatorname{cth}\delta}{\operatorname{sh}\delta}e^{-(1-i)z/\alpha}\right\}+\alpha^3\left\{-\frac{(1-i)\delta^2}{4\operatorname{sh}\delta}\left(\frac{3}{2}+\operatorname{cth}^2\delta+\frac{\beta_0\vartheta}{P}e^{i\tau}\right)\left(\frac{\operatorname{sh}[\delta(z-1)]}{\operatorname{sh}\delta}+\right.\right.$$
$$\left.+e^{-(1-i)z/\alpha}\right)+\frac{(1-i)\delta^2}{8}\left[2e^{-(1-i)(z-1)/\alpha}+\frac{\beta_0\vartheta}{(P-1)P\sqrt{P}}(P\sqrt{P}e^{-(1-i)(z-1)/\alpha}-\right.$$
$$\left.\left.-e^{(1-i)\sqrt{P}(z-1)/\alpha}\right)\right](z-1)+\frac{(1-i)\delta^2\operatorname{cth}\delta}{8\operatorname{sh}\delta}ze^{-(1-i)z/\alpha}\Big\},\qquad(2.19)$$
$$T(z)=\vartheta e^{i\tau}e^{(1-i)\sqrt{P}(z-1)/\alpha}\left[1+\alpha\frac{\delta^2(1+i)}{4\sqrt{P}}(z-1)\right].\qquad(2.20)$$

It follows from (2.19) that the fluctuations of the heat field, caused by surface waves, in turn exert an influence on the value and distribution of the velocity wave field. This contribution has the order of magnitude $0(\alpha)$ and is especially important in the boundary layers. It is interesting to note that the temperature field exerts its main influence on the horizontal component of the velocity field; on the vertical component this influence is an order of magnitude less, that is $0(\alpha^2)$. This can

be attributed to the fact that the gradient of fluctuations of the temperature field in a horizontal direction is of the same order of magnitude as in a vertical direction, but along the vertical the diffusion of heat occurs at a lesser rate than its transfer along the horizontal.

Expressions (2.16), (2.18), (2.19) indicate that in the upper boundary layer there is an appreciable phase shift between fluctuations of the temperature field and the stream function (that is, the vertical velocity component). This phase shift should give rise to an averaged wave heat flow in the vertical direction. In addition, the wave velocity field has a non-zero vorticity. This leads to a stationary flux of momentum and appearance of another secondary effect -- stationary flow.

3. Field of Stationary Velocities

Equations (1.6), (1.7) and the boundary conditions (1.8)-(1.12) describe the total fields of velocity and temperature, including both fluctuating and secondary stationary parts. The solution for the first of them was obtained in the preceding section. In order to determine the stationary parts of the fields we will represent the stream function and temperature in the form

$$\psi(x, z, t)=\tilde{\psi}(x, z, t)+\bar{\psi}(z), \quad T(x, z, t)=\tilde{T}(x, z, t)+\bar{T}(z), \tag{3.1}$$

where the wavy line denotes waves fluctuating with frequency and the line denotes functions nondependent on time. Substituting (3.1) into the initial equation of motion along the x coordinate and averaging for the period of wave motion (or, which is identical in this case, in the phase from 0 to 2π), as

$$\bar{f}=\frac{1}{T}\int_{t_0}^{t_0+T} f\,dt.$$

we obtain

$$\frac{\alpha^2}{2}\frac{\partial^3\bar{\psi}}{\partial z^3}=-\varepsilon\overline{\frac{\partial(\tilde{\psi}, \partial\tilde{\psi}/\partial z)}{\partial(x, z)}}, \tag{3.2}$$

which corresponds to a second-degree equation for mean velocity; therefore, for $\bar{u}=\partial\bar{\psi}/\partial z$ it is necessary to have two boundary conditions. They are obtained by expansion of condition (1.8) into a Taylor series relative to z = 1 with successive averaging of the result of the expansion by period and condition (1.11). Performing these operations, we have

$$\frac{\partial^2\bar{\psi}}{\partial z^2}=-\frac{\varepsilon}{\delta}\left[\overline{\frac{\partial^3\psi}{\partial z^3}\cos(x-t)}-\delta^2\overline{\frac{\partial^3\psi}{\partial x^2\partial z}\cos(x-t)}+\right.$$

$$\left.+4\delta^2\overline{\frac{\partial^3\psi}{\partial x\partial z}\sin(x-t)}\right] \quad \text{when } z=1, \tag{3.3}$$

$$\frac{\partial\bar{\psi}}{\partial z}=0 \quad \text{when } z=0. \tag{3.4}$$

It follows from (3.2) that the temperature field exerts no direct influence on mean velocity. There is only an implicit dependence of $\tilde{\psi}$ on $\tilde{T}$ through the function $\tilde{\psi}$. Accordingly, the mean velocity field can be computed independently of $\tilde{T}$.

Taking into account that only the real part has physical sense, omitting intermediate computations, we immediately write a final expression for mean velocity, being a solution of the problem (3.2)-(3.4), in which $\tilde{\psi}$ is determined by formula (2.19)

$$\begin{aligned}\bar{u} = -\frac{\varepsilon}{\alpha}\Bigg\{&\frac{\sqrt{2}}{2\delta\,\mathrm{sh}^2\delta}e^{-z/\alpha}\,\mathrm{sh}\,\delta z\sin\left(\frac{z}{\alpha}+\frac{\pi}{4}\right)+\frac{\beta_0\vartheta\sin\left(\gamma+\frac{\pi}{4}\right)}{\sqrt{2}P}z\Bigg\}+\\ &+\varepsilon\Bigg\{\frac{\mathrm{sh}\,\delta z}{\mathrm{sh}\,\delta}e^{(z-1)/\alpha}\cos\frac{z-1}{\alpha}-\frac{\beta_0\vartheta\,\mathrm{sh}\,\delta z}{2(P-1)\,\mathrm{sh}\,\delta}\Bigg[\frac{1}{P}\cos\left(\sqrt{P}\frac{z-1}{\alpha}-\gamma\right)\times\\ &\times e^{\sqrt{P}(z-1)/\alpha}-\cos\left(\frac{z-1}{\alpha}-\gamma\right)e^{(z-1)/\alpha}\Bigg]+\frac{e^{-z/\alpha}}{2\,\mathrm{sh}^2\delta}\Bigg[z\frac{\delta\,\mathrm{sh}\,\delta z}{2}\cos\frac{z}{\alpha}+\\ &+\frac{\mathrm{sh}[\delta(z-1)]}{\mathrm{sh}\,\delta}\sin\frac{z}{\alpha}-\mathrm{ch}\,\delta z\cos\frac{z}{\alpha}\Bigg]+\frac{e^{-z/\alpha}}{4\,\mathrm{sh}^2\delta}+\\ &+\frac{\delta\,\mathrm{cth}\,\delta}{2}\left(4+\frac{\beta_0\vartheta\cos\gamma}{P}\right)z+\frac{1}{4\,\mathrm{sh}^2\delta}\Bigg\}.\end{aligned}\tag{3.5}$$

The solution (3.5) shows that the temperature fluctuations caused by surface waves make a substantial increment to the field of mean velocities generated by waves.

Thus, surface waves are propagated in a shear current, the reason for whose appearance was the surface waves themselves. It follows from (3.5) that with some wave parameters the values and vertical gradients of the mean velocities can attain considerable values in the surface layer of the sea. Then it is natural to assume that this can be one of the reasons for the appearance of instability and destruction of surface waves, that is, generation of turbulence in the surface layer of the sea.

Formula (3.5) expresses the velocity of the mean flow in a Euler representation. In order to compute the velocity of transport of masses by waves (Lagrangian velocity of motion of fluid particles) it is possible to use the Longuet-Higgins formula [11]

$$V_A = \bar{u} + \overline{\frac{\partial\tilde{u}}{\partial x}\int\tilde{u}\,dt} + \overline{\frac{\partial\tilde{u}}{\partial z}\int\tilde{w}\,dt}.\tag{3.6}$$

This gives

$$V_A = -\frac{\varepsilon}{\alpha}\frac{\beta_0\vartheta\sin\left(\gamma+\frac{\pi}{4}\right)}{\sqrt{2P}}z+\varepsilon\left\{\frac{\beta_0\vartheta\,\mathrm{sh}\,\delta z}{2P\,\mathrm{sh}\,\delta}\cos\left(\sqrt{P}\frac{z-1}{\alpha}-\gamma\right)\times\right.$$
$$\times e^{\sqrt{P}(z-1)/\alpha}+\frac{e^{-z/\alpha}}{2\,\mathrm{sh}^2\delta}\left[-3\,\mathrm{ch}\,\delta z\cos\frac{z}{\alpha}+\frac{2\,\mathrm{sh}[\delta(z-1)]}{\mathrm{sh}\,\delta}\sin z/\alpha\right]+ \qquad (3.7)$$
$$\left.+\frac{3e^{-2z/\alpha}}{4\,\mathrm{sh}^2\delta}+\frac{\mathrm{ch}\,2\delta z}{4\,\mathrm{sh}^2\delta}+\frac{1}{4\,\mathrm{sh}^2\delta}+\frac{\delta\,\mathrm{cth}\,\delta}{2}\left(4+\frac{\beta_0\vartheta\cos\gamma}{P}\right)z\right\}.$$

It follows from (3.7) that in the transport of masses the fluctuating temperature field plays a still greater role, since the term $O(\varepsilon/\alpha)$ is related specifically to thermal fluctuations and disappears when $\vartheta = 0$. Here, however, it must be emphasized that these conclusions were drawn on the basis of a quasilinear approximation in which the entire analysis is made. In order to investigate these important effects more precisely, the nonlinear problem must be solved.

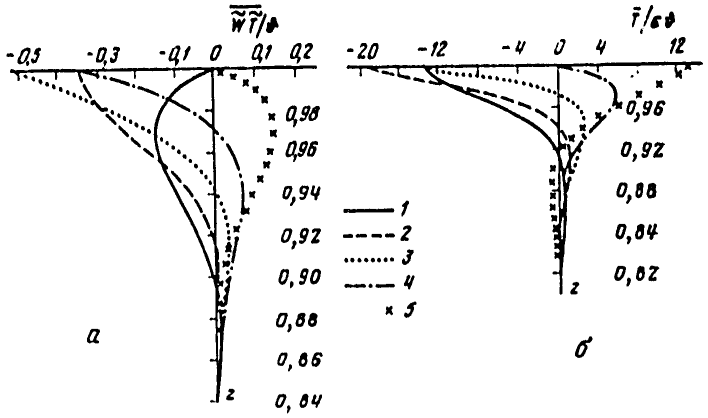

Figure. Depth distribution of stationary heat flows caused by waves (a) and mean temperature (b), caused by a stationary wave heat flow: 1) $\gamma = 0$, 2) $\gamma = \pi/4$, 3) $\gamma = \pi/2$, 4) $\gamma = 3\pi/4$, 5) $\gamma = \pi$; z was normalized at the fluid depth d

4. Averaged Heat Flow and Stationary Temperature Field

The solutions for the nonstationary velocity field (2.19) and temperature (2.20) make it possible to determine, as a function of z, the averaged heat flow in a vertical direction caused by waves. Making the corresponding computations, we have

$$\overline{\tilde{w}\tilde{T}} = \frac{\vartheta}{2\delta}\frac{\operatorname{sh}\delta z}{\operatorname{sh}\delta}e^{\sqrt{P}(z-1)/\alpha}\sin\left(\sqrt{P}\frac{z-1}{\alpha}-\gamma\right), \tag{4.1}$$

where, as a simplification, only the main term of the expansion has been retained.

It follows from (4.1) that in the neighborhood $z = 1 + \alpha(n\pi + \gamma)/\sqrt{P}$ the stationary flow is minimum. It follows that the nonmonotonicity of attenuation with depth for the averaged vertical heat flow, caused by the surface waves, is determined by the phase shift between the surface and the heat wave, and also by the viscosity parameter α, determined by the phase shift between the surface and heat wave, and also by the viscosity parameter α characterizing the degree of wave turbulence. It also follows from formula (4.1) that the rate of attenuation of the wave heat flow with depth is dependent on wave frequency. The flow caused by the high-frequency part of the spectrum attenuates more rapidly, so that the maximum of the spectrum of the averaged wave heat flow with depth should be displaced in the direction of the low frequencies. This conclusion agrees with actual observations made in the ocean.

In the figure a represents the depth distribution of the averaged wave heat flow for different values of the phase shift between the rise in sea level and the amplitude of the thermal disturbance in it when $\alpha = 0.1$, $\delta = 1$, $P = 7$. The figure does not show the flow itself, but the value $Q = \overline{\tilde{w}\tilde{T}}/\vartheta$. It can be seen that both the value and the depth distribution of Q are essentially dependent on γ. When $\gamma = 0$ the maximum of the wave heat flow is situated within the fluid, that is, in this case the main role in heat transfer through the water-air discontinuity is played by diffusion. But already at a shallow depth, when a phase shift appears between the wave velocities and the wave part of temperature, the mechanism of vertical wave heat transport is activated. With other values of the phase shift this process plays a significant role in the upper boundary layer, including the discontinuity itself (all experiments made up to this time show that under real conditions $\gamma \neq 0; \pi$). It is of interest to compare the values of the heat flows caused by wave transport with flows due to evaporation and contact heat transfer. It is known that the mean climatic values of the heat flows in the equatorial and tropical regions of the ocean, caused by the last two mechanisms, are equal to [14] ~400-500 and 40-50 cal/cm^2·day respectively. However, the wave flow Q, computed from (4.1) for waves characterized by the parameters a = 0.5 m, $\omega = 1$ sec^{-1}, $\theta_0 = 10^{-3}$ degree, $\gamma = 1°$, is equal to $Q \approx 38$ cal/cm^2·day, that is, the effect of the wave mechanism for heat transport can be comparable with contact heat transfer. Thus, the process of wave heat transfer through the ocean-atmosphere discontinuity and in the entire upper boundary layer plays an important role, which agrees with the conclusions drawn on the basis of observations [5].

Since there is a wave-produced stationary heat flow in a vertical direction, it naturally forms "its" secondary stationary temperature field. The wave flow is a significant function of depth. Accordingly, the stationary temperature field formed by it also changes with depth, that is, there is a vertical gradient of the stationary temperature field, and as a result, a diffusion stationary heat flow in the vertical direction $Q_g = -\varkappa \partial \overline{T} / \partial z$ also arises. Much as the equation for stationary velocity was derived, by averaging (1.7) we obtain the following equation describing the stationary temperature field

$$\frac{\alpha^2}{2P}\frac{\partial^2 \overline{T}}{\partial z^2} = -\varepsilon \overline{\frac{\partial(\tilde{\psi}, \tilde{T})}{\partial(x, z)}}. \tag{4.2}$$

Since in the considered case the stationary heat exchange between the atmosphere and ocean is accomplished only due to two mechanisms -- wave transport and stationary diffusion, in the steady case, which is investigated here, the total heat flow caused by them must be equal to zero; otherwise there will be heating or cooling of the fluid. In dimensionless form this condition has the form

$$-\frac{\alpha^2}{2P\varepsilon}\frac{\partial \overline{T}}{\partial z} + \overline{\tilde{w}\tilde{T}} = 0. \tag{4.3}$$

In addition, according to (4.1), the wave heat flow attenuates exponentially with depth. Accordingly, the stationary field formed by it also should attenuate exponentially with increasing distance from the water-air discontinuity. Therefore, we require that

$$\overline{T} = 0 \text{ when } z = 0. \tag{4.4}$$

The solution of the problem (4.2)-(4.4) is

$$\overline{T}(z) = \frac{\varepsilon}{\alpha}\frac{\vartheta}{\delta}\frac{\gamma\overline{P}}{\sqrt{2}}\frac{\operatorname{sh}\delta z}{\operatorname{sh}\delta} e^{\sqrt{P}(z-1)/\alpha} \sin\left(\gamma\sqrt{P}\frac{z-1}{\alpha} - \gamma - \frac{\pi}{4}\right). \tag{4.5}$$

In the figure b represents the distribution of mean temperature with depth, computed using formula (4.5) for $\alpha = 0.1$, $\delta = 1$, P = 7 for different γ values. It can be seen that with all γ values there are clearly expressed stationary boundary layers adjacent to the discontinuity. Within the limits of these layers the temperature changes sharply with depth, forming a surface heat film. Depending on γ this film can be "cold" or "warm." Unfortunately, there are no experimental results which represent the changes in film characteristics as a function of γ. Laboratory experiments have been made in which studies were made of the properties of the surface temperature film, but in [4] they were subjected to criticism and the conclusions drawn on their basis were then questionable. Thus, for checking the derived theoretical expressions there must be a purposeful experiment. According to (4.5), under realistic conditions (with $\alpha = 0.1$, $\varepsilon = 0.05$, P = 7, $\delta = 1$, $\vartheta = 10^{-2}$) at the surface of the fluid $\overline{T} \approx 3 \cdot 10^{-3}$ °C. With

$\varepsilon = 0.1, \vartheta = 10^{-1}$ and these same values of the other parameters $\overline{T} \approx 10^{-1}$ °C. Accordingly, surface waves can exert an appreciable influence on formation of the surface temperature film.

If the solution (4.5) is rewritten in dimensional variables, it can be seen that the mean temperature value is inversely proportional to $(\lambda)^{1/4}$, where λ is the wavelength. At the same time, the rate of its attenuation with depth increases with a decrease in λ (the exponent is proportional to $\lambda^{-1/2}$). It therefore can be concluded that the greatest influence on the structure of the surface film should be exerted by short waves and this influence will be greater when their contribution to the total spectrum increases.

Summary

Thus, the solutions show that the stationary vertical heat flow observed in the sea, caused by surface waves, is a joint effect of the nonpotentiality and nonlinearity of the surface waves. Allowance for these factors makes it possible to obtain such peculiarities as the shift of the spectral maximum of the wave heat in the direction of the low frequencies with increasing distance from the ocean surface, its nonmonotonic attenuation, etc. The first peculiarity is confirmed experimentally; for the time being there is no clarity concerning the second.

On the basis of the solutions obtained above it can be concluded that this mechanism is important and it must be taken into account in a study of the peculiarities of the temperature field in the surface layer of the ocean. When the sea surface is in a seeming undisturbed state, in actuality there are capillary waves and they should create a stationary temperature boundary layer -- its thermal film; specifically the effect of short waves here is more important. It is desirable to check this result experimentally. In addition, since an investigation of the properties of the surface thermal film is of great importance in the problem of analysis and interpretation of hydrometeorological data, obtained from satellites and other remote vehicles, there is a need for purposeful experimental and theoretical investigations of this problem.

We emphasize in conclusion that the considered mechanism of the genesis of the stationary temperature boundary layer adjacent to the sea surface is only one of the factors forming the temperature film in the presence of surface waves. In this study we solved the problem in a quasilinear approximation for waves having a small steepness, formulated in a Cartesian coordinate system. However, it is clear that for a more precise description and detailed analysis of the studied effects it is necessary to take into account more fully the nonlinear character of the wave motion and use an orthogonal curvilinear coordinate system tied in to wave movement. In addition, it is also necessary to take into account the initial stratification of the fluid caused by radiation, the absorption of salts and other factors.

BIBLIOGRAPHY

1. O'Brien, E. E., "On the Flux of Heat Through Laminar Wave Liquid Layers," J. FLUID MECH., 28, Part 2, 1967.

2. O'Brien, E. E., Omholt, T., "Heat Flux and Temperature Variation at a Wave Water-Air Interface," JGR, 74, No 13, 1969.

3. Witting, J., "Effect of Plane Progressive Irrotational Waves on Thermal Boundary Layers," J. FLUID. MECH., 50, Part 2, 1971.

4. Witting, J., "Temperature Fluctuations at an Air-Water Interface Caused by Surface Waves," JGR, 77, No 18, 1972.

5. Yefimov, V. V., Zapevalov, A. S., "Spectral Characteristics of Temperature Fluctuations in the Wind Waves Layer," OKEANOLOGIYA (Oceanology), 15, No 4, 1975.

6. Saunders, P. M., "Aerial Measurement of Sea Surface Temperature in the Infrared," JGR, 72, No 16, 1967.

7. Katsaros, K., Liu, Timothy W., Businger, J. A., Tillman, I. E., "Heat Transport and Thermal Structure in the Interfacial Boundary Layer Measured in an Open Tank of Water in Turbulent Free Convection," J. FLUID MECH., 83, Part 2, 1977.

8. Khundzhua, G. G., Andreyev, Ye. G., "Experimental Investigations of Heat Exchange Between the Sea and the Atmosphere in Cases of Small-Scale Interaction," IZVESTIYA AN SSSR, FAO (News of the USSR Academy of Sciences, Physics of the Atmosphere and the Ocean), 10, No 10, 1974.

9. Khundzhua, G. G., Gusev, A. M., Andreyev, Ye. Ye., Gurov, V. V., Skorokhvatov, N. A., "Structure of the Surface Cold Film of the Ocean and Heat Exchange Between the Ocean and the Atmosphere," IZV. AN SSSR, FAO, 13, No 7, 1977.

10. Ginzburg, A. I., Zatsepin, A. G., Fedorov, K. N., "Fine Structure of the Surface Boundary Layer in Water at the Water-Air Discontinuity," IZV. AN SSSR, FAO, 13, No 12, 1977.

11. Longuet-Higgins, M. S., "Mass Transport in Water Waves," PHIL. TRANS., A245, 1953.

12. Dvoryaninov, G. S., "Excitation of Stationary Motion in the Ocean and Atmosphere by Thermal Waves," IZV. AN SSSR, FAO, 12, No 1, 1976.

13. Cole, G., METODY VOZMUSHCHENIY V PRIKLADNOY MATEMATIKE (Perturbation Methods in Applied Mathematics), "Mir," 1972.

14. ATLAS TEPLOVOGO BALANSA OKEANOV (Atlas of Heat Balance of the Oceans), edited by A. G. Kolesnikov, Izd-vo MGI AN UkrSSR, 1970, 88 pages.

5303
CSO: 1870

GEOPHYSICS, ASTRONOMY AND SPACE

UDC 551.241 : [550.312+550.834.32](477+439)

STRUCTURE OF THE CRUST AND UPPER MANTLE IN THE WESTERN UKRAINE BASED ON MATERIALS FROM COMPREHENSIVE INTERPRETATION OF SEISMIC AND GRAVIMETRIC DATA

Moscow GEOLOGICHESKIY ZHURNAL in Russian No 1, 1979 pp 12-22

[Article by A. V. Chekunov and K. A. Bolyubakh]

[Text] Study of the deep structure of the crust and upper mantle of different geological regions of different ages is highly interesting, especially when these regions are immediately adjacent to one another. By comparing differences in the composition, history of formation, and deep structure of these regions we may expect to establish certain empirical patterns that help clarify the mechanism of abyssal processes.

In the western part of the Ukraine, which is crossed by international deep seismic sounding profile III, the situation is especially favorable for solving these questions because this region contains a whole range of sharply differing structures that are related to one another by evolution. From northeast to southwest these structures are the Voronezh Massif, the Dnepr-Donets Depression, the Ukrainian Shield, the Volyn'-Podol'sk Platform, the Subcarpathian Foredeep, the Folded Carpathians, the Transcarpathian Trough, and the Great Hungarian Depression (Pannonian Median Mass).

The study of such diverse structures, and this is true, incidentally, of all tectonic structures in general, can be fully effective only if it is done comprehensively, taking all geological and geophysical information into account. A clarification of just the near-surface geological structure of the sedimentary mantle and upper layers of the basement is no longer satisfactory today, no matter how reliable and detailed it may be, just as establishing the patterns of distribution of just one physical parameter through the entire section of the crust and upper mantle is not satisfactory, even if it is done precisely to great depth. It is necessary to combine studies made by different methods, and not only geophysical methods, for the most diverse regions, especially type regions that differ from one another, and to systematize, compare, and provide comprehensive geological-geophysical-geochemical interpretations of the factual data. After interpreting jointly materials from deep seismometry, gravimetry, and geology for the structures crossed by the

third international deep seismic sounding profile in the Ukrainian SSR and Hungary, the authors of the current report tried to make some contribution to solving this problem.

According to deep seismic sounding data [10-13, 25, and others], the structure of the crust along the third profile is highly variable. Its thickness ranges from structure to structure within broad limits. These changes usually occur abruptly, along fractures that divide the crust into distinct units. Depths to the M discontinuity range from 25 to 65 km. The crust is thinner beneath the Dnepr-Donets Aulacogen (35 km), the Great Hungarian Depression, and the Transcarpathian Trough (25-30 km), and thicker beneath the Flysch Carpathians and Subcarpathian Trough (55-65 km), and beneath the ancient Shepetovka Zone of the Ukrainian Shield (50-55 km). In the rest of the profile the M discontinuity centers around an average depth that is about 40 km. The hypsometric position and thickness of the layers that make up the crust also vary considerably. Depths to the consolidated basement and, correspondingly, the thickness of the sedimentary mantle range from 0 (the Ukrainian Shield) to 10-15 km (Subcarpathian Trough and Carpathians). Because the Conrad discontinuity is unclear at many points, the thickness of the "granitic" and "basaltic" layers cannot always be reliably determined. Nonetheless, it may be stated that the thickness of the "granitic" complex beneath the Ukrainian Shield is large, at least 25-35 km, while the thickness of the "basalt" beneath the Hungarian Depression is very small (3-4 km). In the lower parts of the crust beneath the Carpathians and Subcarpathian Trough is a layer with layer velocity on the order of 7.6 km/sec, intermediate between the velocities in "basalt" and the mantle. This layer appears to correspond to a complex of rocks of mixed crust-mantle composition. The Carpathians as a whole are characterized by general, conformable bedding of all the basic crust boundaries, beginning from the foot of the Flysch complex and ending with the M discontinuity. All these boundaries descend from the Transcarpathians to the Subcarpathian Trough, beneath which they are at maximum depth. The Carpathian "root" is, thus, asymmetrical; it is displaced significantly to the northeast relative to the axis of the mountain structure [10].

The gravitational field in the zone of the third profile is also intricately differentiated. A large regional minimum of gravity with a northwesterly trend stands out distinctly within the Folded Carpathians and Subcarpathian Trough. A large minimum is located in the northeastern part of the profile, within the Ukrainian Shield. South and west of this minimum and also in the Dnepr-Donets Depression and the Transcarpathian Trough there are distinct gravitational maximums. The Great Hungarian Depression and Volyn'-Podol'sk Platform have average values of gravity anomalies. The gravitational field of the large anomalies is complicated by numerous small disturbances.

To construct a deep density cross-section on the basis of the observed gravitational field it is necessary to use data on the structure and physical properties of the crust and upper mantle obtained by other techniques. Without these findings, which are superposed on the desired

density section as constraints, it is possible to calculate an uncountable set of models that satisfy the observed gravitational field [14, 15]. For this reason, the distribution of densities in the upper part of the lithosphere in the regions under consideration was studied on the basis of a deep sounding section [11-13]. The constraints on the density model were not only the geometry of the seismic boundaries but also characteristics of velocity columns that change from one region to another. The use of these columns to determine densities, intervals of their permissible values, and jumps at particular depths was based on the general relationship between velocity and density. This relationship unquestionably exists, although as the result of various factors it is sometimes not very clearly expressed (see Figure 1 below).

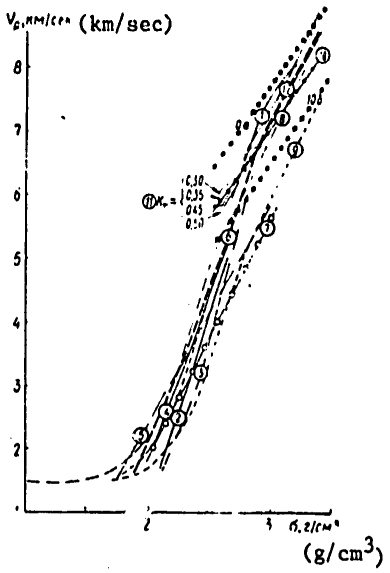

Figure 1. Relationship Between the Velocity of Longitudinal Seismic Waves (P-Waves) and Rock Density (drawn by V. S. Belokurov)

Key: (1) According to I. G. Klushin (1961);
(2) According to N. N. Puzyrev (1959);
(3) According to V. M. Berezkin (1963);
(4) According to B. K. Balavadze and P. Sh. Mindel' (1971);
(5-7) According to N. N. Mikhaylov (1965) --
(5) For the Entire Sedimentary Stratum of the Ukraine from the Devonian to the Paleogene;
(6) For Carbonate Rocks;
(7) For Terrigenous Rocks;
(8) According to D. E. Nef and S. L. Drake (1959);
(9) According to H. V. Menard (1967);
(10) According to M. L. Ozerskaya (1970) for a Pressure of 4 kbar (10a and 10b are the upper and lower boundaries of fluctuation of parameters);
(11) According to M. B. Dortman and N. Sh. Magid (1969) for Different Values of the Texture Coefficient K_t;
(12) Averaged Dependence.

Calculations of sections of the crust and mantle using gravimetric data exclusively, a common practice in the past that is still sometimes done today, must be acknowledged to be unjustified. In such sections the crust is represented as having homogeneous layers (the "granitic" layer with a density of 2.7 g/cm^3) with conformable boundary surfaces, which is not generally confirmed by deep seismic sounding studies. Homogeneous-layer density models compiled on the basis of seismic sections but without considering vertical, lateral, and local changes in density in the layers, which are graphically reflected in velocity sections and columns, are also inadequate.

Densities and permissible intervals of change in density depending on depth were calculated for different segments of the third international deep sounding profile on the basis of data on the distribution of velocities in the crust and the averaging curve (see Figure 1 above and Figure 2 below). The use of such regional graphs $\sigma|H|$, where σ is density and H is depth, made it possible to effectively approach the true distribution of densities in a deep section of the crust and upper mantle. This approximation is not ideal, however, and the graphs are apparently still too generalized because when they were used it was not always possible to achieve full correspondence with observed values for the force of gravity and corrections ranging from ± 0.01 to ± 0.06 g/cm^3 had to be made in the model.

Analysis of the change in the density of rocks in wells with depth compared to data on the densities at great depths showed that the gradient of increase in density observed in the near-surface zone of the crust cannot remain the same, but must decrease considerably. Thus, in the wells of the northwestern part of the Ukrainian Shield, drilled to a depth of 600 m in the sector of the Korosten' Pluton, the gradient in the Rapakivi granite averages 0.08 g/cm^3 per kilometer. If this magnitude were to remain constant, the rock density values at a depth of about 10 km would reach 3.43 g/cm^3, which is unrealistic because such magnitudes are already characteristic of mantle material. According to theoretical calculations, the density of the rock at this depth is not more than 2.85 g/cm^3. It is not impossible that a density inversion may occur in the depth range between 5 and 15-20 km. This is indicated by the discovery of many seismic waveguide regions in this zone of the crust, some within the territory under consideration [3, 13, 25, 27, and others].

The calculated model for the third international deep sounding profile (see Figure 3) is not steeply sloping, nor is it without shortcomings. But it reflects the mosaic, layer-block structure of the crust and takes account of the vertical and lateral variations of density in the layers and blocks. To a significant degree these variations are conditioned by special features of the distribution of velocity parameters. Based on these parameters we may conclude that the drops in density in the upper zones of the crust are much greater than in the lower parts and the underlying mantle. The spectrum of permissible density values narrows with depth. The model under consideration "permits" gravitation by all possible density heterogeneities both in the crust and the mantle, unlike the models of certain authors who attempt (without

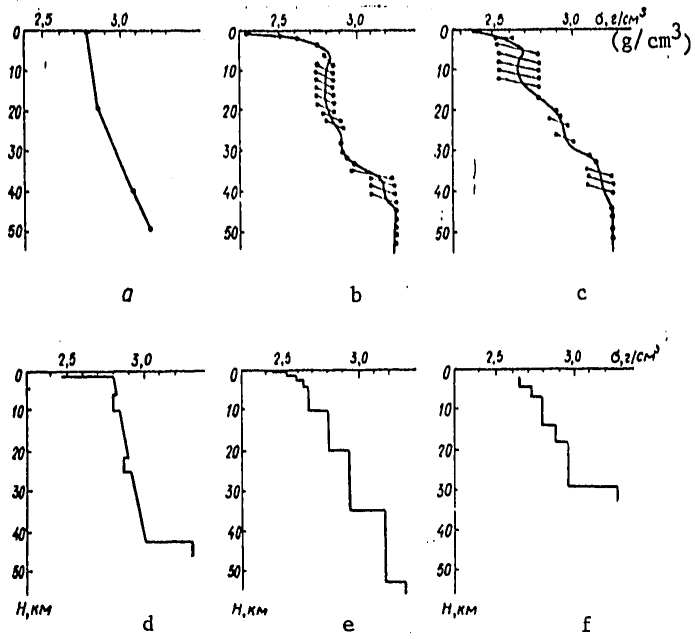

Figure 2. Graphs of the Dependence of Density on Depth.

Key : a) For the Voronezh Masiff (calculated according to T. V. Il'chenko's Velocity Column);
b) For the Dnepr-Donets Depression (according to the findings of K. A. Bolyubakh and A. V. Chekunov);
c) For the Ukrainian Shield (according to the findings of K. A. Bolyubakh and A. V. Chekunov);
d) For the Volyn'-Podol'sk Platform (according to the velocity column of V. S. Geyko and L. P. Livanova);
e) For the Carpathians (according to L. P. Livanova's velocity column);
f) For the Great Hungarian Depression (according to the velocity column of E. Mitukh and K. Pozhgaya).

justification, in our view) to confine all gravitational activity exclusively to the upper part of the crust. There is a sufficient number of indications, obtained by various independent techniques (seismology, deep seismic sounding, calculation of isostatic anomalies, satellite observations, indirect geological data, and the like), of the existence of large deep-crustal and mantle heterogeneities that cannot be ignored. The resolution of the gravimetric method for identification of such heterogeneities decreases with depth, but this does not mean that they do not exist. As for purely gradient-type density models, despite all their unquestioned merits they are only one type of approximation and often fail to take into account the discrete character of the internal structure of the crust, which is manifested in the existence of abyssal

reflections from numerous boundaries where what occurs is not a change in the gradient, but rather a break in the velocity function and an abrupt drop in its values with depth. The optimal density model should, of course, depict both fundamental characteristics of the medium under study, its discreteness and its gradients.

During calculations for the third international deep sounding profile the position of gravitational objects was determined in a three-dimensional variation. The mathematical apparatus of Ye. G. Bulakh and M. N. Markova was used [4]. The interpretation involved determination of the components of the observed gravitational function and eliminating them from the function in sequence. Anamolies caused by petrographic and lithological heterogeneities in the top horizons of the crust were subtracted first. Then the position of the gravitational objects within the crust was determined and the effect created by them was eliminated. As a result of these operations the component of the gravitational field related to density heterogeneities in the upper mantle was isolated. Determination of the center of gravity of the particular anomaly-forming bodies that make up this component yielded depths of 100 km and more. The methodology of this interpretation is set forth in detail in work [2].

It is apparent from the geological-geophysical section (Figure 3) that bodies of increased density, exceeding the average by 0.03-0.25 g/cm^3, stand out in a number of sectors of the upper crust near the basement surface. Such bodies have been noted at the base of the sedimentary stratum of the Transcarpathian Trough, near the deep fracture that separates the trough and the Folded Carpathians, in the region of the Subcarpathian Trough and its zone of connection with the East European Platform, within the Volyn'-Podol'sk Platform, at its contact with the Ukrainian Shield (zone of the Rovno Fault), and in the sectors of the Shepetovka Block and the Korosten' Pluton of the Ukrainian Shield. These bodies differ by geological nature and are not always identified unambiguously. They are caused by density heterogeneities in the lower parts of the sedimentary mantle or upper parts of the basement, possibly in both at the same time.

Some of these heterogeneities have already been outlined earlier. For example, works [7, 16] assumed that there were either quite strongly uplifted blocks of the pre-Cretaceous substrate or thick beds of extrusive rock in sediments lay at the base of the Transcarpathian Trough. In the transition zone between the Subcarpathian Trough and the Volyn'-Podol'sk Platform gneiss strata have been identified in the body of the crystalline foundation in addition to the granitic-migmatic "fabric" [20]. The data now obtained on excess densities confirm that we may expect dense magmatic formations to occur in this region.

Rocks of largely basic composition cause surplus mass in the region of the Korsten' Pluton, the Rovno Fault, and the Shepetovka Block of the Ukrainian Shield. In the Dnepr-Donets Depression certain bodies of increased density are identified on the southwestern side. In the most submerged part of the depression (the graben), the density of the rocks that make up the top of the crystalline substrate increases as one moves from the periphery to the center of the graben.

In the deeper zones of the crust along the third international profile the existence of complex density differentiation of material in a lateral direction is observed. The magnitude of excess density reaches 0.18 g/cm^3. Every region crossed by the profile, and frequently also distinct blocks within them, has its own typical density characteristics. The crust beneath the Great Hungarian Depression and Transcarpathian Trough is generally more dense than beneath the Folded Carpathians and Subcarpathian Trough. The crust is heaviest in the Shepetovka Block of the Ukrainian Shield. The region of the Korosten' Pluton, by contrast, has the lowest density values. The density values beneath the Dnepr-Donets Depression vary within broad limits. Density values that are close to average have been identified beneath segments of the junction of the Subcarpathian Trough and the Volyn'-Podol'sk Platform, the latter with the Ukrainian Shield, and the Dnepr-Donets Depression with the Voronezh Crystalline Masiff.

Identifying the influence of deeper heterogeneities, within the mantle, is a very complex problem. Some general findings, as well as particular (regional) data, make it possible to formulate limiting conditions and, relying on them, to undertake an attempt at its solution. The following is kept in mind.

The depths at which the expected mantle heterogeneities should be located correspond to the usual depths of the asthenosphere layer (the Gutenberg waveguide) so it is logical to conclude that they are, in fact, confined to it. Different authors (9, 28, and others] using different techniques and materials have obtained similar results, putting the roof of the asthenosphere beneath the Carpathians at a depth of 80-90 km. According to the findings of Hungarian researchers [29, 30] it decreases to 60 km under the Great Hungarian Depression. The depth to the foot of the asthenosphere in this region may be considered to be as much as 250 km [1, 8]. The density in the medium surrounding a waveguide is taken to be 3.3 g/cm^3 [6, 17]. In the asthenosphere, which generates basaltic magma and, we assume, consists of 12 percent of this magma [1], the average density of the matter should be lowered accordingly by 0.07 g/cm^3. According to the findings of [1, 19], a waveguide may contain particular interior layers with relatively higher and lower velocities of propagation of elastic waves and, correspondingly, densities. Considering this initial information, calculations were made leading to selection of a model (see Figure 3). Despite the fact that it is certainly quite hypothetical, it correlates quite well with near-surface geological structures.

Lateral changes of density in the asthenosphere appear to be 0.04-0.10 g/cm^3. A definite interrelationship can be identified between the configuration of this layer and distribution of mass within it, on the one hand, and the thickness of the crust investigated by the deep seismic sounding technique on the other. Thus, beneath the Great Hungarian Depression and Transcarpathian Trough, which have thinner crust and are characterized by high thermal flow, the roof of the asthenosphere is uplifted, its thickness is greater, and relatively light material

σ = 3.13-3.25 g/cm^3) clearly predominates in it. Beneath the Folded Carpathians and Subcarpathian Trough where the crust is thickest (up to 65 km) and the heat flow is less, the thickness of the asthenosphere waveguide decreases and it contains the largest proportion of dense (σ = 3.43 g/cm^3) masses. Beneath the Dnepr-Donets Depression heavy material (σ = 3.45 g/cm) in the asthenosphere predominates over light material (σ = 3.15-3.25 g/cm^3). The vertical thickness of the waveguide is minimal (or it may possibly be completely absent) beneath the structures with average crustal thickness and low thermal flow (the Volyn'-Podol'sk Platform, the Ukrainian Shield, and the Voronezh Massif).

These relationships between the structure of the crust and distribution of mass at great depth correspond well to S. I Subbotin's ideas [16-18] concerning the existence of zones of compacted and de-compacted mantle beneath these structures. It is very suggestive that the asthenosphere is thickest, least compacted, and most "disturbed" beneath the region of active, young tectonic deformations and volcanic activity in the Carpathians, that relicts of former activity can still be discerned beneath the older Dnepr-Donets Depression, and that such signs are essentially absent under the long-consolidated, ancient structures of the Ukrainian Shield and Voronezh Massif, where the very existence of a softened asthenosphere is problematic. Against the background of these characteristics, the location of the Eastern Carpathians seems natural; this folded structure occurred at exactly the place where the most active, "live" part of the asthenosphere joins with its most passive, virtually "extinct" part.

The asthenosphere layer does not differ by parameters only beneath different geological structures; it is plain that significant changes in this layer also occur at the contacts between them, which correspond to major, deep fractures. These contacts are the zones of articulation of the Transcarpathian Trough and the Folded Carpathians (the Peripenine Lineament), the Subcarpathian Trough and the East European Platform, the Volyn'-Podoi'sk Platform and the Ukrainian Shield (the Rovno Fault), the Ukrainian Shield and the Dnepr-Donets Depression, and this depression in the Voronezh Massif. The roots of the deep faults, which arise in the mantle, fracture the entire thickness of the crust [17, 18, 26, and others], and carry basaltic material to the upper layers of the crust (which has been geologically documented in all of the zones listed above) could manifest themselves in such changes in the asthenosphere beneath the zones of articulation of major geological structures.

The material cited, together with the findings of works [5, 23, 25], allow us to take up certain issues of the mechanism of formation of these structures. The increased thickness and uplifted position of the roof of the asthenosphere, saturated with relatively light material, beneath the Great Hungarian Depression, which is characterized by high thermal flow and recent, intensive magmatic activity, testifies to active upsurge beneath the depression of heated and de consolidated mantle material that forms the ascending convection flow or asthenolith.

Apparently it occurred as an abyssal source of heat about 50 million years ago, in the Paleogene [5], as the result of phase, polymorphous, or other transformations of matter [17, 18]. It began rising toward the surface at that time. As time passed and it penetrated less dense horizons of the mantle, its upward movement slowed down and today the roof of the asthenolith is at a depth of about 60 km. The movement of material in it, rising in the center and descending (as the result of cooling and compaction) along the periphery, affected the overlying shell in such a way that the crust was subjected to breaking up, tangential stretching, and pulling apart [23, 25]. Mantle material rose beneath the Hungarian Depressions, then spread in the direction of the Carpathians and, apparently, the Dinarides. The compensating descending branches of advection were located along the outer margin of the Carpathian Folded Arc where the smallest thermal flows in the Carpathian region are observed today. This process has caused significant changes in absolutely all the physical parameters of the lithosphere of this region [5]. Beneath the territory of Hungary, apparently as a result of the existence of a large amount of melted material, the velocities of propagation of elastic waves are lowered, the matter is less compact, and electrical conductivity is greater. The Curie isotherm is abruptly uplifted here also. All this caused corresponding geophysical anomalies. The high temperatures created favorable conditions in the crust for the formation of zones of partial melting beneath the Transcarpathian Trough, which is confirmed by the existence there of zones of heightened electrical conductivity and seismic waveguides.

Under the influence of the abyssal mechanism described, the crust of the Carpathian Region has experienced profound transformations. Geologically speaking, they have been very rapid because they have taken place in just the concluding orogenic phase of the Alpine stage, a comparatively short period but one with such important consequences that a reconstruction of even the very recent pre-orogenic structure of the crust of the region is complicated. As a result of these transformations, the following characteristics of the deep structure of the region emerged [23, 25]: 1) the M discontinuity is lowest beneath the Subcarpathian Trough and the Skibovaya Zone of the Carpathians, with depths decreasing uniformly toward the Great Hungarian Depression where they have their minimum values; 2) the Conrad discontinuity is deepest beneath the Subcarpathian Trough; 3) the surface of the "granitic" layer (basement) is lowest beneath the Interior Zone of the Subcarpathian Trough; 4) the primary crustal boundaries in the Volyn'-Podol'sk Platform and in the Carpathians generally lie conformably; 5) the thickness of the "basaltic" layer beneath the Great Hungarian Depression is sharply reduced; 6) the deep fractures along the southwest margin of the East European Platform descend toward the northeast, under the platform; 7) the fractures in the Outer Carpathians, according to geological data, dip to the southwest; 8) the Flysch strata of the Outer Carpathians have been thrust to the northeast, in the direction of the Subcarpathian Trough, and the degree of thrusting increases closer to the trough; 9) magmatic rocks, chiefly of basic composition, are widely developed in the Great Hungarian Depression and Transcarpathian Trough, whereas they are not characteristic

of the Subcarpathian Trough and Flysch Carpathians. These characteristic features are explained by the rising of abyssal, heated asthenolith from the asthenosphere accompanied by a warming of the lithosphere followed by horizontal seepage of the uplifted material in the subcrustal area and a compensatory downflow to the depth of comparatively cold lithosphere bodies, that is, in general, the mechanism described above.

The tangential stretching forces in the crust of the region occurred in the final stage of the rising of the asthenolith, during its outward flow. These stresses led in the Neogene to formation of the Great Hungarian Depression and Transcarpathian Trough in place of the Baikalian, Paleozoic, and Mesozoic folded structures. Stretching accompanied by downwarping of the basement caused the crust to be pulled apart and led to the formation of zones of lowered pressure. Faults opened channels for magma from the mantle to enter; they opened up the partial melting chambers that existed in the crust as the result of heating or caused them to occur by reducing pressure in a high-temperature setting. This caused considerable volcanic activity in the interior zones of the Carpathian Region. As a result of the stretching and heating up, it appears that the "basaltic" layer largely melted and a significant part of its matter, together with the mantle matter in the form of magma, chiefly of basic composition, was forced into the upper layers of the crust, including the sedimentary layer. The result of this process is the almost complete absence of a "basaltic" layer beneath the Great Hungarian Depression and also the existence, primarily around its periphery, of large masses of rock of magmatic origin. The Beregovo and, especially, Transcarpathian (Peripenine) deep faults are of this type; they opened up deep magmatic centers and thus fueled the volcanic activity of the Vygorlat-Gutinskaya Range and Beregovo Mountains. The dimensions of the Transcarpathian Fault allow us to assume that its "roots" are located directly in the body of abyssal asthenolith.

The tangential forces stretching the crust led to displacement of its matter in the direction of the platforms next to the Carpathians. The Carpathian faults along which this displacement mainly occurred acquired a dip toward the center of the asthenolith, and the further from the center they were, the more gentle the dip was. The tangential, centrifugal movement of crustal masses encountered resistance from the surrounding stable platforms. Because the marginal fractures of the East European Platform descend to the northeast, beneath the platform, while the fractures of the Eastern Carpathians dip to the southwest, a "ramp" type structure formed in the zone of articulation. Tangential compression at the edge of the platform together with the effect of the descending advection branch led to burial of a wedge-shaped (narrower at the top) block of crust. Along with the lowered block the Conrad and M discontinuities as well as the surface of the basement descended. As a result, it is here that the greatest depths to these surfaces are observed. Here too the thickness of the lower layers of the crust is sharply increased as a result of the lateral forcing of crustal material from the Great Hungarian Depression and Transcarpathians and its accumulation. The submerging of the basement led to formation of the narrow Subcarpathian Trough, onto which the Flysch strata of the Carpathians

were thrust. Thus, this trough arose as a result of compression of the crust. Because the Subcarpathian Trough and the part of the Carpathians adjacent to it experienced compression and are located above a relatively cool, descending advection branch, magmatic shows are not characteristic for them.

The mechanism of formation of structures of the Carpathian region that we have described, involving the rising of heated, abyssal asthenolith, its outward flow, and the tangential stresses thus caused in the crust provide a good explanation for the arching bend of the Carpathians in plan view, the asymmetry of the "roots" of the Carpathians and Dinarides which are displaced regularly to the northeast and southwest of the axial parts of these mountain structures respectively, and of the movement of mountain masses away from the Hungarian Depression, a phenomenon universally observed in the Carpathians and Dinarides. The action of the mechanism is not yet completed; it continues to create very intensive fields of mechanical and thermal stresses whose discharge finds expression in seismic activity, modern movements of the crust, and the like.

The heavy ultrabasic components of the asthenolith, set in motion, settled in the descending advection branches, leading to a concentration of dense material in the asthenosphere beneath the Carpathians (see Figure 3).

During formation of the Dnepr-Donets Depression, which is an extension structure [21, 22], abundant basaltic magmatic material came from the asthenosphere into the upper layers of the crust. The ultrabasic material left after the basalt fused now forms a relatively compact medium in the asthenosphere beneath the depression (see Figure 3). The principal channels by which the basaltic magma rose up are confined to the central part of the depression, where the densest varieties of rock are observed in its foundation.

Most of the faults of the Korosten' gabbroid pluton, which is located in the northwestern part of the Ukrainian Shield not far from the Dnepr-Donets Depression, dip very gently the northeast, toward the depression [25]. If we imagine a continuation of these faults to depth, they would join with the asthenosphere center beneath the depression. This circumstance allows us to hypothesize that the beginning of the abyssal process in the mantle that later led to the formation of the Dnepr-Donets Depression dates to the Middle Proterozoic, not to the Riphean or Paleozoic. It is apparent that magmatic activity had already begun then in the zone of the depression. It is possible that magma from a single asthenosphere center penetrated into structures adjacent to the depression along distinct, gently sloping faults. This refers in particular to the Ukrainian Shield where, after cooling at depth, it formed the modern, denuded gabbroid plutons (Korosten', Korsun'-Novomirgorod).

The presence of dense magmatic rocks which were also generated in the asthenosphere layer of the mantle is observed in the zones of

articulation of major structures in other segments of the third international profile such as the Rovno Fault. The zones of articulation are more active; the processes of breakage and magmatic activity were periodically renewed in them.

Comprehensive interpretation of geological and geophysical findings on the deep structure of the outer shell of the earth allows us to obtain additional information that is important for understanding the nature and mechanism of the processes taking place in it.

FOOTNOTES

1. Belousov, V. V., "Zemnaia Kora i Verkhnyaya Mantiya Materikov" [The Crust and Upper Mantle of the Continents], Moscow, Nauka, 1966, 123 pp.

2. Bolyubakh, K. A., "Some Questions of the Methodology of Interpreting Gravitational Findings from the Shepetovka -- Chernigov Deep Seismic Sounding Profile," GEOFIZ. SB. AN USSR 1976, No 69, pp 87-91.

3. Bott, M., "Vnutreneye Stroyeniye Zemli" [The Internal Structure of the Earth], Moscow, Mir, 1974, 373 pp.

4. Bulakh, Ye. G., and Markova, M. N., "Metodicheskoye Rukovodstvo i Sbornik Programm dlya Resheniya Obratnykh Zadach Gravirazvedki na ETsVM 'Minsk-22'" [Methodological Guide and Collection of Programs for Solving Inverse Gravimetric Exploration Problems on the Minsk-22 Computer], Kiev, Nauk. Dumka, 1971, 164 pp.

5. Bur'yanov, V. V., Gordiyenko, V. V., Kulik, S. N., et al, "Comprehensive Geophysical Model of the Lithosphere of the Eastern Carpathians," GEOFIZ. SB. AN USSR, 1978, No 83, pp 3-16.

6. Demenitskaya, R. M., "Osnovnyye Cherty Stroyeniya Kory Zemli po Geofizicheskim Dannym" [Principal Features of the Structure of the Earth's Crust Based on Geophysical Data], Leningrad, Gostoptekhizdat, 1961, 223 pp.

7. Lazarenko, E. A., Gnilko, M. K., and Zaytseva, V. N., "Metallogeniya Zakarpat'ya" [Metallogeny of the Transcarpathian Region], L'vov, Izdatel'stvo L'vov. un-ta, 1968, 173 pp.

8. Magnitskiy, V. A., "Sloy Nizkikh Skorostey Verkhney Mantii Zemli" [The Layer of Low Velocities in the Upper Mantle of the Earth], Moscow, Nauka, 1968, 29 pp.

9. Rudnitskiy, V. P., and Chekunov, A. V., "New Information on the Deep Structure of the Soviet Carpathians Based on Data from Seismic Observations of Converted Waves," GEOL. ZHURN. 1970, Vol 30, No 5, pp 106-111.

10. Sollogub, V. B., and Chekunov, A. V., "The M Discontinuity in the Radyanskiye Carpathians and Neighboring Regions," DAN URSR. SERIYA B, 1967, No 6, pp 494-498.

11. Sollogub, V. B., Chekunov, A. V., Pavlenkova, N. I. et al, "Chief Results and Problems of Studying the Crust of the Ukraine by Seismic Methods," GEOFIZ. SB. AN USSR, 1970, No 38, pp 48-63.

12. Sollogub, V. B., Chekunov, A. V., Mitukh, Ye. et al, "Results of Deep Seismic Sounding on International Profiles" in the book "Stroyeniye Zemnoy Kory Tsentral'noy i Yugo-Vostochnoy Yevropy (po Dannym Vzryvnoy Seismolcgii)" [Structure of the Crust of Central and Southeastern Europe (Based on Data from Explosion Seismology)], Kiev, Nauk. Dumka, 1971, 286 pp.

13. Sollogub, V. B., and Chekunov, A. V., "Deep Structure and the Evolution of the Crust," in the book "Problemy Fiziki Zemli na Ukraine" [Problems of Earth Physics in the Ukraine], Kiev, Nauk. Dumka, 1975, 176 pp.

14. Strakhov, V. N., "Some Examples of Equivalence andWeak Uniqueness in the Plane Inverse Problem of Potential," IZV. AN SSSR. FIZIKA ZEMLI 1973, No 5, pp 39-62.

15. Strakhov, V. N., "Toward a Theory of the Inverse Problem of Logarithmic Potential for a Contact Surface," IZV. AN SSSR. FIZIKA ZEMLI 1974, No 6, pp 39-60.

16. Subbotin, S. I., "Glubinnoye Stroyeniye Sovetskikh Karpat po Dannym Geofizicheskikh Issledovaniy" [Deep Structure of the Soviet Carpathians According to Data from Geophysical Studies], Kiev, Izd-vo AN USSR, 1955, 260 pp.

17. Subbotin, S. I., Naumchik, G. L., and Rakhimova, I. Sh., "Protsessy v Verkhney Mantii Zemli" [Processes in the Upper Mantle of the Earth], Kiev, Nauk. Dumka, 1964, 136 pp.

18. Subbotin, S. I., Naumchik, G. L., and Rakhimova, I. Sh., "Mantiya Zemli i Tektogenez" [The Earth's Mantle and Tectogenesis], Kiev, Nauk. Dumka, 1968, 174 pp.

19. Fedotov, S. A., Matveyeva, N. N., Tarakanov, R. Z., and Yanovskaya, T. B., "The Velocities of Longitudinal Waves in the Upper Mantle in the Region of the Japanese and Kuril Islands," IZV. AN SSSR. SER. GEOFIZ. 1964, No 8, pp 1185-1191.

20. Fil'shtynskiy, L. Ye., "Toward an Interpretation of the Gravity Anomalies of the Western Frontiers of Volyn' and Podolia," in the book "Geofizicheskiye Issledovaniya na Ukraine" [Geophysical Studies in the Ukraine], Kiev, Tekhnika, 1970, pp 158-163.

21. Chekunov, A. V., "TheDnepr-Donets Depression as the Result of Tangential Stretching of the Crust," GEOL. ZHURN, 1966, Vol 36, No 4, pp 30-39.

22. Chekunov, A. V., "The Mechanism of Formation of Aulacogen-Type Structures (with the Example of the Dnepr-Donets Depression)," GEOTEKTONIKA, 1967, No 3, pp 3-18.

23. Chekunov, A. V., "Some Issues of Tectogenesis and Evolution of the Crust," GEOFIZ. SB. AN USSR, 1968, No 26, pp 72-88.

24. Chekunov, A. V., "Symposium on the Physical Properties, Composition and Structure of the Upper Mantle," GEOFIZ. SB. AN USSR, 1972, No 50, pp 77-80.

25. Chekunov, A. V., "Struktura Zemnoy Kory i Tektonika Yuga Yevropeyskoy Chasti SSSR" [The Structure of the Crust and Tectonics of the Southern Part of European USSR , Kiev, Nauk. Dumka, 1972, 176 pp.

26. Chekunov, A. V., and Kuchma, V. G., "The Origin of Faults and Their Manifestation in the Crust of the Ukraine," DAN USSR. SERIYA B, 1976, No 8, pp 702-704.

27. Chekunov, A. V., Livanova, L. P., and Geyko, V. S., "Deep Structure of the Crust and Some Features of the Tectonics of the Transcarpathian Trough," SOV. GEOLOGIYA, 1969, No 10, pp 57-68.

28. Shechkov, B. Ya., and Yurkevich, O. I., "Determining the Thickness of the Crust in the Ukrainian Crystalline Massif by the Dispersion of Surface Waves," GEOFIZ. SB. AN USSR, 1962, No 1 (3), pp 68-75.

29. Adam, A., "The Electric Structure of the Crust and Upper Mantle in Hungary on the Basis of Magnetotelluric and Relative Telluric Frequency Sounding," in Geofiz. kozl. XIII kotet, 2 szam, Budapest, 1964, pp 141-161.

30. Posgay, K., "Mit Reflexionsmessungen bestimmte Horizonte und Geschmindigkeits verteilung in der Erdkruste und im Erdmantel," in Geofiz. kozl., XXIII kotet, Budapest, 1975, pp 13-17.

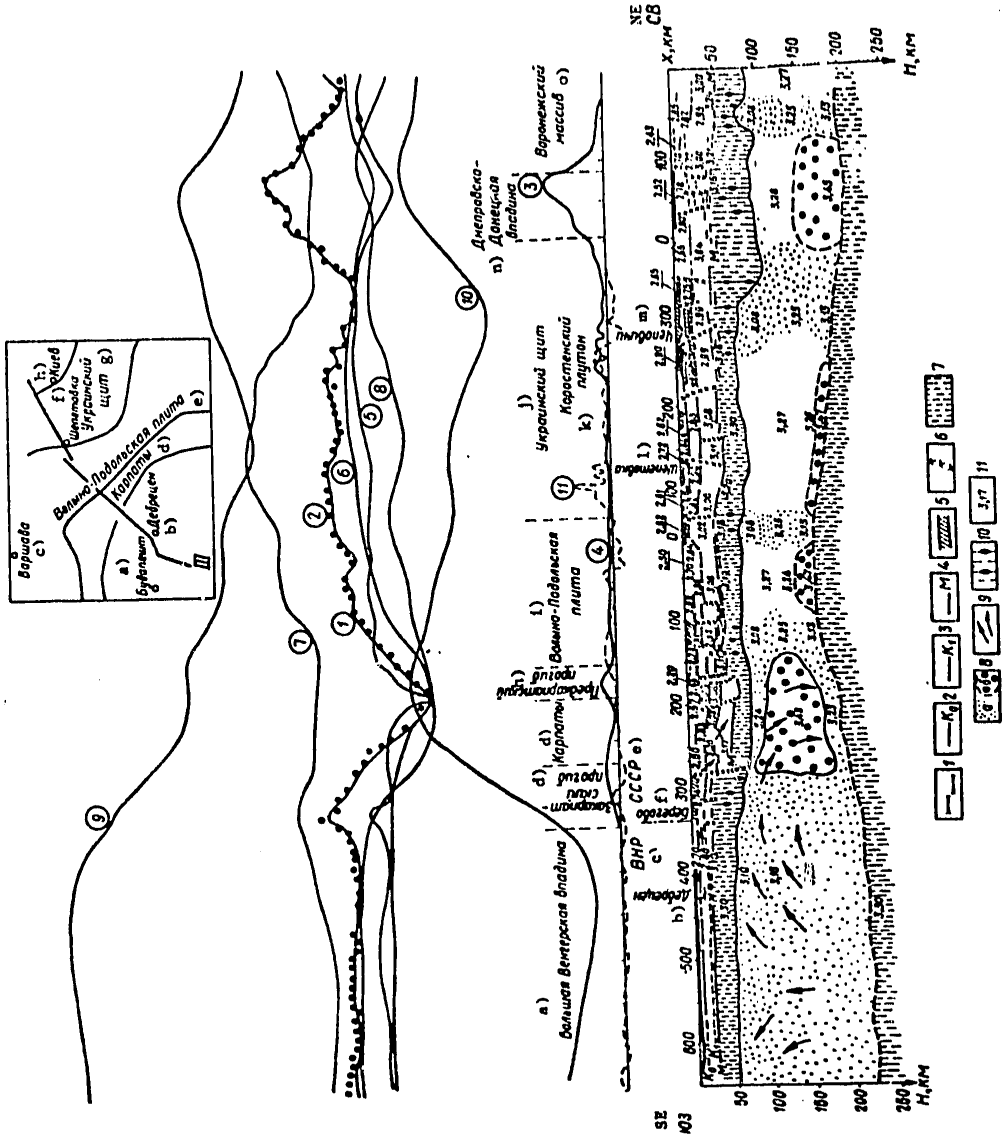

Figure 3. Geological-Geophysical Section of the Crust and Upper Mantle along International Deep Seismic Sounding Profile III.

Key : 1) Crust with Seismic Boundaries According to Deep Seismic Sounding Data;
2) Basement Surface;
3) Conrad Discontinuity;
4) M Discontinuity;
5) Segments of Increased Density in the Crust;
6) Faults;
7) Parts of Mantle above and below Asthenosphere;
8) Asthenosphere with Sectors of Relatively Lower (a) and Higher (b) Density;
9) Direction of Movement of Material in the Mantle and Crust;
10) Basaltoid Magma Channels;
11) Density (g/cm^3).

[Encircled numbers indicate curves of gravity anomalies : 1 — observed; 2 — calculated

Components of curve 2 calculated : 3 — from local bodies; 4 — from larger objects; 5 — from lateral heterogeneities in the sedimentary mantle and basement; 6 — from the "basalt" layer; 7 and 8 — from lateral heterogeneities in the crust; 9 — from the M discontinuity 10) from lateral heterogeneities in the upper mantle; 11 — the curve of the vertical component of an anomalous magnetic field

[Place Names]

a) Great Hungarian Depression;
b) Debrecen;
c) Hungary;
d) Transcarpathian Trough;
e) USSR;
f) Beregovo;
g) Carpathians;
h) Subcarpathian Trough;
i) Volyn'-Podol'sk Platform;
j) Ukrainian Shield;
k) Korosten' Pluton;
l) Shepetovka;
m) Tsepovichi;
n) Dnepr-Donets Depression;
o) Voronezh Masiff.

[Place Names on Small Inset Map]

a) Budapest;
b) Debrecen;
c) Warsaw;
d) Carpathians;
e) Volyn-Podol'sk Platform;
f) Shepetovka;
g) Ukrainian Shield;
h) Kiev.

11176
CSO: 8144/1168-E

GEOPHYSICS, ASTRONOMY AND SPACE

EXPERIENCE GAINED IN COMBINING SEISMIC METHODS IN STUDYING THE NORTHERN EDGE OF THE CASPIAN DEPRESSION

Moscow GEOLOGIYA NEFTI I GAZA in Russian, No 10, 1978 pp 5-9

[Article by T. A. Akishev, R. U. Ashimov, V. P. Komarov, and B. A. Khrychev, Iliyskaya Geophysical Expedition: "Experience Gained in Combining Seismic Prospecting Methods in Studying the Northern Edge of the Caspian Depression"]

[Text] The great promise of the presence of oil and gas in the subsalt deposits of the Caspian Depression's northern peripheral zone has been confirmed in recent years by the discovery of the Zapadno-Teplovskoye and Gremyachinsk gas-condensate fields. A large volume of seismic studies have been accomplished here now which permitted refining and, in some cases, even changing previously existing concepts on the plutonic structure of this region. In 1969-1975, the Iliyskaya Geophysical Expedition of YuKTGU [expansion unknown] conducted a study of the plutonic geological structure of the Caspian Depression's northern slope zone. Studies with the MOV [reflected-wave method] were accomplished in a zone 50-70 km wide between the settlements of Chingirlau and Novoalekseyevka, and using KMPV [correlation method of refracted waves]--in a zone 100-150 km wide between the settlements of Semiglavyy Mar and Martuk (Fig. 1).

The procedure and results of these works were examined in detail earlier [1, 2].

As a result of these studies, new information was obtained on the plutonic geological structure of the Caspian Depression's northern peripheral zone.

The surface of the foundation (along the bottom of the salt) in the zone of the Zhadovskaya step and the Irtek-Ilekskaya flexure, which coincide spatially with the zone of the peripheral gravitational step, occurs at a depth of 6-7 km (Fig. 2) and there are no abrupt scarps in its relief. A region of the gently sloping occurrence of the foundation at a depth of 7-8 km--the Ilekskaya step complicated by the Berezovskiy and Koblandinskiy projections--has been mapped south of the gravitational step and east of the settlement of Burli.

In the area of the Ilekskaya step, MOV work by the Iliyskaya geophysical expedition disclosed the Koblandinskoye, Tamdinskoye, and Akrapskoye local uplifts within the limits of which the surface of the subsalt Paleozoic is at a depth

of 5.5-6 km, while further west MOV-MOGT [expansion unknown] work by the Ural'sk geophysical expedition disclosed local Karachaganakskoye, Aksayskoye, Konchebayskoye, and other uplifts with a depth of roof occurrence for subsalt deposits of 4-5 km. Thus, the spatial confinement of the subsalt Paleozoic local uplifts to the Ilekskaya step was established (see Fig. 1).

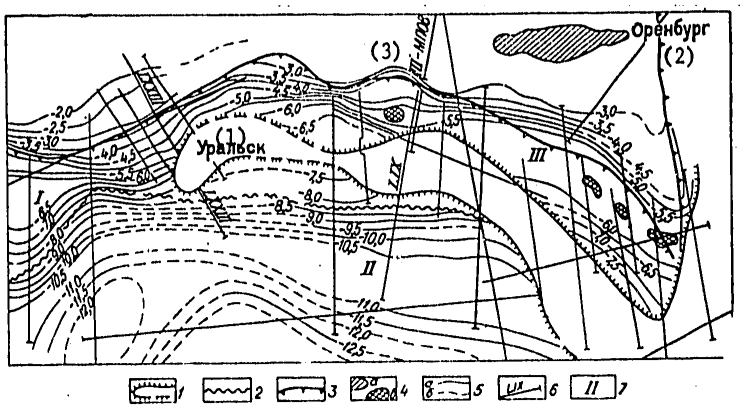

Figure 1. Diagram of the spread of subsalt sulfate-carbonate deposits on the northeast of the Caspian Depression. 1- limit of spread of subsalt sulfate-carbonate deposits; 2- limit south of which the roof of subsalt sulfate-carbonate deposits (d_4^{os}) occurs deeper than the bottom of the salt-bearing Kungur(Π_1); 3- peripheral gravitational step; 4- local uplifts of surface of subsalt deposits according to data: a- of seismic prospecting and drilling; b- seismic prospecting; 5- isohypses of the surface of subsalt sulfate-carbonate deposits (km) according to KMPV data: a- reliable, b- hypothetical; 6- KMPV profiles, GSZ [deep seismic sounding]; 7- steps: I- Kalmyk-Chabanskaya, II- Chelkarskaya, III- Ilekskaya.

Key:
1. Ural'sk
2. Orenburg
3. MPOV

West of the settlement of Bueli the inner zone of the depression near the periphery is several times narrower and the surface of the foundation is subsided very abruptly here--from 6-7 to 10-12 km, and further toward the center of the depression up to 20 km. South of the settlement of Semiglavyy Mar KMPV work disclosed the Kalmyk-Chabanskaya step with the depth of occurrence of the subsalt Paleozoic surface of 6-6.5 km.

APPROVED FOR RELEASE: 2007/02/09: CIA-RDP82-00850R000100050022-1

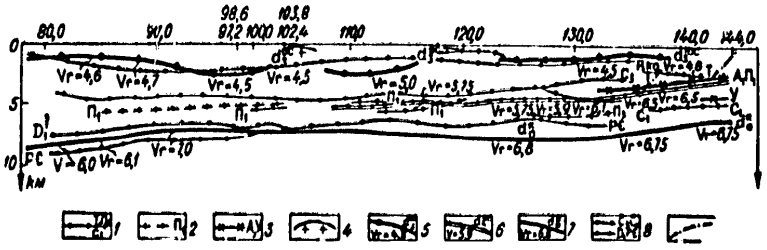

Figure 2. Comparison of MOV, MPOV [transmitted transformed wave method], and KMOV data for the LIX profile. Reflecting horizons: 1- T, $П_1$, C_1 (from data of the Ural'sk geophysical expedition), 2- $П_1$ (from sounding data of the Spetsgeofizika [Specialized Geophysical] Trust, 3- A, У (from data of the Orenburg geophysical office); refractive boundaries: 4- salt surface on arches of domes; 5- boundary in supersalt deposits d_3^{os}, 6- surface of subsalt sulfate-carbonate deposits d_4^{os}, 7- surface of foundation d_0^k; 8- boundary of exchange on surfaces: C_3--upper Carboniferous (bottom of salt), C_1--lower Carboniferous, D_1--in Devonian lows; P_{ϵ} -- Pre-Cambrian foundation; 9- fractures from MOV data.

Information was obtained for the first time on the lithology of the subsalt sedimentary complex from KMPV data.

It was established that in the inner zone near the periphery (south of the gravitation step) the thickness of the subsalt carbonate mass of the upper Devonian-lower Permian decreases from 2.5 to 1 km and then peters out completely. Farther to the south, carbonates appear in a section within the limits of the Central Caspian Depression where they occur 1-3 km deeper than the bottom of the salt. Only west of the city of Ural'sk are the subsalt carbonates from the inner zone near the periphery continuously traced in the area of the Central Caspian Depression (see Fig. 1).

An analysis of MOV-MOGT, KMPV, and MPOV work permits us to evaluate the capabilities of various methods in the following manner and to judge the expediency of their rational combination in studying various seismological zones.

1. MOV-MOGT provide information on the relief of boundaries in the subsalt, supersalt, and sometimes the salt-bearing strata with extremely high accuracy. As a rule, however, MOV-MOGT does not ensure the reliable study of the foundation surface which controls the structure of at least the lower part of the subsalt deposits and the lithology of the subsalt deposits. In the zone of subsalt flexure, regular reflections from the salt bottom and deeper subsalt horizons cannot be recorded. The reflecting horizons are not always

unambiguously identified through the correlation discontinuity zones. Complication of the wave field in the peripheral zone is graphically illustrated by the intermittent section presented in [3].

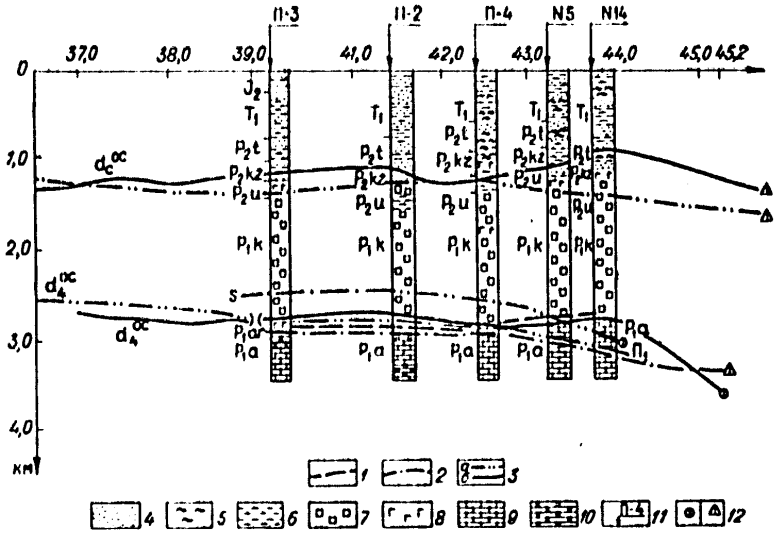

Figure 3. Comparison of data from deep drilling with results of MOV and longitudinal and nonlongitudinal profiling with KMPV on profile LXXIII (Zapadno-Teplovskaya area).
1- roof of salt-bearing Kungur and roof of sulfate deposits in the base of the Kungur from drilling data; 2- reflecting boundaries S and Π_1; 3- refracting boundaries d_4^{ss} (roof of salt-bearing Kungur) and d_4^{os} (roof of sulfate deposits in base of Kungur) from data of longitudinal (a) and nonlongitudinal (b) profiling with KMPV; 4- sand; 5- clay; 6- aleurolite; 7- rock salt; 8- gypsum and anhydrite; 9- limestones; 10- dolomites; 11- deep-drilled wells; 12- seismogeological boundaries in the plane of the section (a) and not in the section plane of the wells (b).

2. KMPV determines the relief of the foundation surface and the surface relief and outlines of the spread of subsalt sulfate-carbonate deposits (the boundary d_4^{os}). In this way, the problem of studying the lithology of the subsalt complex is solved. The shortcomings of the method are low accuracy of the structural formations along the subsalt boundary d_4^{os} in relation to MOV-MOGT which is caused by the wave's penetration into the carbonate mass

which leads to the smoothing-out of abrupt relief forms and by the specific nature of the reflected waves kinematics.

3. Nonlongitudinal profiling with KMPV was tested in the zone of subsalt flexure. A comparison of data from drilling, MOV-MOGT, and longitudinal and nonlongitudinal profiling with KMPV (Fig. 3) permitted establishing that on an upthrown side of a flexure the data from drilling, MOV-MOGT (reflecting horizons Π_1 and S), and KMPV (refracting horizon d_4^{08}--the roof of anhydrites in the base of the Kungura) show satisfactory convergence. However, the low-amplitude Zapadno-Teplovskaya structure (well 5.14) is reliably recorded only from nonlongitudinal profiling with KMPV. Longitudinal profiling did not permit disclosing it. MOV-MOGT materials are characterized by low quality both in this area and especially to the south. A similar result was obtained at other intersections of the subsalt flexure. Shortcomings of nonlongitudinal profiling are the low accuracy in determining the absolute depth of a boundary, as a result of which the tie-in from drilling or MOV-MOGT data is necessary, and the distortion of the incident wave front by the salt domes in the area of the point of explosion. The careful selection of its location on the most homogeneous sections is necessary to eliminate this.

4. The transmitted transformed wave method (MPOV) was tested by the Spetsgeofizika Trust in the peripheral zone of the Caspian Depression [4].

We compared the materials from MOV, KMPV, and MPOV for the profile LIX KMPV (see Fig. 2). The reflecting horizon A or Π_1 (roof of the subsalt Paleozoic) coincides with the refracting horizon, according to KMPV. At the same time, horizon C_3 (roof of the subsalt Paleozoic), according to MPOV data, occurs considerably higher. The discrepancy in the data of these methods reaches 1-1.5 km. We know of numerous examples where MPOV has been employed successfully in areas with a simple seismogeological structure where there are no abrupt seismic boundaries above the surface being mapped or in areas where the results of MPOV can be checked by drilling data rather frequently.

In areas with a complex seismic section, such as the Caspian Depression, which are characterized by the presence of several (often three) strong seismic boundaries located above the surface of the foundation, determination of the nature of the waves in subsequent arrivals is an extremely difficult and frequently unresolvable task. It is for this very reason that the discrimination and stratification of PPS-type transformed waves here is an extremely problematical task. Another complexity in the interpretation of MPOV data is that there are no data on the rate of propagation of transverse waves in the area of the investigations. All this limits the employment of MPOV to study the structure of subsalt deposits and the surface of the foundation of the Caspian Depression. This is also confirmed by experimental work carried out by the Iliyskaya geophysical expedition in 1969.

An analysis of the capabilities of various methods permits us to substantiate both the assumption of their rational combination and the procedure for the conduct of field work in various seismogeological zones.

The regional stage of KMPV studies can now be considered concluded everywhere with the sole exception of the section of the peripheral zone between Ural'sk and the settlement of Burli. Here, it is necessary to accomplish several submeridional profiles using the procedure which ensures the continuous tracing of the subsalt refracting boundary and the foundation surface.

All the KMPV profiles which have been developed should be duplicated by MOV-MOGT since only the combination of these methods permits the study of the foundation relief and the section and lithology of the subsalt deposits. The procedure for KMPV and MOV work was examined earlier [1, 2].

In the zone of subsalt flexure, it is recommended that MOV-MOGT be combined with nonlongitudinal KMPV profiling. The procedure for nonlongitudinal KMPV profiling for seismogeological conditions of the Caspian Depression's peripheral zone was designed for the recording of waves which have been refracted on the surface of subsalt sulfate-carbonate deposits (P_4^{os}) and the surface of the salt (P_3^{os}) from different azimuths. This permitted consideration of the salt's relief in the construction of the subsalt refracting boundary and obtaining two seismogeological sections with consideration of drift. The spacing of the seismic receivers is 100 meters and the size of the charge is from 200-500 to 1,500 kg.

The initial object for further geological-geophysical studies is provided by the subsalt flexure, on the upthrown side of which a number of local low-amplitude uplifts have been disclosed--the Tsyganovskoye, Gremyachin, Vostochno-Gremyachin, Teplovskoye, Zapadno-Teplovskoye, and others, in which regard commercial inflows of gas condensate have been established on the Gremyachin and Zapadno-Teplovskoye uplifts.

Another object of study is the interior zone of the Caspian Depression near the periphery where the depth of occurrence of the subsalt deposits' surface is 5-6 km. Most promising here is the area of the Ilekskaya step to which the subsalt local uplifts are spatially confined. Within its limits, searches should be conducted not only for traps of the anticlinal type, but also for nonanticlinal zones of the stratigraphic and lithological petering out of subsalt carbonate rocks and zones of increased jointing and karst formation which are connected with the ancient weathering crust. The study of the Ilekskaya step should be conducted by a combination of MOV-MOGT and KMPV methods, in which regard KMPV will solve the task of throwing light on the lithography of the rocks and delineating the zones where subsalt carbonates peter out.

The Kalmyk-Chabanskaya step which is located west of the settlement of Kamenka is an object for the second phase.

BIBLIOGRAPHY

1. Komarov, , V. P., Mironenko, V. M., Khrychev, B. A., and Tsimmer, V. A. "Study of a Section of the Sedimentary Mantle and the Foundation of the Caspian Depression by a Combination of Seismic Methods." In the book:

"Razvedochnaya geofizika na rubezhe 70-kh godov" [Prospecting Geophysics on the Boundary of the 1970's]. Moscow, Nedra, 1974, pp 580-585.

2. Komarov, V. P., Khrychev, B. A., and Tsimmer, V. A. "Geological Structure of the Northeastern Part of the Caspian Depression from Seismic Data." SOVETSKAYA GEOLOGIYA, No 2, 1976, pp 125-130.

3. Al'zhanov, A. A., Geyman, B. M., Golov, A. A., et al. "Direction and Procedure in Oil and Gas Prospecting Work in the Northern Peripheral Zone of the Caspian Depression." GEOLOGIYA NEFTI I GAZA, No 1, 1976, pp 7-11.

4. Fomenko, K. Ye., Vilenchik, A. M., Grineva, T. I., et al. "Regional MPOV Seismic Studies in the Northern Peripheral Zone of the Caspian Depression." GEOLOGIYA NEFTI I GAZA, No 7, 1971, pp 51-57.

6367
CSO: 8144/1169

GEOPHYSICS, ASTRONOMY AND SPACE

UDC 553.98.061.4.082:550.832(574.1)

STUDY OF ROCK DENSITIES IN THE CASPIAN DEPRESSION SECTION USING GRAVITATIONAL LOGGING

Moscow NEFTEGAZOVAYA GEOLOGIYA I GEOFIZIKA in Russian No 10, 1978
pp 28-32

[Article by V. F. Kononkov, B. V. Bobynin, V. V. Butazov, A. Ya. Zhigalin, A. I. Volgina, A. S. Pavlov, and O. K. Kozak of the Soyuzgeofizika Science Production Association, the Institute of Geography of the Academy of Sciences USSR, and the Russian Hydrological Institute]

[Text] Prospects for increasing reserves of petroleum and gas in the lateral zone of the Caspian Depression are linked to the discovery of lithological and stratigraphic traps confined in the reefogenic formations and carbonate reservoirs of the subsalt stratum of sedimentary rock of Lower Permian, Carboniferous, and possibly Devonian age [2].

Works [1-3] have pointed out the lack of a clear solution to the problem of searching for traps and evaluating their productivity because of the absence of information on the true density of large volumes of rock.

Experimental gravimetric tests were made in wells together with highly precise gravitational and magnetic exploration from the surface in the lateral zone of the Caspian Depression to obtain additional information on density characteristics.

In the Volgograd region gravitational logging was done in well 3-N at the Nikolayevskaya site to a depth of 2,800 meters with a cutting face of 3,200 meters; well 278-A at the Aleksandrovskaya site to a depth of 2,100 meters with a cutting face of 4,162 meters; well 276-N-N at the Novo-Nikol'skaya site to a depth of 1,850 meters with a face of 4,162 meters (see Figure 1 below). In the Saratov region gravitational logging was done in well 6-N at the Miloradovskaya site to a depth of 1,390 meters with a cutting face of 1,785 meters.

The study sites belong to different tectonic elements. Thus, the Miloradovskaya and Nikol'skaya sites are located directly within the boundaries of the lateral zone and its immediate outer margin, while the Novo-Nikol'skaya and Aleksandrovskaya sites are located in the inner, near-lateral interdome zone of the Caspian Depression.

Figure 1. Map of the Region in which Geophysical Work Was Done in 1974-77:

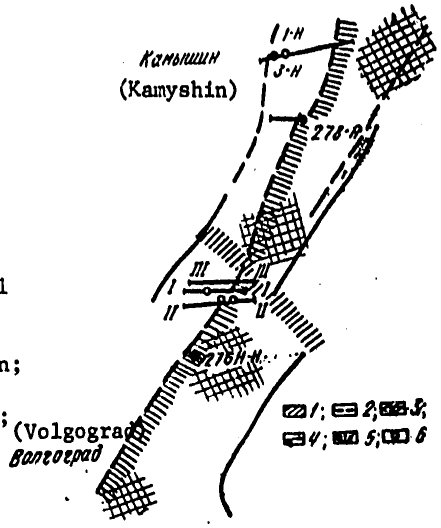

Key:
1) Zones of High Gradients of Gravitational Force;
2) Boundaries of Second-Order Zones Determined by Composite Geophysical Descriptions;
3) Zones of Maximum Gravitational Force;
4) Profiles Studied by Scientists from the Institute of Geography and Russian Hydrological Institute Using High-Precision Gravitational and Magnetic Exploration;
5) Wells in which Gravitational Logging Was Done;
6) Wells Drilled;
(H) Nikolayevskaya Site;
(A) Aleksandrovskaya Site;
(П) Primorskaya Site;
(H-H) Novo-Nikolayevskaya Site.

The affiliation of the objects of study with different tectonic elements was reflected both in the techniques of gravitational logging and in the results of determining rock densities in the geological section. Gravitational logging at the study sites was done with measurements at fixed points primarily using the top-to-bottom technique. The mean quadratic error of measurement within the range 0.15-0.3 milligals insures determination of the density of rocks in the geological section on the vertical with a precision from 0.01 to 0.05 grams per cubic centimeter at intervals of 100 meters.

When calculating the apparent density σ_{ad} along the shaft of the wells by the top-to-bottom technique we used the following equation (P. I. Lukavchenko, 1955):

$$\sigma_{ad} = \frac{1}{0.0838h}\left[g_i - g_{i+1} + 0.3086h + g^{p}_{i+1} \pm \Delta\right]. \quad (1)$$

After simplification calculations were made according to the formula

$$\sigma_{ad} = 3.68 + 11.933\,\frac{\Delta g}{\Delta z}, \quad (2)$$

where Δz is the distance in meters on the vertical and Δg is the difference in force of gravity between the top and bottom observation points.

The results of the determination of rock density of the geological section of the slope (side) of the depression and its western margin are given in Figure 2 below.

As was observed above, measurements of the force of gravity were made in wells 6-M, 3-N, and 1-N together with high-precision gravitational and magnetic exploration from the surface to determine the density characteristics of the lateral (slope) zone and outer margin. We will briefly discuss below the results obtained from measurements in these wells.

In well 6-M at the Miloradovskaya site gravitational logging was done by the loop increment technique, from the bottom to the top and from the top to a depth of 1,390 meters. With a precision of observation $\xi = \pm 0.28$ milligals, the error in determining density was ± 0.03 g/cm^3 with an observation interval of 100 meters. Eleven runs were made.

The cross-section of the well was compiled from geological materials of the Lower Volga Territorial Geological Administration. To a depth of 630 meters the section is represented by terrigenous deposits, beneath which is the salt of the Kungurskiy Stage of the Lower Permian (P_{1kg}) with interlayers of anhydrites. The density graph constructed from gravitational logging data reflects a change in density from 1.8 to 2.8 g/cm^3. From the mouth of the well to a depth of about 500 meters the apparent rock density σ_{ad} changes unevenly from 2.06 to 2.27 g/cm^3, probably caused by the more dense packing of the rock owing to geostatic pressure, which increases at depth. In the interval 500-630 meters σ_{ag} increases sharply to 2.66 g/cm^3. This is apparently related to the appearance of dense sandstones and, possibly, unrecorded interlayers of anhydrites in the section. On the density graph $\sigma_{ad} = 2.66$ g/cm^3 corresponds to them. Lower in the section, to a depth of 700 meters, the sandstones alternate with layers of anhydrites and σ_{ad} increases to 2.73 g/cm^3. Even lower, down to 1,390 meters, interlayering of sand and anhydrites is observed. In this interval σ_{ag} varies in a wide range, from 2.03 to 2.59 g/cm^3. Comparing the lithological section of the well with the density graph it appears that pure rock salt has a $\sigma_{ad} = 2.03$ g/cm^3. In the interval 800-1,000 m where interlaying of salt and anhydrites is observed σ_{ad} increases to 2.54-2.59 g/cm^3. Down to 1,300 m practically pure salt is found, characterized by a σ_{ad} from 2.03 to 2.10 g/cm^3. According to data from the Dergachevskiy NER [expansion unknown], a layer of anhydrites is identified in the interval 1,197-1,223 m, but it is not reflected in the density graph. From a depth of 1,300 m σ_{ad} increases with depth to 2.47g/cm^3, probably related to the presence of anhydrites. In the western part of the outer lateral margin of the depression gravitational logging was done in well 3-N at the Nikolayevskaya site to a depth of 2,800 m.

At well 3-N (see Figure 2), measurements of the force of gravity were done with a precision of $\varepsilon = \pm 0.25$ milligals, which makes it possible to determine rock density with an error of ± 0.03 g/cm^3. The density

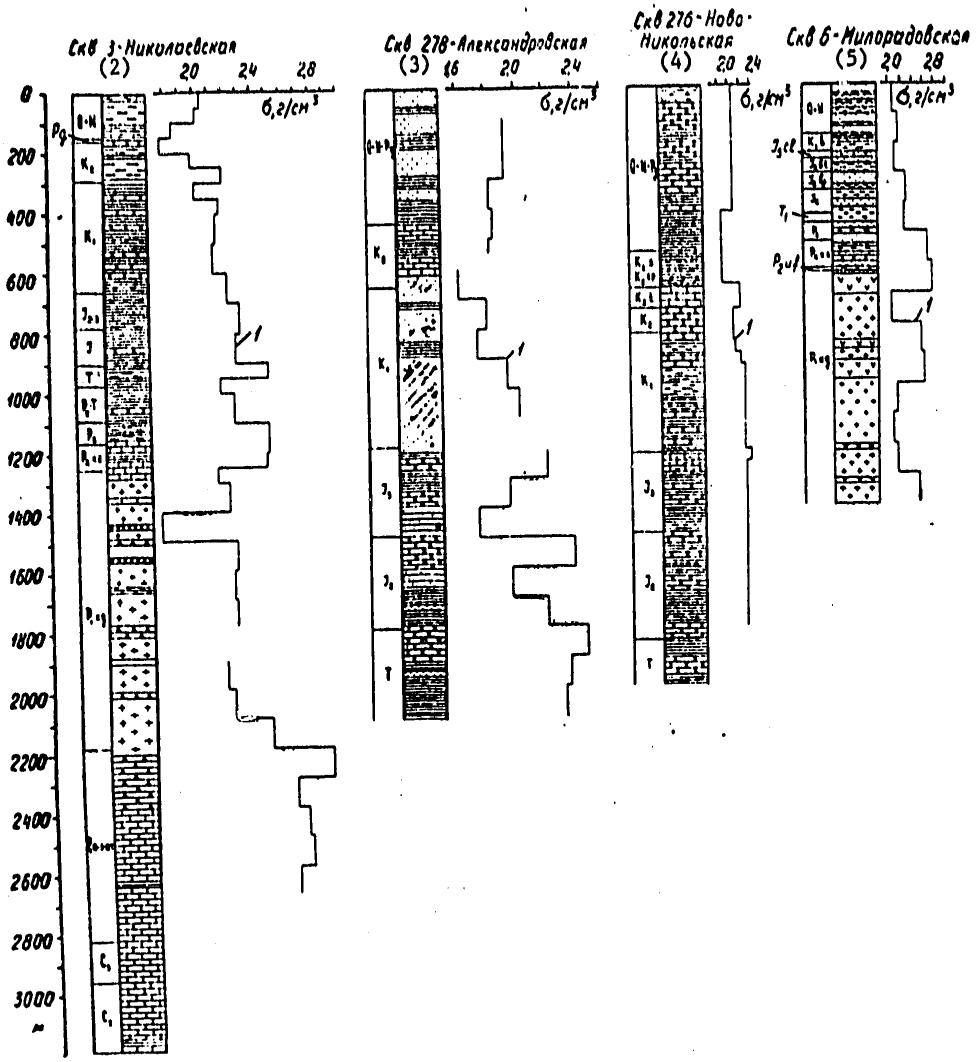

Figure 2. Results of Determination of Rock Densities by Gravitational Logging, Done by the Institute of Geography and Russian Hydrological Institute Jointly with the Soyuzgeofizika Science-Production Association in 1974-1977.

Key: 1) Density Graph;
2) Well 3, Nikolayevskaya;
3) Well 278-Aleksandrovskaya;
4) Well 276, Novo-Nikol'skaya;
5) Well 6, Miloradovskaya.

graph as a whole reflects change in rock density from 1.7 to 2.7 g/cm^3. The above-salt deposits here are sandy-clayey rocks of relatively small thickness (1.2 km). The apparent density to a depth of 1,160 m shows a tendency to increase.

In the depth interval 1,160-1,260 m, represented by limestones of the Kazan' Stage of the Upper Permian (P kz), σ_{ad} = 2.52 g/cm^3. Lower in the section salt occurs with thin interlayers of anhydrites; σ_{ad} = 2.25-2.28 g/cm^3. In the interval 1,400-1,500 m magnesium salts of contrasting density stand out; σ_{ad} = 1.77 g/cm^3. The depth interval 2,200-2,300 m is represented by pure anhydrites with σ_{ad} = 2.95 g/cm^3. Beneath the anhydrite beds at a depth of 2,400 m on the section are limestones with densities of 2.70-2.78 g/cm^3. The description of the density section of the inner margin of the western slope of the depression is given with the examples of well 278-A and 276-N-N. Gravitational logging on the section to a depth of 2,100 m was done at well 278-Aleksandrovskaya, located in the interdome zone. Three runs were made by the looping increment technique. The precision of measurement was ε = ±0.11 milligals, which makes it possible to determine σ_{ad} with a precision of ±0.01 g/cm^3 at intervals of 100 m. The density graph along the section represented by terrigenous beds reflects a change in σ_{ad} in the range 1.63-2.43 g/cm^3. The upper part of the section until a depth of 600 m is represented by interlayering sand and clay with a characteristic σ_{ad} = 1.95 g/cm^3. In this interval, moreover, account must be taken of the lateral gravitational effect of the salt domes, which may cause underestimation of the σ_{ad} of the rocks of the section under study. In the interval 600-1,300 m the density of the rocks increases from 1.8 to 2.2 g/cm^3. Lower on the section density changes unevenly. In the intervals 1,500-1,600 m and 1,800-1,900 m, represented by dense sandstones, it reaches its maximum values (2.43 g/cm^3).

The description of the density section of the inner margin of the southeastern slope of the depression is reviewed using the example of well 276 at the Novo-Nikol'skaya site (see Figures 1 and 2). This well is in the interdome zone, close to the lateral scarp. The geological section along the shaft of the well was compiled from material provided by the Nizhnevolzhskneft' Association. Gravitational logging was done to a depth of 1,850 m. With a precision of measurement of the force of gravity of ε = ±0.25 milligals, the precision of determination of rock density is ±0.03 g/cm^3. Thirteen runs were made using the techniques of complete repetition and looping increments.

Along the shaft of the well density was determined at intervals (each 100 m) and taking account of lithological complexes. The density graph showed a general change in density from 1.87 to 2.50 g/cm^3. The upper part of the section, represented to 420 m by interlayers of clay and sandstones, has a σ_{ad} = 1.97-2.05 g/m^3. In the interval 420-650 m the apparent density is 1.87 g/cm^3. The interval 650-720 m is composed of limestones and has σ_{ad} = 2.24 g/m^3, while at depths of 720-860 m the section is represented by sandstones with density of 2.12 g/cm^3.

Lower on the section are limestones (K_2) with higher density (up to 2.45 g/cm^3), then again lower the σ_{ad} again decreases to 2.38 g/cm^3. Overall the section is represented by sand and clay beds whose density increases at depth. Well 276-N-N is located in the zone of salt dome tectonics, so additional calculations were made and the effect of the salt domes on change in the force of gravity in the well, which influences the determination of rock density, was estimated.

Studies showed that the gravitational effect created by the salt domes exercises a significant influence on the density of rocks of the section. This effect must be taken into account in drawing the density graph. For example, on the corrected density graph the sandstone stratum at a depth of 1,300-1,400 m in well 276-N-N has the same σ_{ad} (2.50 g/cm^3) as higher on the section. Without taking account of the effect of the nearby salt dome the rock density in this interval was estimated at 2.27 g/cm^3.

Study of the density sections of the wells showed that anhydrites and carbonate rocks have fairly high density and the magnesium salts have comparatively low density. At the same time the apparent density of sedimentary rocks both among different petrographic groups and within each of them changes in a broad range by area and at depth. This is a result of the aggregate of geological factors affecting sedimentary rocks during their entire period of existence. Sedimentary rocks in the uplifted parts of the lateral scarp and on its outer margin differ significantly by density from rocks in the dropped part and within the lateral margin with well-developed salt dome tectonics characterized by very thick beds above the salt.

In drawing the density graphs by area, therefore, the effect of the salt domes on the readings of well gravimeters must be taken into account and corrections made for the non-horizontal bedding of the layers under study and the effect of other factors.

The table below was compiled on the basis of data from gravitational logging. It shows the densities of sedimentary rocks in the above-salt stratum and rocks within the limits of the entire western lateral zone of the Caspian Depression depending on their geological age.

It can be seen from the table that the density of sedimentary rocks within the lateral zone is indirectly related to their geological age through the depth of occurrence of the rocks.

The density of rocks of the same age varies greatly: the deviation reaches 0.3 g/cm^3. The density of the above-salt beds ranges from 1.99 to 2.28 g/cm^3, even though a constant density of 2.3 g/cm^3 for the intermediate layer is generally accepted in interpretation of materials from high-precision surface gravimetric exploration. Failure to take account of density deviations from this constant value causes significant distortions in the results of geological interpretation of gravimetric data.

Geological Age of Rocks	Rock Density (g/cm^3) in Wells			
	6-M	3-N	278-A	276-NN
P—Q	2.10	2.03	1.87	1.98
K_{1-2}	2.10	2.13	1.79	2.19
	2.18	2.32	2.10	2.39
T	2.25	2.38	2.40	--
P_2	2.47	2.51	--	--
P_1	2.07	2.28	--	--
Above-Salt Beds	2.28	2.22	1.99	2.19

FOOTNOTES

1. Kononkov, V. F., Volgina, A. I., and Kozak, O. K., "Results of the Use of High-Precision Gravimetric Exploration to Find Reefogenic Masses in the Volgograd Region" NEFTEGAZOVAYA GEOLOGIYA I GEOFIZIKA No 5, Moscow, VNIIOENG, 1975.

2. Pavlov, N. D., and Mushnikova, Z. F., "New Findings on the Structure and Petroleum-Gas Prospects of the Subsalt Deposits of the Southwestern Caspian Region" NEFTEGAZOVAYA GEOLOGIYA I GEOFIZIKA No 6, Moscow, VNIIOENG, 1977.

3. Sergeyev, L. A., Ballakh, I. Ya., Kononkov, V. F. et al, "Poiski Neftyanykh i Gazovykh Mestorozhdeniy s Pomoshch'yu Pryamykh Geofizicheskikh Metodov" [Prospecting for Petroleum and Gas Deposits Using Direct Geophysical Techniques], Moscow, Nauka, 1973.

11,176
CSO: 8144/1168 D

SCIENTISTS AND SCIENTIFIC ORGANIZATIONS

MEETING OF DIRECTORS AND LEADING WORKERS OF GEOLOGICAL PROSPECTING ORGANIZATIONS OF THE USSR MINISTRY OF GEOLOGY

Moscow SOVETSKAYA GEOLOGIYA in Russian No 3, 1979, pp 3-7

[Article: "Consolidation of What Has Been Achieved"]

[Text] The meeting of the aktiv of directors and leading workers of geological prospecting organizations of the USSR Ministry of Geology in participation with representatives of Party, Soviet and Trade Union agencies convened 12 January 1979 and discussed the speech of USSR Minister of Geology, Comrade Ye.A. Koslovskiy "Summary of the Work of Enterprises and Organizations of the Ministry of Geology for 1978 and Problems in Ensuring Fulfillments of the 1979 Plan for the Increase of Effectiveness and Quality of Geological Prospecting Operations Resulting from Decrees of the November (1978) Plenum of the CPSU Central Committee and Conclusions and Arrangements Discussed in the Address of Secretary General of the CPSU Central Committee Chairman of the Presidium of the USSR Supreme Soviet Comrade L.I. Brezhnev at This Plenum."

It was emphasized, at this meeting, that the November (1978) Plenum of the CPSU Central Committee is an important boundary mark in the struggle of the Soviet people for the realization of the historical decrees of the 25th CPSU Congress of the social and economic program of development of the country in the 10th Five-Year Plan. Comrade Brezhven's speech at this Plenum included a profound analysis of results of development of the national economy during the last 3 years of the 10th Five-Year Plan and a delineation of tasks and the development of a program of action directed toward the successful fulfillment of the tasks of 1979 and of the Five-Year Plan as a whole.

The 10th session of the USSR Supreme Soviet of the 9th convocation discussed and adopted laws concerning the State Plan of Economic and Social Development of the USSR and the USSR State Budget for 1979.

Geological prospectors, like all Soviet people, received the decrees of the November (1978) Plenum of the CPSU Central Committee and the session of the

USSR Supreme Soviet with great enthusiasm. Workers of geological organizations are responding to the concern of the Communist Party and Soviet government concerning further economic and cultural well-being with unselfish labor, are displaying initiative and are activating existing reserves of production in order to fulfill and overfulfill the plan tasks and the socialist obligations assumed.

As a result of intensive labor and political activity and the extensive development of socialist competition for a worthy welcome of the 1st anniversary of the USSR Constitution and the 61st anniversary of the October Revolution, geological organizations have ensured fulfillment of the basic tasks of the State Plan for 1978 and of the socialist obligations assumed.

The annual plan of increment and consolidation of supplies are being fulfilled for all forms of minerals. The 3-year plan of increase of supplies for 20 minerals is being fulfilled for the 1st anniversary of the USSR Constitution. According to production totals for 1976-1978, fulfillment of the Five-Year Plan of consolidation of the GKZ [State Commission of Mineral Supplies] USSR of supplies of 9 minerals are being fulfilled.

The economic effectiveness and quality of geological prospecting operations increased. In 1978 more than 65 percent of the geological reports approved in the GKZ USSR received good or outstanding evaluations.

Successful operations are underway for discovery of raw material--mineral resources for existing and planned territorial industrial complexes. The prospects of oil and gas bearing in western Siberia are improving; a new raw material base for oil extraction is being prepared on Buzach Peninsula in the Kazakh SSR and a new gas-bearing region in the lower Volga Region has been discovered. The reserve of explored coal regions in basic coal basins of the country are being increased significantly.

The raw material base of ferrous metallurgy, non-ferrous metallurgy and of the chemical industry is being improved. Major deposits of underground waters are being explored in order to ensure the water supply of many towns, industrial regions and agricultural areas.

Attaching great importance to the preparation of new mineral--raw material bases in the area of the BAM [Baykal-Amur Mainline], geological prospecting operations conducted in this region were increased 2.3-fold during the 3 years of the Five Year Plan. During the current five-year plan, prospecting of major deposits in the BAM zone [the Udokan copper deposit, the Kholodnin zinc and lead deposit and others) will be completed.

Scientific research and design organizations are conducting important work in forecasting the presence of mineral deposits and in the development of new high-productivity geological prospecting techniques and progressive technology of operations.

As a result of comprehensive socialist competition and the introduction of scientific and technical achievements, many geological organizations have achieved high technical and economic indicators of performance. In 1978, 120 deep test drilling brigades, 1218 column drilling brigades and 78 tunneling brigades worked at the limits established for the 10th Five-Year Plan. Drilling and tunneling brigades (88) have fulfilled 4-year plans and 8 brigades have fulfilled 5-year plans.

Excellent results in fulfillment of the socialist obligations assumed were achieved by deep prospecting drilling brigade headed by USSR State Prize laureate M.D. Avramitz from the "Khar'kovneftegazvedka" trust; by Hero of Socialist Labor N.D. Glebov from Glavtyumen'geologii and Hero of Socialist Labor A.A. Zhukov from the Orenburg Territorial Geological Administration; by V.S. Solov'yev, A.A. Khalin and V.A. Makar from Glavtyumen'geologii; column drilling brigades, directed by USSR State Prize laureate A.E. Nitsak from the Irkutsk Territorial Geological Administration and SSR State Prize Kazakh laureate I.S. Dontzov from the north Kazakhstan Territorial Geological Administration; tunneling brigades headed by brigade leader G.S. Akhmetzhanov from the Administration of Geology of the SSR Kirghiz and by USSR State Prize laureate A.A. Polyakov from Glavgeologorazvedki and many others.

There are still serious deficiencies in the work of geological organizations.

Thus, according to results for 3 years of the 10th Five-Year Plan, the plan for increasing petroleum supplies is unfulfilled and, in addition to this, the lag in growth of petroleum supplies which occurred in 1976-1977 in regions of Siberia, the Timano-Pechorsk oil and gas bearing province and Orenburgskaya Oblast (and also in regard to gas) in the Yakut ASSR still has not been made up. Search operations for oil and gas in eastern Siberia are proceeding slowly. One of the causes of the low efficiency of oil and gas operations is, in some cases, the low quality preparation by geophysical methods of structures for deep drilling.

The set volume of deep prospecting drilling for 1978 was not fulfilled by Ukhtin (85 percent of the plan) and Orenburg (88.1 percent) territorial geological administrations, the "Krasnoyarskneftegazrazvedka" (53.3 percent), "Yakutneftegazvedka" (83.1 percent) trusts, Mingeo RSFSR as a whole (90.2 percent) and some other organizations. The non-fulfillment of deep prospecting drilling volume restrains timely preparation of oil and gas supplies in major oil and gas bearing regions of the country.

Search operations for coking coals (of which there is a shortage) are proceeding slowly in Pechorsk Basin and Kuznetz Basin. Fulfillment of the Five-Year Plan for increasing tin reserves and phosphate raw material created stressful conditions.

From the beginning of the Five-Year Plan, the task concerning the increase of labor productivity at geological prospecting operations has been, on the whole, underfulfilled by the USSR Ministry of Geology.

The capital construction plan for 1978 was only 86.9 percent fulfilled and the plan for putting into operation residential area for the same year was fulfilled by only 85.9 percent.

Some geological organizations are not taking adequate measures for the careful and rational expenditure of material resources, allocated for conducting geological prospecting operations. Losses from lost time, accidents and discards are great. There are instances of a wasteful attitude toward the consumption of energy and fuel resources.

There is a high instability in some organizations due to shortcomings in the provision of work conditions and housing and domestic services required. Lax labor discipline results in occupational injuries. There are deficiencies in the selection and distribution of personnel and in the organization of educational work.

The level of organization of socialist competition does not comply fully with the requirements of the November (1978) Plenum of the CPSU Central Committee. The work of progressive collectives is inadequately studied and disseminated. Plan assignments for deep prospecting drilling are not fulfilled by 35.7 percent of the working brigade, for column drilling by 28.9 percent and for tunneling operations by 26.5 percent.

The meeting of activists of directors and progressive production workers of geological organizations of USSR Ministry of Geology with participation of representatives of Party, Soviet and Trade Union agencies resolved:

1. To approve completely the entirety of the November (1978) Plenum of the CPSU Central Committee, the conclusions and aims proposed in the address of Secretary General of the CPSU Central Committee, Chairman of the USSR Supreme Soviet Comrade L.I. Brezhnev at this Plenum, and to base the activity of all geological organizations of the Ministry of Geology on them.

2. The assembly of active workers assumes that the most important tasks of republican ministries and administrations of geology, of organizations of union subordination and of the central apparatus of the Ministry are:

concentration of efforts of geological organizations on the solution of complicated scientific and technical and production problems of the sector for further increase of mineral--raw material reserves, primarily in regions of operating mining enterprises and in newly mastered regions of the country, for fulfillment and overfulfillment of the plan task and socialist obligations of 1979 and the 10th Five-Year Plan for the increase of proven supplies of minerals and the consolidations of them in the GKZ USSR;

further intensification of the struggle for the increase of effectiveness and quality of search and prospecting operations due to improvement of scientific prediction, evaluation and methods of prospecting

deposits of useful minerals, improvement of preparation of structures for deep prospecting drilling, introduction of progressive geophysical and geochemical methods during search and prospecting for mineral raw material;

increase of labor productivity at geological operations on the basis of wide dissemination of progressive experience, more complete utilization of the achievements of science and acceleration of scientific and technical progress;

realization in 1979 of measures for making up the 1976-1977 deficit in growths of supplies of minerals, primarily the deficit in petroleum for Tyumenskaya Oblast and Orenburgskaya Oblast and the northern European part of the USSR and the deficits in fulfillment of the Five-Year tasks for tin in Magadanskaya Oblast and for phosphate raw meterial in the Yakut ASSR;

unconditional fulfillment of tasks of the 1979 plan and the socialist obligations undertaken for the growth and consolidation in GKZ USSR of supplies of mineral raw material for production of fertilizers, underground waters for irrigation and land reclamation, which are highly important for further development of agriculture;

fulfillment of plans of capital construction, reequipping of production areas at the sites of geological operations, plans of renovation and expansion of plants and enterprises, construction of industrial-laboratory bases of scientific research organizations; reduction of volumes of uncompleted constructions; improvement of organization of constructions realized by economic procedures;

ensurance of fulfillment of the 1979 plan and the socialist obligations for expansion of output of consumer goods and the improvement of the assortment and quality of them;

improvement of economy measures, reduction of non-production expenditure and loss including those due to down times, accidents and rejects; improvement of the use of fixed capital, careful, rational expenditure of material and technical supply, allocated for geological prospecting operations;

strict observance of plan, production and labor discipline, intensification of the mobilizing and organizing role of the plan and the furthest possible improvement of the system of planning and economic incentive of the structure of administration and methods of economic operation in the sector;

improvement of the forms of organizational operation, manifestation of a maximum specificity, efficiency and practicality in operation; considering it to be necessary: constantly to concentrate attention on

problems of economic and scientific-technical development of geological organizations, to ensure effective control over utilization of decisions made to increase the personal responsibility of management personnel for fulfillment of plans, for improvement of the conditions of work and life of geological prospectors.

3. To approve the initiative of the collective of the Irkutsk territorial geological administration and of collectives of leading tunneling and derrick-installing brigades, who have accepted the increased socialist obligations for 1979; to expand socialist competition in the sector significantly, and direct it toward the pre-term fulfillment of the annual and Five-Year plans, for search for the realization of production reserves, bringing up lagging tasks to the level of those in the lead for the purpose of achieving excellent final results.

4. To approve "Basic Measures of the Ministry of Geology of the USSR for Fulfillment and Overfulfillment of the 1979 plan and the 10th Five-Year Plan, for the Increase of Effectiveness and Quality of Geological Prospecting Operations, Flowing from the Decrees of the November (1978) Plenum of the CPSU Central Committee, of the Conclusions and Aims, Stated in the Address to the Plenum of Secretary General of the CPSU Central Committee, Chairman of the Presidium of the USSR Supreme Soviet Comrade L.I. Brezhnev to take into account observations and additions expressed by participants of the actives.

5. To recommend completion of work for the adoption of socialist obligations and counter plans by all geological organizations in January 1979 and to complete organizational work for their fulfillment.

The meeting of active members of directors and progressive workers of geological organizations with participation of representatives of Party, Soviet and Trade Union agencies assured the CPSU Central Committee and Comrade L.I. Brezhnev personally that, guided by the decrees of the November (1978) Plenum of the CPSU Central Committee, geological prospectors are doing everything necessary for fulfillment of the historical decrees of the 25th CPSU Congress for further expansion and strengthening of the mineral raw-material base of our country.

2791
CSO: 1870

PUBLICATIONS

SUCCESSIVE LINEARIZATION METHOD IN PROBLEMS OF OPTIMIZATION OF FAST-NEUTRON REACTORS

Moscow METOD POSLEDOVATEL'NOY LINEARIZATSII V ZADACHAKH OPTIMIZATSII REAKTOROV NA BYSTRYKH NEYTRONAKH in Russian 1978 signed to press 9 Dec 1977 pp 1-4, 88

[Annotation, table of contents and introduction from the book by V. V. Khromov, A. M. Kuz'min and V. V. Orlov; Atomizdat, 1650 copies, 88 pages]

[Text] A solution of the complete optimization problem of fast-neutron power reactors is considered based on the method of successive linearization. A statement of the problem is given as well as a brief characterization of the optimization methods applicable in reactor design, mathematical models for the description of neutron-physical and heat-engineering characteristics of a nuclear reactor are discussed; the method of successive linearization using formulas of the theory of small perturbations and the algorithms of linear programming is discussed; a designed optimization complex for programs and problem solution is described with various criteria of optimality.

The book is intended for a wide circle of readers engaged in the development of methods and computation programs and in the optimization of nuclear reactors, as well as graduate and upper-division students specializing in the field of atomic energy.

Fig. 13, tab. 8, Bibliography 72 titles.

Table of Contents

* * * * *

Introduction

In the next decades nuclear engineering will become one of the principal producers of electric energy (and possibly of heat, too) in most industrially developed countries of the world. Predictions indicate that in 1980 the output of the atomic power plants (AES) of the world will approach 200 million kW of electric power, and by the year 2000 it will reach a level of 1.5-3 billion kW. Nuclear engineering will allow the solving of energy problems of areas and countries poor in conventional fuel; it will lower environmental pollution from combustion products of organic fuel and conserve the

reserves of valuable fossils, such as oil, gas and coal, for chemical synthesis [1].

However, nuclear engineering, called to solve the problem of fuel resources, itself faces a problem no less complex. Indeed, although the uranium reserves of the earth are huge, only an insignificant part of them is found in relatively rich deposits (5-7 million tons at the cost 10$/kg). Thermal reactors on which present-day nuclear engineering is based consume in their life-time (~30 years) 3-5 thousand tons of natural uranium for 1 million kW of electric power. A comparison of these figures shows that the known reserves of cheap uranium would suffice for nuclear engineering only on such a scale as will be reached in the next decades. And transition to poorer ores would result in a considerable increase in the cost of electric energy produced by the AES. The situation will not change qualitatively even should geological prospecting detect nuclear fuel resources which are several times larger.

Among the many ways of solving (even partially) the fuel problem of nuclear engineering (improvement of thermal-neutron reactors, prospecting for new uranium deposits and development of cheap methods of extracting uranium from poorer ores, various methods of processing nuclear raw material (^{238}U, ^{232}Th) into nuclear fuel with the help of accelerators, nuclear blasts or thermonuclear installations) the fast-neutron breeder reactors represent the principal, best prepared scientific and technological trend. The introduction of fast reactors into nuclear engineering makes its resources practically inexhaustible. In principle, this problem may be solved in another way, based on thermonuclear synthesis. However, thermonuclear engineering is still in the emergence stage.

Presently only the first of the fast power reactors have begun operation (BN-350 in the USSR, Phenix in France, PFR in England) and the power engineers face the task of accumulating experience in industrial operation of such reactors. The creation of serially produced high-power fast reactors with optimal indices is a matter of the near future. Attainment of the best indices requires careful optimization, and the optimization task turns out to be rather complicated since most varied factors are closely linked with each other.

In the optimization process one has to take into consideration, side by side with the neutron-physical aspects, also materials strength, thermodynamics and others; and sufficiently complete economic characteristics of fuel and equipment must be used as criteria. Solutions of such complex problems--which could provide not only qualitative, but also quantitative answers to practical questions arising in designing--are attainable only due to the use of electronic computers. The present book describes an approximate computation model and expounds one of the methods of optimization of fast reactors, which has been developed precisely for the automated search for optimal constructions and parameters of fast reactors.

The reader should keep in mind that fast reactors and the mathematical methods of their optimization are in the initial stage of development. The neutron-physical data used in the calculations, and to an even greater extent, the heat-engineering and strength properties of materials and the cost indices entering into economic criteria exhibit a high degree of uncertainty. Therefore in the future the optimization problem should be formulated as a minimum (or maximum) problem under conditions of uncertainty of the initial data.

Also the computation models require improvement; they should ensure that essential factors are taken into account accurately enough, and at the same time they should not be overloaded with unimportant details. Finally, the extremum-finding procedures are themselves in need of improvement and optimization.

12157
CSO: 1870

PUBLICATIONS

ORBITS OF COMMUNICATIONS SATELLITES

Moscow ORBITY SPUTNIKOV SVYAZI in Russian 1978 signed to press 25 Aug 78 pp 2, 239-240

[Annotation and table of contents from book by G. M. Chernyavskiy and V. A. Bartenev, Izdatel'stvo "Svyaz'", 2800 copies, 240 pages]

[Text] This book is devoted to certain aspects of designing satellite communications. In the book an analysis is made of the orbit of a satellite and the influence of its parameters on the characteristics of communications satellites. High-elliptic orbits of the "Molniya" type and a stationary orbit are observed in detail. Questions are submitted concerning guaranteeing the function of several satellites combined in a system. Ways of ensuring continuous, stable communication with an assigned service territory using satellites are shown. Methods are cited for estimating the coverage zone of a communications satellite and for deriving coordinates to guide the antennae of ground stations.

The book is intended for scientific workers in the field of space technology and radio communications.

Table of Contents

9376
CSO: 1870

PUBLICATIONS

SIMULATION OF COMMUNICATION SYSTEM CHANNELS

Moscow MODELIROVANIYE KANALOV SISTEM SVYAZI in Russian 1979 signed to press 17 Nov 78 pp 2, 94

[Annotation and table of contents from book by A.P. Galkin, et al., Izdatel'stvo "Svyaz'", 5400 copies, 96 pages]

[Text] The possible use of methods of simulating communication channels when developing and constructing communications systems is shown. The possible ways of constructing imitators of communication channels are studied, and the methods devised from them are examined. Certain questions on the use of imitators when developing and constructing communication systems are submitted. The structural plans of the most expedient imitators of communication systems and examples of their use to increase the effectiveness of the development and testing of communication systems are cited.

This book is intended for engineering and technical workers involved with the development of communication systems and can be useful to scientific workers and students in the upper classes in the corresponding fields.

Table of Contents

9376
CSO: 1870

PUBLICATIONS

UDC 681.372

COMPUTER PROGRAMS FOR RADIOELECTRONIC GEAR DEVELOPMENT

Moscow MASHINNAYA OPTIMIZATSIYA ELEKTRONNYKH UZLOV REA (Machine Optimization of Radioelectronic Gear Electronic Assemblies) in Russian 1978 signed to press 26 Jun 78 pp 2, 192

[Annotation and table of contents from book by Anatoliy Georgiyevich Larin, Dmitriy Ivanovich Tomashevskiy, Yuriy Mikhaylovich Shumkov, and Valeriy Mikhaylovich Eydel'nant, "Sovetskoye radio", 10,700 copes, 192 pages, with illustrations]

[Text] The book is devoted to questions of elaborating and implementing a problem-oriented complex of programs for the analysis and optimization of radioelectronic circuits for moderate-output electronic computers. It provides a description of a complex of programs developed and designed to process radioelectronic circuits of moderate complexity.

The book is intended for engineering and technical workers involved in the elaboration of electronic devices for automation, radioelectronics, and measurement equipment. It will also be useful for VUZ students.

Contents Page

Contents Page

7869
CSO: 1870

PUBLICATIONS

SELF-TUNING MEASURING AMPLIFIERS WITH TEST SIGNALS

Moscow SAMONASTRAIVAYUSHCHIYESYA IZMERITEL'NYYE USILITELI S PROBNYM SIGNALOM in Russian 1978 signed to press 10 April 78 pp 2, 97

[Annotation and table of contents from book by I.P. Grinberg and S.A. Taranov, Izdatel'stvo "Energiya", 7000 copies, 97 pages]

[Text] A new class of amplifiers proposed by the authors, self-tuning measuring amplifiers with test signals (SIUP), is examined, their construction principles are observed, and amplifiers are analyzed with various methods of signal discrimination.

It is shown that self-tuning measuring amplifiers are nonlinear, unstationary and non-independent automatic regulation systems. The transient processes in the amplifiers are studied using the method of finite intervals proposed by the authors, and stability is observed using the method of harmonic balance. The estimation relationships needed to determine the errors in self-tuning measuring amplifiers are derived.

This book is intended for scientific workers and engineers studying and devising amplifying devices, and also for graduate students and students in the upper grades of institutions of higher education specializing in electronic and radio technology.

Table of Contents

9376
CSO: 1870

PUBLICATIONS

UDC 621.3.019

ANALYSIS OF THE RELIABILITY OF ELECTRONIC MEASURING EQUIPMENT IN ITS DESIGNING

Moscow ANALIZ NADEZHNOSTI ELEKTRONNOY IZMERITEL'NOY APPARATURY PRI YEYO PROYEKTIROVANII (Analysis of the Reliability of Electronic Measuring Equipment in Its Designing) in Russian 1978 signed to press 20 Jan 78 p 2, 111

[Annotation and table of contents from book by Aleksandr Davydovich Krop, edited by V. N. Sretenskiy, Izdatel'stvo "Sovetskoye radio", 8200 copies, 112 pages]

[Text] This book treats the main problems of the reliability of electronic measuring equipment (EIA) during various stages of its designing. It examines the special characteristics of the designing of this type of equipment. It gives engineering methods of the evaluation of reliability and defines the role of the subdivision of reliability in the process of EIA designing.

The book will be of interest for engineers and technicians connected with the problems of reliability and designing of electronic measuring devices.

Figures -- 22, tables -- 23, bibliography -- 35 titles.

Contents

10,233
CSO: 1870

PUBLICATIONS

UDC 621.311.1:681.3+621.398+621.316.925

SIMULATION AND AUTOMATION OF ELECTRIC POWER SYSTEMS

Kiev MODELIROVANIYE I AVTOMATIZATSIYA ELEKTROENERGETICHESKIKH SISTEM (Simulation and Automation of Electric Power Systems) in Russian 1978 signed to press 9 Jan 78 p 2, 151-152

[Annotation and table of contents from a collection edited by L. V. Tsukernik (chief editor) et al, Izdatel'stvo "Naukora dumka," 1550 copies, 160 pages]

[Text] This collection treats the problems of the development of methods, algorithms, and programs of computations on electronic computers for the analysis of stationery and transitional modes of electric power systems, computation of short-circuit currents and equivalent parameters, as well as complex simulation in solving these problems. It describes the results of studies and development of systems of automatic control, regulation, and devices of circular remote control. A number of articles deals with the determination of quality indexes of measuring converters of current and voltage, and the development of devices for automatic tuning of the compensation of the capacitive currents of a network.

This collection is intended for scientists, engineers, and technicians engaged in the problems of operation modes, relay protection, and automation of power systems, as well as for specialists in the use of computers in electric power engineering.

Content

10,233
CSO: 1870

PUBLICATIONS

PRODUCTION OF SEMICONDUCTOR CASINGS

Moscow PROIZVODSTVO KORPUSOV POLUPROVODNIKOVYKH PRIBOROV (Production of Transistor Bodies) in Russian 1978 signed to press 30 May 78 p 2, 183-184

[Annotation and table of contents from a book by Oleg Sergeyevich Moryakov, "Vysshaya shkola", 8,000 copies, third edition, adapted and supplemented, 184 pages, with illustrations]

[Text] Described in the book are the engineering processes for manufacturing varying types of semiconductor casings. Presented are casing designs and material characteristics, basic methods for obtaining glass and ceramic junctions with metal, hermetic sealing of crystals with electron-hole junctions and plastic integral structures, metal and ceramic component seals with solid solders, as well as methods of application of galvanized surfaces and of casing output control.

The third edition has been supplemented with a description of the special features of casing designs for powerful SVCh [microwave] semiconductors, as well as of new engineering processes for working with high-silica ceramic.

Contents Page

Contents Page

Contents Page

7869
CSO: 1870

PUBLICATIONS

UDC 621.3.049.77

NEW BOOK ON APPLICATION OF MICROCIRCUITS

Moscow MIKROSKHEMY I IKH PRIMENENIYE (Microcircuits and Their Use) in Russian 1978 signed to press 4 Dec 78 pp 2, 246-247

[Annotation and table of contents from book by Vladimir Aleksandrovich Batushev, Viktor Nikolayevich Veniaminov, Venedikt Grigor'yevich Kovalev, Oleg Nikolayevich Lebedev, and Andrey Ivanovich Miroshnichenko, "Energiya," 150,000 copies, 248 pages, with illustrations, Mass Radio Library, Publication 967]

[Text] Presented in the book is general information concerning integrated microcircuits, the principles of building various radioelectronic devices based upon them are examined, and possibilities of employing microcircuits in amateur radio operations are demonstrated. Microcircuit classification and the requisite reference data has been presented.

The book is intended for amateur radio operators experienced in the field of semiconductor electronics.

Contents Page

Contents

Contents Page

7869
CSO: 1870

END